Universitetet
i Stavanger

FACULTY OF SCIENCE AND TECHNOLOGY

MASTER'S THESIS

Study program/specialization: Study program: Master's Degree Programme in Offshore Technology Specialization: Subsea Technology	Spring semester, 2009 Confidential
Author: Akaradech Apornsuvan	AKARADECH A. (signature author)

Supervisors: Prof. dr. Arnfinn Nergaard (UiS)
Anders Ledin (FMC Production Services AS)

Title of Master's Thesis: Concept design of self-contained remotely controlled running tool

ECTS: 30

Subject headings: -WCP Running tool -Ultra deepwater RLWI deployments -Riserless Light Well Intervention	Pages: 68 + attachments/other: 109 Stavanger, 15/06/2009 Date/year

Abstract

Riserless Light Well Intervention (RLWI) technologies nowadays become a cost-effective solution to improve oil recovery rate from existing subsea wells with high operational efficiency. However, when deploying RLWI packages to an ultra-deepwater subsea well, some operational downtime may be occurred due to line entanglement. Operational downtime in oil and gas industry poses a serious risk to project economics therefore the RLWI operation need to be developed to minimize its potential downtime and optimize its overall performance.

The new concept of running tool (RT) system for deploying RLWI packages is initiated to minimize submerged lines, resulting in lower possibility of line entanglement. This concept is to replace a traditional RT with a guidelineless RT for ultra-deepwater RLWI operations. The success of the new RT concept can also be further applied for installing other subsea structures without long operational periods, the need of guidelines and the use of a work-class ROV.

An overview of fundamental equipment and systems for the new RT is reviewed with state-of-the-art applications. The essential systems include thruster system, control system, communication system, navigation system and sensors, and energy system. It is important to focus on the thruster system, a main energy consumer and a main system used to adjust the position of the well control package (WCP) during the operation.

The theory of hydrodynamics and assumptions of module geometries were used to establish the relationship between global forces and moments acting on the RT and WCP in the sea water. The new RT concept is evaluated assuming the RLWI operation is located at 3,000 m water depths in Angola Sea. The hydrodynamic forces in each operational step are calculated to design the required thrust of the thruster system in the deployment and retrieval operations.

Some results reveal that there are at least two operations that need further studies; during stacking the WCP onto the XT re-entry hub and during the retrieval of the RT and WCP back to the surface vessel. The lack of real-time transmission requires that the communication and the control system should be further investigated. According to the tremendous environmental forces on the RT and WCP module in the shallow zone, the thruster system cannot provide enough thrust to control the movement of the RT and WCP module during the retrieval operation, thus the guide frame system need to be modified to assist the retrieval operation.

Acknowledgements

I would like to take this opportunity to thank Anders Ledin who was my supervisor in FMC production services AS for his great assistance and consultancy. I also would like to thank Vidar Sten-Halvorsen and Bjarne Neumann, FMC Production services AS, for giving me useful comments and a chance to write my master thesis.

I am grateful to Peter Michael Guest, Guest Drilling Consultants Ltd, for sharing his long professional experiences in offshore operations.

I wish to express my gratitude to Professor Arnfinn Nergaard, University of Stavanger (UiS), for all his supports and guidance during the work.

The last thanks, but it is not least, go to my family for a lot of support and encouragement.

Table of Contents

List of Tables

List of Figures

List of Abbreviations

AUV	Autonomous Underwater Vehicle
CAPEX	Capital Expenditure
DGPS	Differential Global Positioning System
DHSV	Down Hole Safety Valve
DOF	Degree Of Freedom
DP	Dynamic Positioning
DVL	Doppler Velocity Log
EQD	Emergency Quick Disconnect
HAIN	Hydroacoustic Aided Inertial Navigation
HMI	Human-Machine Interface
HPU	Hydraulic Power Unit
INS	Inertial Navigation System
IWOCS	Installation/Workover Control System
LBL	Long Base Line
LLP	Lower Lubricator Package
LS	Lubricator Section
LUB	Lubricator Tubular
MEG	Monoetheylene Glycol
MODU	Mobile Offshore Drilling Unit
MULBL	Multiple User Long Base Line
OD	Outer Diameter
OPEX	Operational Expenditure
P&A	Plugging and Abandonment
PCH	Pressure Control Head
PWM	Pulse Width Modulation
Re	Reynolds number
RLWI	Riserless Light Well Intervention
ROV	Remotely Operated Vehicle
RPM	Revolutions per Minute
RT	Running Tool
SCM	Subsea Control Modules
SSBL	Super Short Base Line
SSLBL	Super Short and Long Base Line
ULP	Upper Lubricator Package
UUV	Untethered Underwater Vehicle
WCP	Well Control Package
XT	Christmas tree

List of Variables

Symbol	Name	Unit/descriptions
ρ	density of sea water	[kg/m^3]
τ	torque	[Nm]
C_a	added mass coefficient	
C_d	drag coefficient	
C_m	mass coefficient	$1+C_a$
F_b	buoyancy	[N]
F_d	drag force	[N]
F_i	inertia force	[N]
W_s	submerged weight	[N]
a_m	acceleration of the module	[m/s^2]
a_r	relative acceleration	[m/s^2]
m_a	added mass	[kg]
r_m	moment arm	[m]
$\dot{u}$	horizontal acceleration	[m/s^2]
v_c	current speed	[m/s]
v_m	advance speed of the module	[m/s]
v_r	relative velocity	[m/s]
v_w	the maximum horizontal velocity of water particle	[m/s]
$\emptyset$	velocity potential	[m/s]
A	area	[m^2]
D	diameter	[m]
H	wave height	[m]
Hs	Significant wave height	[m]
I	moment of inertia	[kgm^2]
L	angular momentum	[Nm s]
T	wave period	[s]
a	acceleration	[m/s^2]
d	water depth	[m]
g	acceleration of gravity	[N/s^2]
k	wave number	[m^{-1}]
m	mass	[kg]
u	horizontal velocity	[m/s]
v	velocity	[m/s]
∇	volume of the object	[m^3]
α	angular acceleration	[rad/s^2]
λ	wavelength	[m]
ν	kinematic viscosity	[m^2/s] (sea water $\cong$ 1.17 x 10^{-6} m^2/s)
ω	angular frequency	[s^{-1}]

1 Introduction

In the early days, oil and gas fields have been produced from dry trees where production facilities are located above the sea level. The dry trees are a basic concept for a number of topside platforms such as a steel jacket platform, fixed concrete platform or gravity based structure (GBS) jackup, tension leg platform (TLP) and jack-up platform. The main characteristics of the dry tree development are the large amount of CAPEX and the low amount of OPEX.

When offshore exploration and production (E&P) business has strived towards deeper water field or marginal field applications, subsea production systems have become an outstanding choice. The subsea production systems are favorable for several offshore fields in Norway, Gulf of Mexico, West Africa, Brazil and others.

Despite a great number of subsea production systems deployed during the last decades, the drawback of the subsea production systems is higher OPEX and lower recovery rate than dry tree concept. The lower oil recovery rate can be caused by the lack of proper well services to maintain production level, which is normally due to high service costs such as rig day rates and equipment used for subsea fields.

Several subsea technologies, however, have been improved to overcome the deficiencies of subsea production systems during the last decades. A cutting edge technology being used to improve production of existing subsea wells is Riserless Light Well Intervention (RLWI). The RLWI enhances cost effectiveness for subsea well intervention and help to close the production gap between topside and subsea wells. When the cost of well intervention is significantly reduced, well intervention can be regularly performed to accomplish the target of oil recovery rate.

The use of wire-rope guidelines with a running tool is nowadays a typical guidance system to deploy and retrieve the RLWI system. The running tool is a clamp mechanism hanging from the surface vessel with guide arms. This technique is used to limit the movement of the running tool along with the guidelines vertically. The clamp inside the running tool is used to lock the WCP. The running tool configuration is dependent on the RLWI sections needed to be deployed.

1.1 Current Limitations

RLWI operations in deepwater zones, at depths greater than 1,000 meters, are much more challenging than in shallow water. The deployment of the RT with guidelines becomes unmanageable due to line entanglement. The guidelines probably tangle with other guidelines, umbilicals or ROV umbilical and these guidelines could also snap due to the entanglement. Such failures could result to long operational downtime.

1.2 Motivations

Thriving oil and gas in ultra-deepwater fields can represent several challenges and advantages throughout the offshore industry. One of these challenges is to employ RLWI in ultra-deepwater fields while minimizing operational downtime in the process.

The operational downtime can pose a serious risk to project economics because rig costs could exceed the projected budget. The rig cost may be more than 50 percent of the total operational cost. In addition to extra rig costs, the E&P company must suspend the oil/gas production, resulting in the loss of the company revenue. Minimizing downtime is so important that operators can save extra rig time and enhance success rates of the RLWI services.

By using a new guidelineless deployment concept, an operator can be able to deploy WCP to XT without the need for traditional guidelines. The RLWI operation would require only four lines in the water; the two IWOCS umbilical lines, the ROV umbilical and the wireline. Therefore, the lesser the lines, the lesser the chance of the line entanglement.

In addition, the new concept can minimize payloads on the surface vessel by removing the winch systems and heave compensation systems used to support guidelines. The new concept practically eliminates operational times typically required for connecting and disconnecting guidelines.

1.3 Objectives of Thesis

Main purpose of the thesis is to establish a design concept for a new WCP RT that can be used to deploy the WCP assembly for ultra-deepwater RLWI operations without a traditional guideline system. The thesis scopes include:

- Outline deployment and retrieval operations of the new WCP RT.
- Analysis for the possible implementation of the self-contained concept for the new WCP RT system.
- Designing the thruster system and essential systems for the new WCP RT.
- Calculating the required thrust used to adjust the position and direction of the RT and WCP.

1.4 Outline of Thesis

This thesis can be divided into four main sections: description of components/systems needed for the new RT, outline of the thruster system, simplification of hydrodynamic equations for the RT and WCP model, and then analyses of the possible implementation of new RT.

Chapter 2 introduces overview of the RLWI, its main systems and WCP RT. The installation operation for WCP is also described.

Chapter 3 presents brief marine operations for deployment and retrieval of WCP with a guidelineless RT concept. This chapter describes essential systems and environmental considerations.

Chapter 4 develops a design concept for each system. This chapter presents simplified concept of a control system that can be implemented for heading and positioning control systems. This chapter also discusses advanced communication, navigation and energy systems applicable for ultra-deepwater operations.

Chapter 5 emphasizes on the design of the thruster system. It discusses pros and cons of different thruster designs and types of motors.

Chapter 6 identifies global forces acting on the RT and WCP module in order to understand characteristics of the module during operations.

Chapter 7 reviews related hydrodynamic forces acting on the model and expresses essential hydrodynamic equations of the system. The simplification of the hydrodynamic model is also discussed for the design of control system.

Chapter 8 performs analyses of the guidelineless RT application in Angola Sea. The environmental conditions and operation requirements are identified. This chapter gives a summary of environmental forces, required thrust and energy consumptions for the operations. The estimations are done by using MathCAD.

Chapter 9 carries out design specifications of the guidelineless RT system.

Chapter 10 summarizes and discusses the overall results with suggestion for future study of the new RT concept.

Appendix A lists key parameters used in the thesis

Appendix B provides main formula for the analysis, e.g. wave equation and moment of inertia.

Appendix C describes assumptions of module rotations of the RT and WCP module

Appendix D presents calculations, results and graphs from MathCAD.

2 Riserless Light Well Intervention (RLWI)

The RLWI system offers operators a safe and profitable method to perform live well intervention without the traditional need for an expensive mobile offshore drilling unit (MODU). The RLWI carries out the light intervention from low-cost dynamically positioned monohull vessels. The monohull vessels can move between oil fields much faster than a traditional mobile intervention rig.

Furthermore, The RLWI system can save rig time by the removal of installation operation for rigid workover risers or anchor lines, thus providing operators a shorter period of intervention. Reducing the well intervention cost of the service vessel is main driver for the development of RLWI technology. The RLWI has become a routine operation with increasing demands of well intervention and high operational efficiency. The RLWI system can result in additional production volumes from mature subsea wells intervention.

The RLWI can typically perform several applications [1]: production logging, perforating/re-perforation, zone isolation (plug/ straddle), inspection/repair/ installation of insert DHSV, milling of short scale bridges, camera runs: visual or x-ray, well killing operation, pumping operations/scale treatments, selective tracer injection or sampling, change out of gas lift valves, sleeve operations. There is also a potential that the scope of RLWI operations can cover P&A operations of subsea wells and change out of subsea trees.

Lessons and input from existing Mark I equipment and operations have been implemented in the system and equipment design of RLWI Mk II as follows [2, 3]:

- Water depth capacity increased from 500 to 3,000 m
- New control system architecture
- New Upper Lubricator and Pressure Control Head design
- Subsea grease injection reservoir and pump system
- Electro-hydraulic umbilical is replaced with a single electric ROV-type umbilical

The new generation of RLWI system called Mk II is to be launched for field operations in April 2009. The main sections of RLWI Mk II are Well Control Package (WCP), Lubricator Section (LS) and Pressure Control Head (PCH).

Well Control Package (WCP)

The WCP is the heaviest module and the first module installed on the XT re-entry hub. The WCP is functioned as a main safety barrier of the well intervention. WCP is composed of shear/seal ram able to cut and seal wireline, coiled tubing and wireline tool string. The WCP supply hydraulic pressure and communication to XT functions. It also has a system that can flush hydrocarbons back into the well. The bottom section of the WCP is equipped with a XT connector, functioning as an interface between The XT re-entry and WCP.

Lubricator Section (LS)

The LS assembly is the longest assembly unit in RLWI and is a pressure containing cylinder used for inserting the downhole tool package into the well under full pressure. The LS consists of three sections; Upper Lubricator Package (ULP), Lubricator Tubular (LUB) and Lower Lubricator Package (LLP).

Upper Lubricator Package (ULP)

The ULP assembly is the connection between the LS and PCH section. ULP includes a wireline cutting ball valve, capable of shearing up to 7/16 inch braided cable and sealing the 7 inch lubricator bore [4]. The ULP also has to supply viscous grease for PCH unit via the circulation outlet. ULP is designed to have an interface with a running tool for handling system.

Lubricator Tubular (LUB)

The LUB is a temporary storage position for the wireline tool string on the way down into the well or on the way out. According to the elimination of the large umbilical line from the topside, the LUB provides a grease storage and grease injection pump for maintaining pressure control and circulation of well fluids.

Lower Lubricator Package (LLP)

The LLP assembly is a connection between the LS and WCP section. The LLP acts as the safety joint capable to disconnect the LS from WCP in the event of an emergency disconnect. The LLP unit includes SCM, HPU and circulation hoses. The elimination of the elctro-hydrolic umbilical requires HPU moved from the topside to be fabricated in the LLP unit.

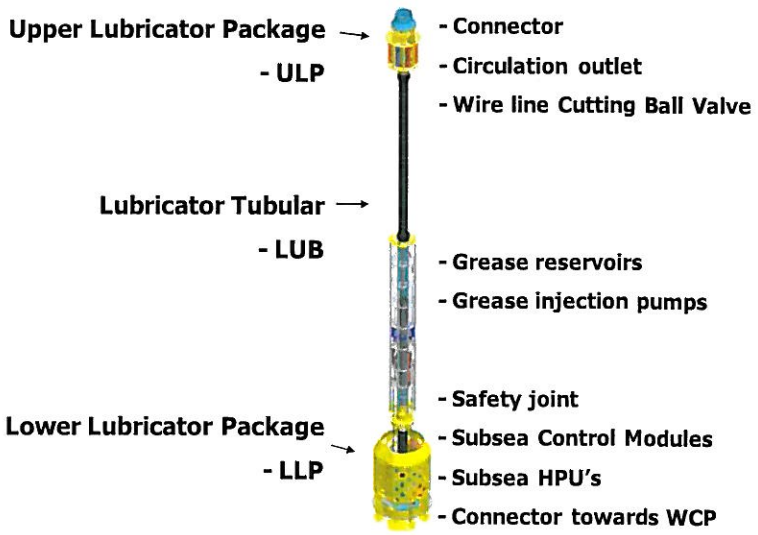

Figure 2-1 Lubricator Section (LS) [2].

Pressure Control Head (PCH)

The Pressure Control Head (PCH) is connected to the top of LS section. It is functioned as a pressure barrier that can seal around moving wireline. It is assembled with static rubber seals activated on stationary wireline, which can reduce a risk of losing tool string. During wireline operations, the pressure barrier is achieved by injecting viscous grease in to the flow tube inside PCH. The pressure difference between well pressure and hydrostatic could be 200 bars[5]. When grease pressure is higher than existing well pressure, it can keep oil and gas to remain inside the PCH and well.

Umbilical Termination Head (UTH)

WCP is accommodated Umbilical Termination Head (UTH) that can be connected and disconnected by use of ROV mechanically. Hydraulic disconnect system can be used in case of Emergency Quick Disconnect (EQD), while mechanical disconnect system can be activated in case of over tensioning. In the UTH, electric signals from fiber optic lines are converted and transmitted to copper lines. The UTH has two terminal connectors for a subsea electric connector and a chemical injection stab.

Umbilical lines

The size of umbilical lines used in RLWI Mk II is smaller than RLWI MK I by removing hydraulic umbilical. As stated previously, there are control and chemical umbilicals connected with the UTH. The OD of control and chemical (MEG) umbilical lines are 38 mm and 51 mm respectively [2]. In contrast, RLWI Mk I use a larger umbilical line which is an elctro-hydrolic line with OD 116 mm.

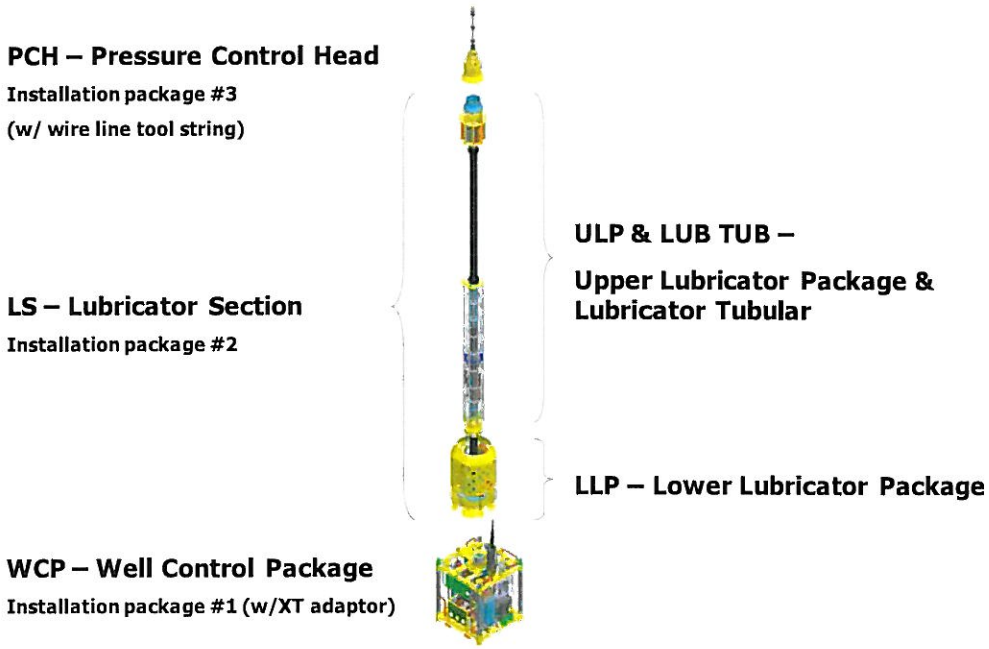

Figure 2-2 Complete RLWI MK II Stack [2].

Running Tool (RT)

The RT is a special tool used to handle the main section of the RLWI system onto the XT. For RLWI Mk II, there are three similar types of RTs used for deploying WCP, LS and PCH units. The main part of RTs is a clamp mechanism inside the RT. The clamp is used to lock WCP and normally unlatched by hydraulically actuated cylinders. The RTs are basically composed of guide arms and funnels, which are slotted to permit insertion and removal of guidelines and limit the RT to move vertically along the guidelines. Locking gates at the funnels are used to avoid accidental removal of guidelines from funnels.

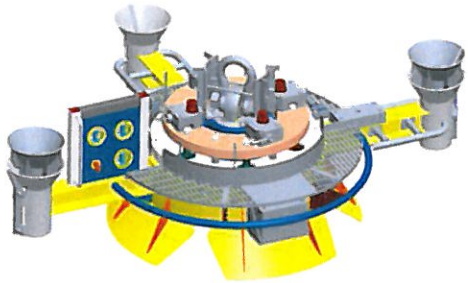

Figure 2-3 WCP running tool for RLWI Mk II [6].

2.1 The Installation Operation for WCP

This part describes the current installation operation for WCP.

- The surface vessel is securely positioned near the subsea template.
- Three guidelines (metal wires) are required for running WCP module and there are only two guidelines required for LS and PCH units.
- The guidelines are established to the guideposts; both at the subsea mounting base and at the module handling tower on the surface vessel.
- The WCP is connected with UTH and XT adapter and The WCP is lifted to an inspection place.
- The tension on the both umbilical reels is set before running the WCP through the splash zone. The tension on the both umbilical reels must be set again after the WCP is below 50 m water depths.
- The WCP is lifted to the module handling tower before launching it to the sea.
- The RT and WCP module is launched though the moon pool on the surface vessel using a cursor system (guide frame) to reduce the effect of the waves in the splash zone.
- Having reached at the bottom of the cursor system, the WCP will be released from the locking system on the cursor system.
- The deployment of the WCP is stopped when the distance between XT re-entry hub and the bottom of the XT adaptor is approximately 6 meters to allow a supporting ROV inspect the re-entry hub on the XT.
- The ROV is also utilized to monitor the alignments and connections during landing.

- Main winch will be set to active heave compensation when landing WCP on the XT re-entry hub.
- After the WCP has landed on the XT, the ROV opens all mechanical safety locks on WCP RT by installing hot stabs into receptacle on WCP RT. The ROV supply the hydraulic power into the actuator system to unlock the WCP RT from the WCP.
- The ROV verifies that the WCP RT is fully unlocked and The XT connector is lock from HMI or by ROV.
- The WCP RT is retrieved back to the surface vessel.
- The protection cap on WCP re-entry hub is installed by the ROV.

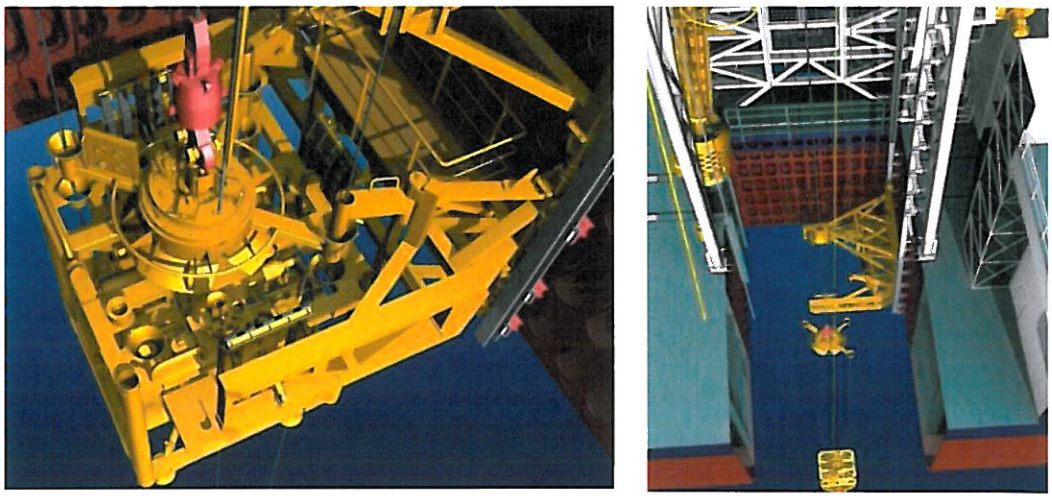

Figure 2-4 The deployment of the RT and WCP module at the bottom of a moon pool (left). The retrieval of the RT to the cursor system (right) [6].

Bearing in mind that the operation may be changed due to the continuous development of RLWI MK II.

3 Deployment and Retrieval Guidance for the New WCP RT

According to ISO 13628-1: 2005, the typical guidance systems to deploy equipment to the seabed from a floating vessel can be accomplished by the use of either wire-rope guidelines or guidelineless techniques[7]:

> "The guideline method uses tensioned wires and equipment-mounted guide sleeves to orient and guide the equipment from the vessel to its final position on the seafloor.
>
> The guidelineless method uses dynamic position reference system to indicate the relative position between the landing point and the subsea equipment. The subsea equipment is maneuvered by moving the surface vessel, until the equipment is positioned over the landing point. The equipment is then lowered to the landing point and brought into the final position by mechanical guidance."

It is possible to apply the guidelineless concept for the deployment of WCP in deepwater zones. The concept appears favorable because the elimination of the long guidelines improves potential line management, reducing the chance of line entanglement.

Nevertheless, when the guidelineless concept is implemented for ultra-deepwater zones, the long distance between the surface vessel and the seabed could be a challenging factor for the operator to perform the final adjustment of the object over the landing point.

The guidelineless concept can be further developed by installing thruster systems on the RT to do final positioning of the WCP rather than controlling the surface vessel.

3.1 Main Missions of Deployment and Retrieval of the WCP

The main operations involved with the deployment and retrieval of the RLWI package can be divided in four operations;

1. The deployment of the RT and WCP to XT
2. The retrieval of the RT back to the surface vessel
3. The deployment of the RT to WCP
4. The retrieval of the RT and WCP back to the surface vessel

The following section will describe the operation #1, the deployment of the RT and WCP to XT. This operation will be executed in an ultra-deepwater zone where the effect of waves to the RT and WCP module can be negligible. The force acting on the module will be lesser compared to operations in shallow water zones; however, the remote operations to position the WCP on the XT re-entry hub can pose as a main challenge.

3.2 The Deployment of the RT and WCP to XT

There are at least two possible deployment operations of the WCP assembly with the new guidelineless RT concept. Of the two approaches to deploy the WCP, the first is an existing method, as the WCP is connected with UTH before the deployment. An alternative method is to deploy the WCP without UTH and after the WCP lands onto the XT re-entry hub, the UTH is connected with WCP using ROV assistance.

The Deployment of the RT and WCP with UTH

The WCP is connected with the UTH before it is deployed into sea water. During deployment, there are three lines in sea water; steel cable attached with the RT and two umbilicals (control and chemical umbilicals) connected with the UTH.

To prevent line entanglement, the thruster, navigation and autopilot system on the RT must be able to orient the heading of the WCP within a rotation limit.

The navigation system and communication system are needed to support the RT system. The communication signal can be an acoustic link and bypassed to the UTH. The energy supply for the RT systems can be designed as a hybrid system.

After the surface vessel is propelled to move the WCP assembly in a close vicinity to the XT, the final adjustment of the WCP position is executed.

Since stacking the WCP on the XT re-entry hub is a critical operation, the operator takes control of all thrusters to manually adjust the heading and position of the WCP module in the correct alignment.

After the landing of the WCP is confirmed, the RT is slowly moved away from the XT to prevent potential entanglement between the steel cable of RT and umbilical lines of UTH.

The Deployment of the RT and WCP without UTH

The RT and WCP module is lowered to the sea with only one steel cable line. After the WCP is stacked on the XT, UTH with umbilical lines is connected to WCP. This method allows the RT and WCP module rotate freely. To reduce the torture effect inside the steel cable, a swivel shackle can possibly be used to hang the RT, rather than a traditional shackle.

After the surface vessel is propelled to move the WCP assembly in a close vicinity to the XT, the final adjustment of the WCP position is executed.

Since stacking the WCP on the XT re-entry hub is a critical operation, the operator takes control all thrusters to manually adjust the heading and position of the WCP module in the correct alignment.

The navigation system and communication system are needed to support the RT system. All systems on the RT are energized from the battery packs on the RT.

Without an umbilical line, after the landing of the WCP is confirmed, the RT can be retrieved back to the surface vessel quickly.

Methods	Advantages	Disadvantages
The Deployment of the RT and WCP with UTH	-Large energy sources. -Electrical signal transmitted via UTH and acoustic link	-Requirement of an autopilot system -Additional drag from the two umbilicals. -Potential line entanglement.
The Deployment of the RT and WCP without UTH	-Less drag force -Less energy consumption -Less complex control system -Allow of rotation during deployment	-Energy constraint. -ROV operations to connect the UTH

Table 3-1 Comparisons of deployment methods.

The deployment of the RT and WCP without UTH is more favorable because the thrusters are not often operated for controlling the heading of the WCP while running WCP down to the XT. In essence, the deployment can eliminate drag force from the two umbilical lines and the chance of the line entanglement.

3.3 The Retrieval of the RT and WCP back to the Surface Vessel

When the RLWI is stacked down, the WCP RT is deployed to retrieve the WCP back to the surface vessel though the moon pool by using the guide frame on the vessel. The required systems in the operation are similar to the deployment of the RT and WCP to the XT as described previously. However, the thruster system is used to orientate the position of the RT and WCP in the correct position in accordance with the guide frame.

3.4 System Configuration of the New WCP RT

The design basis is to make a guidelineless RT as simple as possible while meeting functional requirements for the operations. Design considerations are briefly described as follows:

- The maximum operational limitation of the WCP RT is around 3,000 m water depths.
- Environmental loads, e.g. waves and sea current, can cause the deviation of heading and position of the RT and WCP module.
- The thruster system must be able to generate sufficient thrust to adjust the rotation and translation of the RT and WCP module during operations.
- By controlling rotating speed of thrusters, the RT and WCP module travel with a constant velocity.
- The navigation system and sensors on the RT are used to provide data and guidance for position control system of the RT and WCP module.
- The control system for thruster system must support automatic and manual modes.
- The energy should be supplied from battery packs stored on the RT. Depending on the operation; it can also be supplied from an electrical wire or a hybrid system.
- Hydroacoustic communication appears practical to minimize the drag force.

3.5 Environmental Considerations

The following considerations are overview of design considerations of the RT and WCP module in deepwater zones:

- Hydrodynamic forces: related to propulsive and maneuvering system
- Hydrostatic pressure: related to pressure-resisting structures, electrical and mechanical systems exposed to pressure
- Temperature: related to sensitivity of materials at low temperature and acoustic navigation and communications. A large temperature difference between the operating temperature and the local air temperature could affect mechanical thermal expression which can shatter the seal, resulting ingress of sea water into electrical circuits.
- Density of water: related to acoustic navigation and communications
- Salinity: related to structure corrosion and acoustic navigation and communications

4 Conceptual Design for the WCP RT

The conceptual design is the first design stage that identifies all possible methods based on the operational requirements. This stage provides a review of the state-of-the-art applications, which are based on well proven principles, systems and equipment useful for making decisions in the next design stages.

The simplicity, modularization and redundancy are the main design basis for the new WCP RT. The following systems are essential for the WCP RT to perform the adjustment of the WCP assembly; thruster system, control system, communication system, navigation system and sensors, and energy sources.

4.1 Thruster System

The design of the thruster system takes priority over other components, because it is an essential transmission system to transmit the power to the water, usually a thrust force. The thruster is used to control translation and rotation of the RT and WCP module. Moreover, the main energy consumption of the RT system is the thruster system. Figure 4-1 represents a common propulsive system. The controller controls the revolution speed of the motor, shaft and propeller to achieve a desired thrust.

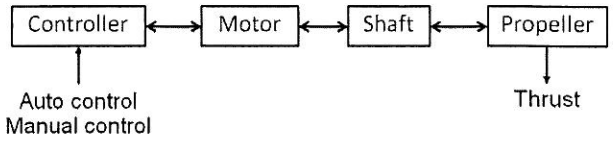

Figure 4-1 Block diagram of propulsion system.

The design concept of the thruster system is further described in chapter 5.

4.2 Control System

Control systems basically consist of: input signal, controller, system and output. After the controller has received the input signal, it can command the system to function in order to achieve the correct output. Two main control systems are needed for controlling the motions of the RT and WCP module:

- Automatic control system (Autopilot control) can help to guide and control the orientation and position of the WCP module in set paths. The control system need to be pre-programmed based on the mission. To adjust rotations and positions of the RT and WCP module in sea water, the data from navigation system and sensors is transmitted to controller and calculated to control the thruster system.
- Manual control system is used to support the operation by sending the control input from the operator through user interfaces (e.g. Joystick). It can be a backup system when the automatic control system has a faulty function.

There are two main principles used in control systems: an open-loop controller and a closed-loop controller.

The open-loop controller of systems is not able to compensate for any unexpected condition because no output is fed back to the controller. It can initially control the system to meet the desired output but it cannot guarantee that the output is still correct afterwards.

A closed-loop controller or feedback controller can improve the accuracy of an open-loop system with a feedback loop that can change the input of the system. There are two types of feedback control systems: positive feedback controller and negative feedback controller see figure 4-2.

Positive feedback controller: The output from a positive feedback controller has of divergent behavior; the system tends to reinforce or reduce its output developed over a period of time.

Negative feedback controller: The output of the system is measured by sensors and is fed back to the controller. The controller is able to determine the error of the system between the measured output and the reference to dynamically compensate for system disturbances such as terrain, wind speed or wind direction. This also rectifies the error caused by internal failures e.g. losses inside a system.

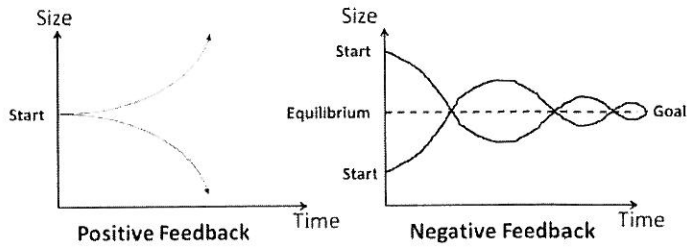

Figure 4-2 Positive and negative feedback control loop.

4.2.1 Design of the Autopilot

This part describes a fundamental control system of autopilot system for controlling the orientation and direction of the RT. The control system used in this design is called a closed-loop controller. The following sequences, for example, describe a feedback control system that can be used for maintaining the heading of the RT, see figure 4-3:

1. After the mission is set at the controller, navigation system and sensors will detect the deviation and feed the signal back to the control processor.
2. The controller manipulates the input data to measure the difference between the reference and the measured output under the system. The controller uses the measured error to adjust the system inputs to the system.
3. Thruster system is triggered to compensate the rotational deviation. To save energy, the controller will commence the thruster system when the rotational degree of the running tool is over the pre-set margin.
4. The thruster system is activated to adjust the orientation of the running tool.
5. As the thrusters are operated based on the input data, the running tool rotate back toward its original direction.

6. The controller removes the command when the position sensors on the RT detects that the orientation is correct again.

The computer program calculates the required steering and thruster output of each thruster using the information fed from several sensors such waves drag, current drag, location of thrusters and gyrocompass. Feedback control systems can be divided into two different types; PID control and model-based control.

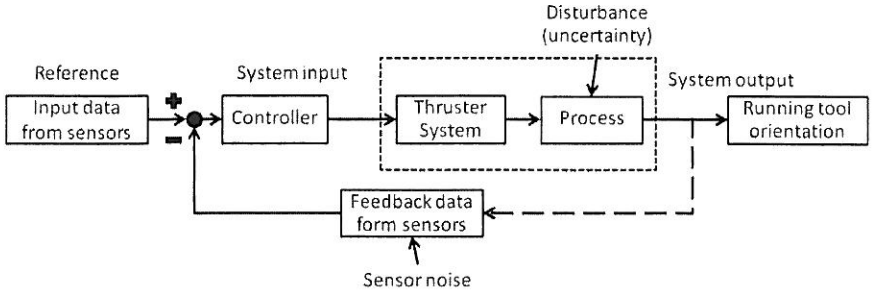

Figure 4-3 Feedback block diagram for controlling the running tool orientation

4.2.2 PID controller

The Proportional Integral Derivative (PID) control technique is probably the most popular choice in feedback control design because of the relative ease of implementation.

The system errors, 'e', is the different values between the input and one output variable, i.e. e(t) = r(t)-y(t). The error signals are manipulated by the proportional, integral, derivative blocks. The desired closed-loop controller can be obtained adjusting the gains in the three branches (K_P, K_i and K_d) of the PID function. The results of all three branches are added together in the summation block before they are transmitted to the process block, see figure 4-4.

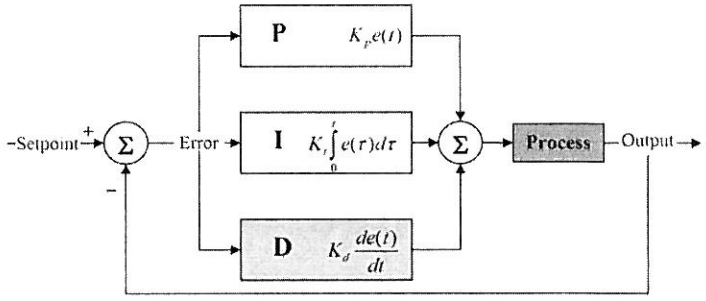

Figure 4-4 Block diagram of a PID controller[8].

Where

K_P	=	proportional gain
K_I	=	integral gain
K_D	=	derivative gain

The characteristics of a control system for the RT should be of low output error and low overshooting with a quick response. The K_P of PDI should be optimized to reduce most error and the K_i value should be tuned at around 1 to prevent overshooting. The K_d should be set as low as possible to provide a quick response; however, when using the small K_d, the effect of noise that can interrupt the system should be evaluated.

Using only PID controllers may not be sufficient to secure complex positioning systems. Hence, a mathematical modeling of the vehicle is preferably used to provide controllers more hydrodynamic and other data concerning the vehicle characteristics such as mass and drag.

4.2.3 Model-based control

A transfer function is a mathematical model used to represent input and output variable of the system. Mathematical models are derived by Laplace transformation.

$$H(s) = \frac{output}{input} \qquad \textbf{4-1}$$

For heading control, the 1st-order Nomoto's model is the most popular model for vessel design due to the simplicity and accuracy. The models can be applied to control the rotation of the WCP by considering yaw rate, r and direction of thrust, δ. The time domain differential equation of the 1st-order Nomoto's model is:

$$\dot{r}T + r = K\delta \qquad \textbf{4-1}$$

Where

r	=	angular velocity [rad/s]
$\dot{r}$	=	angular acceleration [rad/s^2]
T	=	time constant [s]
K	=	process gain constant [1/s]

The application of Laplace transformation of the 1st-order Nomoto's model can be expressed such that[9]:

$$H(s) = \frac{r}{\delta}(s) = \frac{K}{(1+Ts)} \qquad \textbf{4-2}$$

The mathematical models of the RT and WCP module are further described in chapter 7. A theory and table of Laplace transforms are widely available in many mathematical literatures. Further control theories regarding Model-based control and PID control in maneuvering for marine applications can be found in [9-13].

4.3 Communication System

The communication system is aimed to transfer data back and forth between the RT system and the operator on the surface vessel. The data, including control system and navigation system, are necessary for the thruster system to adjust the motions of the RT and WCP

module. Main considerations regarding communication are bandwidth and maximum range as well as speed of transmission.

The communication signals between the RT and the surface vessel can remotely be transmitted via a fiber inside an umbilical line or acoustic communication though sea water. The hydroacoustic link is seemingly more suitable solution for ultra deep water operations because transmitting acoustic signal does not require a line in the sea water.

A typical acoustic single (pulse) is transmitted from the transducer to the seabed transponder with a speed of approximately 1,500 m/s through the sea water[14]. At water depth of 3,000 m., the reception at transmitter on the surface vessel can receive signal 4 seconds after transmission, as shown in figure 4-5. At the same depth, after the operator send a signal, it will take at least 2 seconds to transmit the signal through the sea water. Further information regarding acoustic communication can be found in Crocker(1998) [15] and Elson (2004) [16].

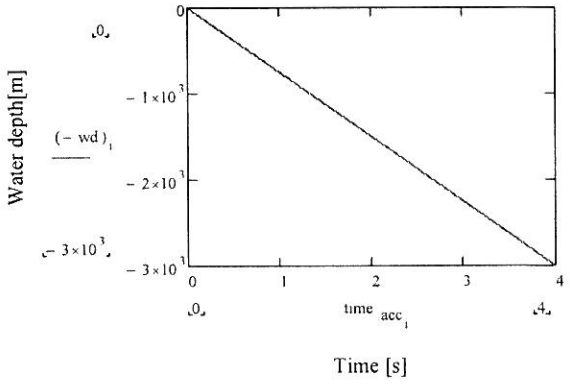

Figure 4-5 Transmitting time calculation.

Summary

The lack of real-time transmission can be troublesome for controlling the thrusters on the RT. The inefficient communication system can become serious problem as the RT performs operations in greater depth. There are at least three alternatives for improving the communication system;

1. The communication signals are simply transmitted through a fiber line.
2. The supporting ROV is equipped with an acoustic receiver to acquire the acoustic signals from the transmitter. The signals can be bypassed through a fiber line in ROV umbilical whereby the signals can travel faster than though sea water.
3. The acoustic signals can be transmitted through the steel cable hanging from the surface vessel.

Considering the third method, it is quite difficult to ensure that the signals are not disturbed from environmental noise on the vessel. The 1st and 2nd methods are more applicable for the operation; however, it is not decisive to select either 1st or 2nd method. The 1st method

can provide fast communication but the wire in the 1st method will cause additional drag to the RT and WCP system. An umbilical can be directly connected to the RT system by using ROV when the WCP is close to the XT to provide communication path and electricity between the RT and the surface vessel for the critical operation. Connecting the wire could be, however, challenging operations while maneuvering the WCP and ROV concurrently.

The 2nd method requires the modification of ROV umbilical as well as extra time to convert signals between acoustic signals and electrical signals from ROV to the surface vessel. Before finalizing the system, a more helpful tool is computer simulations that could help in the analysis the responses of the control system.

4.4 Navigation System

The navigation system is used to provide the operator the data of the RT and WCP module e.g. locations, orientations and speeds of the module. ROVs are regularly used to monitor and locate the WCP during RLWI deployment operations. The loss of ROV visibility can be, however, happened due to marine debris or darkness. The operator can always achieve accurate and nearly instant data from advanced navigation technologies. The widely used navigation system for underwater vehicles is called hydroacoustic positioning.

4.4.1 Hydroacoustic Positioning

The hydroacoustic link functions as an acoustic tether that locates the vehicles position. The acoustic positioning basis consists of a transponder (receivers) and a transducer (transmitter). The transponder immediately responds the pulse, which can be configured to provide a depth telemetry signal. As the velocity of sound through water is known, the positional algorithms can calculate the correct depth and the position of the object. The main principles of hydroacoustic positioning used in marine operations are SSBL, SBL and LBL.

Super Short Base Line (SSBL)

The SSBL system consists of a transponder (at a seabed reference or a moving object) and a multi-element transducer (attached at the vehicle) to provide three-dimensional transponder positions relative to the vehicle, see figure 4-6. As both the range and angle to an acoustic transponder are measured, the transducer position in the space referred to the transponder is known.

Short Base Line (SBL)

The principles of the SBL system are similar with that of the SSBL system, except that the calculation of the SBL system is taken from an array of at least three transponders mounted transducers, see figure 4-6.

Long Base Line (LBL)

The LBL system requires a subsea transponder array to give sufficient measurement data for calculating the location of the transducer mounted with the object because the calculation

is based on only range measurements[17], see figure 4-6. The LBL system requires more time for deployment and calibration of subsea transponder array. All distances between the transponders and the relative depths must be measured. The accuracy of the LBL system is depending on the geometry of the transponder array and the location of the vessel in the array, the actual S/N, and the errors in sound velocity [14].

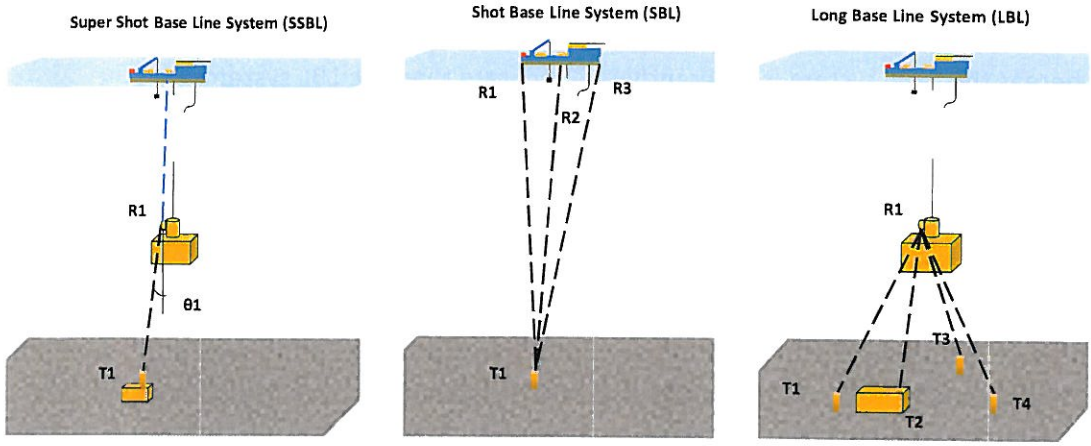

Figure 4-6 SSBL (left), SBL (middle) and LBL (right).

Multiple User Long Base Line (MULBL)

The MULBL systems can allow existing LBL systems to operate with one common transponder below the sea surface. The MULBL systems can be converted from LBL setting a new software mode. As a result, the MULBL can reduce a number of transponders needed for the field and can avoid collusions of transponder frequency caused by multiple transponders working in close area. Further information and positioning sequences can be found in [14, 18].

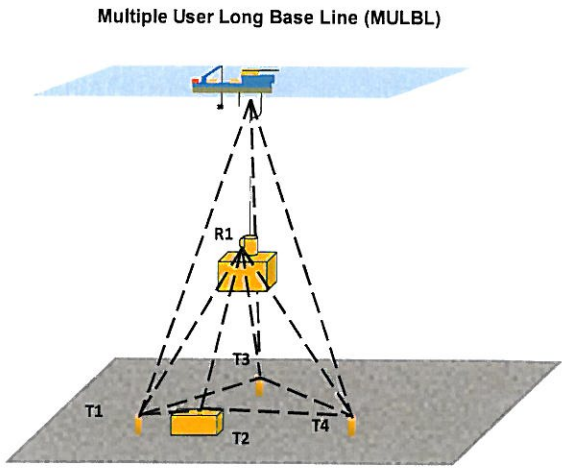

Figure 4-7 Multiple User Long Base Line (MULBL).

Summary

The commonly used navigation systems for underwater vehicles are SSBL and LBL. The SSBL system accuracy (standard deviation) is approximately 0.2 percent of slant range, and the update time increase 1 second for every 700 m extra depth while the LBL system accuracy is within 1 meter regardless of depth and its update time is from 2.5 seconds to 6 seconds dependant on water depth[19]. As can be seen in table 4-1, at 3,000 m water depths, the LBL system is more suitable for the missions and works well in deep water operations whereas the SSBL system is inherently less accurate than the LBL system.

Systems	System accuracy(standard deviation) [m]	Update time [s]
SSBL	6	4
LBL	1	2.5-6

Table 4-1 Comparisons of hydroacoustic positioning systems.

Three or more DP systems are normally utilized to support a surface vessel, a support vessel and the new WCP RT. According to the MULBL advantage over the LBL system, it is more practical to replace the LBL with the MULBL concept for the operation to reduce transponders employed in the field.

4.4.2 Navigation Aid System

Inertial Navigation System (INS)

The INS is a measurement instrument attached on the moving object to track its position, attitude and velocity without the need for external references. The INS includes several sensors such as accelerometers, three-axis gyroscopes and other motion-sensing. Nonetheless, there would always be errors occurring in each measurement. The errors can grow with progression of time because each type of sensors work based on the integration of signals over time.

Hydroacoustic Aided Inertial Navigation (HAIN)

With advancements in hydroacoustic link, Hydroacoustic Aided Inertial Navigation (HAIN) system is implemented to combine advantages of acoustic and AIN. The Aided Inertial Navigation (AIN) is a system that integrates the inertial navigation system (INS) with an external (aiding) sensor to improve navigation accuracy of a vehicle reducing a drift of the INS over time.

Having been calculated from INS (navigation equations), the attitude, velocity and position of the object are corrected by the Kalman filter, see figure 4-8. The Kalman filter can compare the measured data with aiding sensor measurements e.g. a Doppler Velocity Log (DVL), pressure sensor and Differential Global Positioning System (DGPS) [20].

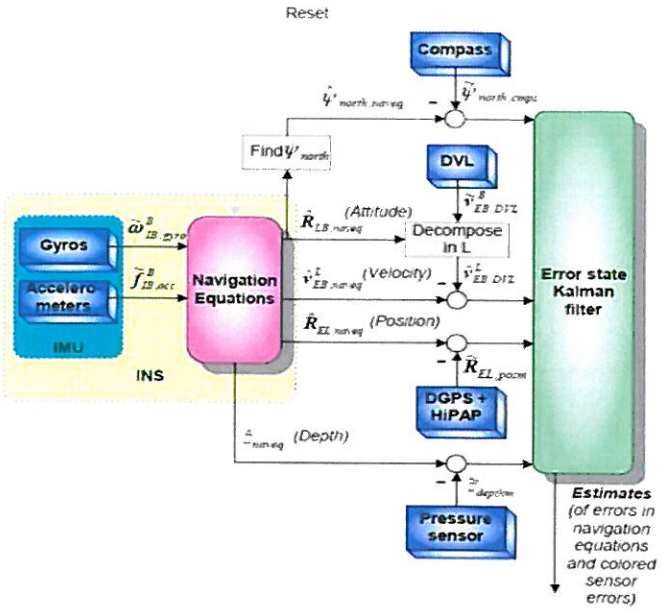

Figure 4-8 HAIN processing - block diagram [21].

HAIN can reduce the errors and noise problems in the calculation of the navigation equations over time. Compared to the use of INS system alone, the combination of the HAIN system and the INS will improve accuracy and performance of the navigation system.

4.4.3 Acoustic Performance and Operational Range

There are many factors that could limit accuracy and range of the system. The common factors involved reliability of a navigation system are[14]:

- Transmitted power
- Transmission loss
- Transducer configuration
- Directivity and bandwidth of receiver
- Environmental noise
- Requirements to signal/noise ratio for reliable signal detection
- Ray-bending and reflected signals

The accuracy of the system depends on the signal-to-noise (S/N) ratio, at the receiving transducer. The signal-to-noise (S/N) ratio is the strength of signal relative to the background noise. The higher the S/N ratio, the lower the interruption of noise.

A main concern of hydroacoustic links is noise disturbance from nearby thrusters and surrounding objects (e.g. acoustic interference from other DP systems). For all noise sources, noise level is inversely proportional to frequency[22]. A rule of thumb - noise level drops approximately 10 dB per decade with increasing frequency. Typical navigation frequencies are from 20-30 kHz and at this range, ambient noise level is very low[14].

Figure 4-9 shows that the higher the frequency, the higher is the accuracy of the system.

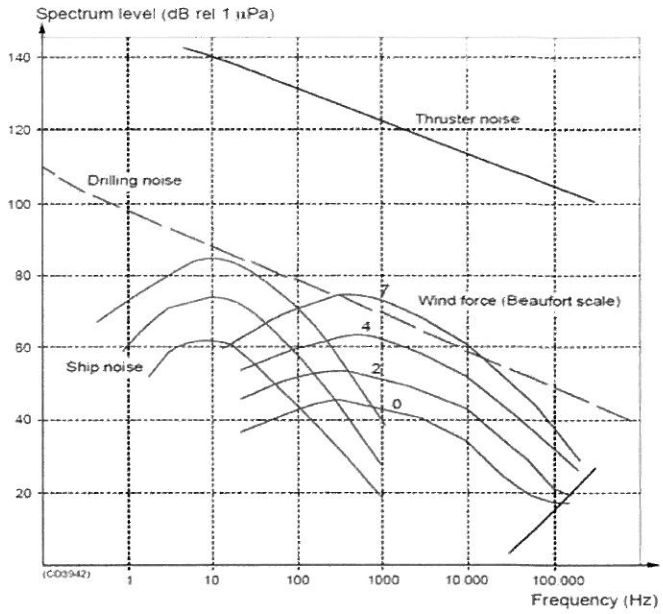

Figure 4-9 Environmental acoustic noise level [14].

Noise from thruster can change depending on the thrusters and the direction of the thruster. In general, thrusters with variable RPM/fixed pitch generates less noise than thrusters with fixed RPM/variable pitch and running a thruster on low RPM/high pitch generates normally less noise than a thruster on high RPM/low pitch[22].

Furthermore, the transducers should be mounted away from any thrusters and parts that may introduce air into the water surrounding the acoustic elements. Air can disrupt the calculation of the time delay between the transducer and transponder, causing the error for navigation system.

An error in the assumed sound speed profile can cause a significant mistake for navigation system. To enhance accuracy of the system, a correct entry of the velocity of sound in sea water is needed because the velocity of sound is an increasing function of water temperature, pressure and salinity.

The loss of communication system can become serious problem as the RT performs operations in greater depth. Hence the operational range of the communication system should cover the operational area. According to LinkQuest, the working range of the acoustic signal can exceed 3,000 meters [23]. Further information regarding acoustic can be found in Crocker(1998) [15] and Elson (2004) [16].

4.5 Energy System

The energy sources are required to supply the RT system including several systems such as thruster system, control system, sensors and navigation system. The energy can be transferred from the surface vessel directly via an electrical wire, from batteries packed on the RT or a hybrid system.

Surface Source

This method requires an electrical wire connected between the surface vessel and the RT system. The diameter of the wire increases according to the requirement of the power that need to supply the RT system.

The advantage of this method is that the RT system can be supplied with unlimited energy; however, its main drawback is that the additional thruster power is required to overcome drag from the electrical wire, and the chance of twist lines can also rise.

Battery System

Batteries are the most often used energy system in several underwater vehicles e.g. AUVs. and ROVs. The advent of battery technology can provide high energy density to meet many applications.

Hybrid System

The advantages of the surface source and battery system can be combined using the concept of hybrid system. This design can eliminate the electrical wire hung from the surface vessel while providing large energy supply to the RT system.

As the UTH is connected with the WCP, the electrical energy from the surface vessel can be transferred to the WCP and it can also supply the RT systems via an electrical wire connected between the RT and WCP system. After the WCP lands on the XT, the RT systems will be energized from the battery packs on the RT itself.

Comparisons of Energy Systems

Table 4-2 compares the advantages and disadvantages between the use of surface source, battery system and hybrid system.

Systems	Advantages	Disadvantages
Surface source	-Large energy sources. -Battery packs used as a redundancy system. -Able to combine electricity wire with communication line as a byproduct.	-Potential downtime due to line entanglement. -Additional drag from an electrical wire. -Requirements of supporting systems.
Battery system	-No drag force from a wire. -Minimal potential downtime due to line entanglement. -No requirements of supporting system e.g. winch.	-Requirements of some room on the RT. -Limited energy sources.
Hybrid System	-Similar to the surface source. -Less drag forces and deployed line then the surface source.	-Similar to the surface source. -Additional drag from an UTH. -Require a system to supply energy from WCP.

Table 4-2 Comparisons of energy systems.

To minimize drag forces and the presence of lines underwater, the battery system is chosen. There are two main types of battery systems; primary batteries and secondary batteries.

Primary batteries are non-rechargeable which can only undergo a single cycle, whereas secondary batteries are electrically rechargeable.

Primary Batteries

Primary batteries are either dispensable (one-time use) or ones which require mechanical replacement of the active material consumed during operation. The types of primary batteries can be zinc carbon batteries, alkaline batteries, button cell batteries, and lithium batteries.

Secondary Batteries

The energy density of secondary batteries is typically lower than primary batteries. The most common types of secondary batteries are nickel cadmium (Ni-Cd), sealed lead-acid (Pb), nickel metal hydride (Ni-MH), and lithium ion (Li-ion). Interestingly, another type of batteries is silver-zinc battery that has been developed to offer high performance, clean technology and safety battery[24].

Summary

Secondary batteries can provide more economical then primary ones. Even if the secondary batteries are expensive, they save money in the long run because of rechargeable capability.

To compare each type of batteries, the term energy density, as watt-hours per kilogram (Wh/kg) and energy/size, is used to compare each type of energy sources. A comparison of the different secondary batteries is shown in the figure 4-10.

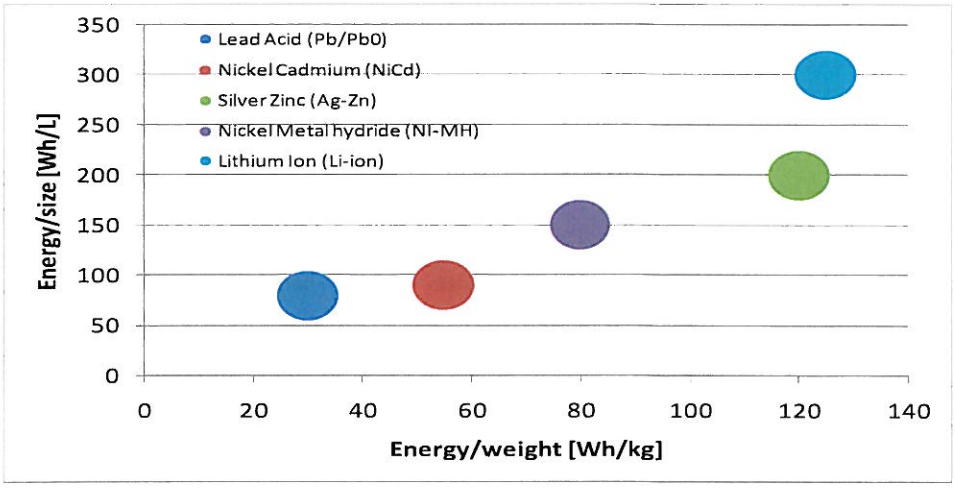

Figure 4-10 Characteristics of secondary batteries.

As can be seen, the properties of the Li-ion battery are superior among others, so the Li-ion battery is the chosen battery for the RT system. Moreover, Li-ion batteries have been proved using as primary and backup resources in many subsea applications e.g. XTs or subsea systems.

Additionally, the selection of the battery should be considered with the following factors:

- Reliability and safety
- Forbidden and hazardous chemical sustains
- Range of operating temperature
- Battery cycle life
- Cost per energy
- Maintenance requirement

For offshore works, high reliability and safety can be primary factors that can outweigh cost and other factors. The higher energy batteries may have a potential of higher violent explosion under certain circumstances.

5 Design of the Thruster System

5.1 Design Concepts of Thruster Placements

Maneuvering the RT and WCP module can be achieved by varying thruster output e.g. directions and RPM of propellers. The thruster system must have the ability to generate thrust to move the RT and WCP module in the full 360 degrees as environmental forces are omnidirectional. There are numerous placement options for thrusters on the RT to allow varying degrees of maneuverability. There are three of the more feasible designs described.

Four Fixed Thrusters

This design is similar to the placement of ROVs thrusters for horizontal translation. The movement and rotation of the RT and WCP module is controlled using a computer system to control speed and direction of the propellers. Each thruster can be independently powered in either positive or negative direction, resulting in forward or backward thrust. The speed of each thruster motor can be also adjustable to match with mission requirements. If one thruster fails or even two thrusters fail, other thrusters can generate thrust for controlling the WCP motion with careful handling.

The main disadvantage of this system is inefficient thrust generated especially in translation. This is due to the fact that vectors of thrust are against each other.

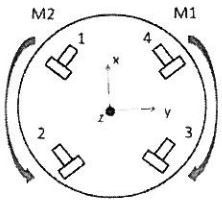

Translational and rotational moment	Thruster
x-axis	(1,4) , (2,3)
y-axis	(3,4*) , (2*,1)
M1	1,2,3*,4*
M2	1*,2*,3,4

(*) indicates reverse thruster forces

Figure 5-1 Four-fixed-thruster design on the RT.

Three Fixed Thrusters

The three-fixed-thruster system is designed to reduce one thruster unit from the previous design, without degrading the manipulability of the RT system. Like the four-fixed-thruster design, the movement and rotation of the RT and WCP module is controlled by managing speed and direction of each thruster. Although one thruster fails, controlling another two thrusters carefully can still be possible to adjust the WCP position and rotation.

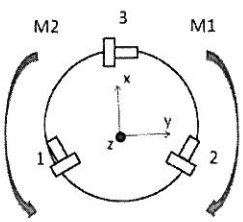

Translational and rotational moment	Thruster
x-axis	1,2
y-axis	1*,2,3
M1	(1,2*,3)
M2	(1*,2,3*)

(*) indicates reverse thruster forces

Figure 5-2 Three-fixed-thruster design on the RT.

Two Steerable Thrusters

This concept is distinguished from the two previous designs in that it can provide higher degrees of maneuverability with fewer thrusters. This concept is initiated from azimuth thrusters used in highly maneuverable tugs or large ships.

Each thruster is rotational in any direction around a vertical axis individually by using a servo motor. The servo motors provide the thruster system the ability to direct the thrust in all directions. This design requires less power and complexity both mechanically and electronically. Nevertheless, it needs additional systems e.g. control systems, electrical supply, and rotating mechanisms for the servo system to rotate the thruster units. Each wake direction of the thruster system is dependent on the accuracy of the servo system.

Since there are two thruster systems, all equipment and control systems for thruster motors and servos are so critical. Although there is a thruster failure, it can be possible to control the WCP with only one thruster system if it can produce enough thrust force.

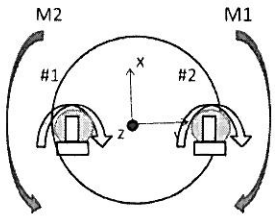

Translational and rotational moment	Direction of thrust wake	
	#1	#2
x-axis	-x axis	-x axis
y-axis	-y axis	-y axis
M1	-x axis	x axis
M2	x axis	-x axis

Figure 5-3 Two-steerable-thruster design on the RT.

Comparison of Thruster Designs

A comparison list of the main advantages and disadvantages of the three concept designs is presented in table 5-1.

Design aspects	Four Fixed Thrusters	Three Fixed Thrusters	Two Steerable Thrusters
Ease of maintenance	High	High	High
Ease of modification	High	High	High
Manipulability	Moderate	Moderate	High
Redundancy	High	Moderate	Moderate
Space availability	Low	Moderate	High
Efficient thrust for rotation	High	High	High
Efficient thrust for translation	Moderate	Moderate	High
Weight tight	Low	Moderate	Moderate
Summary (total point) (High=1, Moderate=0.5 and Low=0)	5.0	5.5	7.0

Table 5-1 Comparisons of concept designs for the thruster system.

As can be seen from the preceding table, designing the new RT with two steerable thrusters shows more advantageous and feasible when compared to the other designs.

5.2 Thruster Selection

5.2.1 Thruster Motors

Motor controllers are designed to provide thruster both speed and rotational direction. For underwater applications, hydraulic and electric drive systems are commonly used to fulfill the transmission requirements. The efficiency of the thruster system is important factor for the efficient operation of the RT system with battery packs. The inefficient thruster leads to higher energy consumption, which can exhaust energy of the RT system.

Hydraulic Drive

The hydraulic system has multi-conversion stages of mechanical energy from a prime mover to electrical energy to power an electrical motor which drive a hydraulic pump. The pump delivers pressured fluid to hydraulic motor to rotate a propeller shaft. Electrical servo vales are used to control the outlet of thrusts by regulating the fluid flow to each separate unit.

The advantage of the hydraulic drive is that it is a preferred delivery power system for a heavy duty. For the same load application, hydraulic motors are relatively smaller size than electric motors. Large workclass ROVs in the market place are, for example, usually powered by hydraulic system because of the high thrust and power requirement in order to provide stable movements.

Hydraulic systems are, however, inherently inefficient because of conversion losses of energy. The hydraulic systems require devices; hydraulic reservoir and hydraulic pump and associated hoses as well as connectors. The hydraulic system efficiency, a combination of the hydraulic unit's efficiency and the motor efficiency, requires several conversions of energy from electrical to mechanical, from mechanical to fluid and from fluid to mechanical energy. The thrusters may receive only 40% to 60% of the power supplied by the feeder[25].

Electric Drive

Small underwater vehicles, e.g. AUVs, are propelled with electric thrusters due to power constraints and required efficiencies. In essence, electric thrusters can eliminate the need for large HPUs, servo valve manifolds, and other hydraulic systems. This can improve reliability of the thruster system by reducing subsystems. The table 5-2 compares the advantages and disadvantages of hydraulic motor and electric motor for underwater applications.

Drive Systems	Advantages	Disadvantages
Hydraulic motor	-High power and torque	-Low efficiency -Large weight and size -Requirement of a reservoir of hydraulic fluid, a pump and a large motor -Potential of hydraulic fluid leakage
Electric motor	-High efficiency and reliability -Weight tight -Less associated components	-Low power and torque

Table 5-2 Comparisons between hydraulic and electric motors.

The electrical drive is more favorable than the hydraulic drive when considering the system efficiency and space allowance on the RT.

Main Characteristic of AC and DC motors

The selection of AC or DC motor can be partly influenced by the types of primary energy supply. AC motors are desirable when the energy is supplied via a tether from the vessel, whilst DC motors are more favorable when the energy is supplied from batteries. Another factor that needs to be considered is the operational performance of the AC and DC motors.

AC motors

AC motors are very reliable, simple to design/construction and requires low maintenance with a few moving parts (rotor and bearing) [25]. A shortcoming of the AC motor system is its speed control and inefficiency. The speed and direction of AC motors can be controlled by varying the characteristic of the AC waveform, such as frequency, phrase and voltage. As little as 50% to 65% of the originally supplied power could be transferred to the thrusters, after the electrical power and motor controller losses are taken into account [25].

DC motors

DC motors are preferred when energy is supplied from batteries. DC motors can generally produce higher torque and more precise speed than AC motors. The obvious disadvantage of DC motors is the use of commutator bars and brushes, which can require a great deal of maintenance. However, advanced brushless motors can prevent the wear problems and provide more lifetimes than brushed electric motors and starting currents of the brushless electric motors are lower than that of brushed ones[26]. Without electrical switching, brushless motors can also generate lower electrical noise than brushed motors[27]. The efficiency of the motor brushless DC motor can be as high as 95% [25]. Nevertheless, the drawbacks of brushless motors are more complex controllers and expensive than brushed motors.

Compared to the brushless AC motors, the brushless DC motors can normally provide more thrust[28]. Furthermore, the brushless DC motors are suitable to drive the RT because the systems on the RT system are energized from battery packs.

Comparisons of Available Thrusters

The selection of available DC thrusters in the market can be firstly evaluated by comparing bollard pull and thruster efficiency (i.e. the ratio of thrust output to power input). The required thrust is determined based on the advance speed of the module and drag forces. The bollard pull of the candidate thrusters must be greater than the required thrust with a safety factor. The more powerful the thruster system of the RT, the stronger the sea current in which the RT can operate. Hence, the high thruster performance can extend the RLWI operational area. Another main goal is to select thrusters with high thrust to power ratio because the thruster system is the main energy consumer in the RT system.

5.2.2 Propeller Considerations

A propeller is a main part that converts the driving power into a thrust force to control the motion of the RT and WCP module. Critical design parameters of a thruster design are diameter of the propeller and its pitch, whereas other parameters (e.g. hub size, the number of blades and blade thickness etc.) are less influence on the power and torque requirements of the thruster design [29]. A fixed-pitch propeller appears to be the most suitable design for underwater vehicles in terms of simplified design while the others are used in marine vessels. Thrusters are often mounted with a ducted shroud or a kort nozzle to favorably increase the efficiency of the thrusters.

In addition, the rotation of the propellers should be considered to prevent a torque steering effect, a rolling of the module in the direction of propeller rotation. When two or more thrusters operating at the same plane of motion, there will be a counter-reaction to this turning moment [30], see figure 5-4. With the counter rotation, the WCP will have difficulty landing on the XT re-entry hub therefore the propeller must rotate in the opposite direction against another propeller to counteract the rotation of the module.

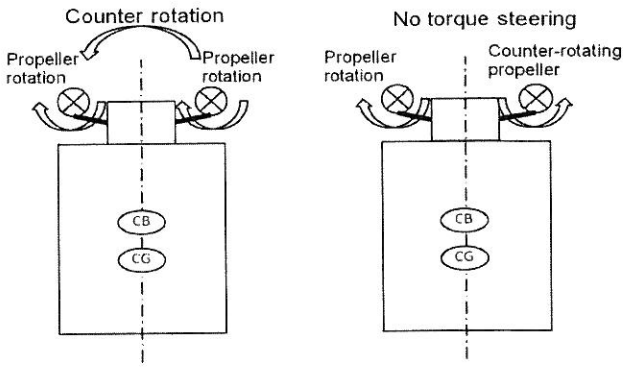

Figure 5-4 Thruster rotational effect upon vehicle.

5.3 Additional Systems

DC Motor Speed Controller

The simplest way to control the rotational speed of a DC motor is to regulate its supplied voltage. The higher voltage the DC motor is supplied, the higher speed the DC motor can rotate. However, this method can cause power loss on control circuit.

An alternative method so-called pulse width modulation method (PWM) is preferred to control DC motor for many applications. A PWM generator is important to generate the correct frequency and timing of PWM signals transmitted to the speed controller. The speed controller controls the motor speed by turning on and off the operating power to the motor. More information about PWM controlling can be found in [31, 32]

DC to DC Converter

In order to supply enough power to thruster motors, a voltage converter (or DC to DC converter) can be used to convert a direct current of battery packs from one DC level to other DC levels. One of DC to DC converter theories is Split-Pi technology which can boost the DC level with high efficiency over 97%[33].

Power monitor

The power monitor is used to ensure that adequate power is supplied to the thrusters. It is essential equipment as a low voltage will result in the unexpected thrust characteristics from the motors.

6 Forces and Moments Affecting the RT and WCP Module

When the RT and WCP module is submerged, they can be exposed to many forces causing rotation and translation. These forces can be caused by waves, ocean currents, torsion inside steel cable, or impact from marine animals. In this thesis, forces and moments are assumed to be induced by waves and ocean current disregarding other sources.

6.1 Waves

Linear wave theory is the simplest wave theory that is used to give a rough approximation of the characteristics of waves. Three parameters needed in describing wave theory are wave period (T), wave height (H) and water depth (d).

The velocity potential Ø= f(x,z,t) of a wave component is:

$$\emptyset\ (\boldsymbol{x}, \boldsymbol{z}, \boldsymbol{t}) = \left(\frac{\pi H}{kT}\right) \cdot \frac{cosh\ [k(d+z)]}{sinh\ (kd)} \cdot \boldsymbol{sin}\ (\boldsymbol{kx} - \boldsymbol{\omega t}) \qquad \textbf{6-1}$$

Where

k	=	wave number [m^{-1}]
x	=	distance of propagation [m]
z	=	vertical distance from mean free surface (positive upward) [m]

The horizontal velocity is given by: $u = \frac{\partial \emptyset}{\partial x}$

$$\boldsymbol{u} = \left(\frac{\pi H}{T}\right) \cdot \frac{cosh\ [k(d+z)]}{sinh\ (kd)} \cdot \boldsymbol{cos}\ (\boldsymbol{kx} - \boldsymbol{\omega t}) \qquad \textbf{6-2}$$

The horizontal acceleration is given by: $\dot{u} = \frac{\partial \mathrm{u}}{\partial t}$

$$\dot{\boldsymbol{u}} = \left(\frac{2\pi^2 H}{T^2}\right) \cdot \frac{cosh\ [k(d+z)]}{sinh\ (kd)} \cdot \boldsymbol{sin}\ (\boldsymbol{kx} - \boldsymbol{\omega t}) \qquad \textbf{6-3}$$

The maximum horizontal velocity for deep water is:

$$\boldsymbol{u} = \left(\frac{\pi H}{T}\right) \cdot \boldsymbol{e}^{kz} \qquad \textbf{6-4}$$

The maximum horizontal acceleration for deep water is:

$$\dot{\boldsymbol{u}} = \left(\frac{2\pi^2 H}{T^2}\right) \cdot \boldsymbol{e}^{kz} \qquad \textbf{6-5}$$

The equation 6-5 expresses that the magnitudes of water velocity and acceleration decrease with increasing water depth. In deepwater zones, the horizontal velocity and acceleration of deepwater waves can be nearly zero,($e^{kz} \approx 0$).

6.2 Ocean Currents

Ocean currents are driven by wind generated currents, tail currents, circulation currents, and loop as well as eddy currents. It is difficult to provide a correct prediction of current

profiles because currents, varying in both space and time, are dependent on many parameters such as water depth, topography and local oceanographic climates.

The deeper water the water in the ocean, the lower the current is. The deepwater currents can be simply assumed to be less than or equal to 0.5 knots, (0.255 m/s)[25].

Field measurements are recommended to provide more information on specific sea currents. For most applications, current velocity vectors (magnitude and direction) are assumed to be dependent on only depth. DNV-RP-C205 (2007) represents simple models for design current profiles, if field measurements are not available[34].

6.3 Hydrostatics

Hydrostatic pressure is considered whether equipment is capable of withstanding pressure with increasing water depth. A range of working depths defines the strength of material required to counter high pressure. Pressure increases approximately 1 atm per every 10 m of depth. Extreme hydrostatic pressure may cause material facture that leads to structures or mechanical damage. This requires all wetted components and seals must be capable of withstanding high pressure when the module operates in ultra deep waters. The internal pressure of a hydraulic thruster motor must always be over the external pressure, exerted by water at any water depth, to prevent water entering to the motor housing and burn the motor.

Buoyancy

Buoyancy is an upward force that applies to submerged objects. Based on the Archimedes law, the forces are calculated from the displacement volume of the objects and the density of the fluid as the following equation:

$$F_b = \rho \cdot \nabla \cdot g \qquad \textbf{6-6}$$

Where

F_b	=	buoyancy [N]
ρ	=	density of sea water [kg/m^3]
∇	=	volume of the object [m^3]
g	=	acceleration of gravity [m/s^2]

6.4 Hydrodynamics

Hydrodynamic theory is fundamental to explain the relationship between the module motions and the environmental loads. When water particles are moving around a vehicle, hydrodynamic forces can generate various horizontal and vertical loads on the vehicle, including drag forces, added mass forces and lift forces.

Morison's Equation

Morison's equation can be used to estimate hydrodynamic forces on marine structures and vessels. The Morison's equation accounts for drag and inertia forces. The Morison's equation is applicable when the following conditions are satisfied:

- The diameter of the object is smaller than one fifth of wavelength, $D < \frac{\lambda}{5}$. If it is larger, acceleration will vary over the object and defection/reflection must be taken into account.
- The assumption of the fluid flows having a constant acceleration is invalid until regular sinusoidal waves break when $\frac{\mathrm{H}}{\lambda} \geq 0.14$.

The RT and WCP are both satisfied the Morison's condition, see table A-2 in appendix A.

Drag Forces

Drag is a force that opposes the motion of a vehicle through sea water or act in a direction opposite to the velocity of sea water when the vehicle is stationary. Drag forces consists of both skin friction drag (surface drag) and pressure drag (eddy-making drag or vortex shedding). The drag forces of a moving object along its longitudinal axis are calculated using the classic drag equation:

$$F_d = -\frac{1}{2} \cdot C_d \cdot \rho \cdot A \cdot v_r \cdot |v_r| \qquad \textbf{6-7}$$

Where

F_d	=	drag force [N]
C_d	=	non-dimensional drag coefficient
ρ	=	density of sea water [kg/m^3]
A	=	cross-sectional Area perpendicular to the flow [m^2]
v_r	=	relative velocity between the object and fluid [m/s]

The relative velocity,v_r, can be expressed as the relative velocity between the velocity of observed object, v_m , and the maximum horizontal velocity of water particle ,v, i.e. $v_r = v_m - v$. The minus sign indicate the direction of the drag force, for example, when the object is stationary, the v=0 and the drag force will act in the same direction of water particle movement. The drag equation represents nonlinear effect of hydrodynamic forces.

Inertia Forces

Inertia forces are caused when fluid flow over a small object with constant acceleration. The inertia forces are contributed from "Froude-kriloff" and accelerating particles. The Froude-kriloff forces are fluid exciting forces on the object. If a submerged object is removed from water, the pressure against the surface of the "imaginary" object causes forces that are enough to give acceleration to the mass. The forces per unit length are given as:

$$F_{FK} = m \cdot a = \rho \cdot \nabla \cdot a \qquad \textbf{6-8}$$

Where

m	=	mass of the fluid displaced by the object [kg]
ρ	=	density of sea water [kg/m^3]
∇	=	volume of the object [m^3]
a	=	maximum horizontal water particle acceleration [m/s^2]

Another part is the force caused by accelerating particles. When fluid near the real object is dragged along the fluid flow, this will generate some forces. Forssen (1994) suggests that added (virtual) mass, m_a, should be understood as pressure-induced forces and moments due to a forced harmonic motion of the body which are proportional to the acceleration of the body [12].The added mass is required in the accurate calculation of object accelerations. The total mass forces acting on the object are:

$$\boldsymbol{F_i = (m + m_a)a = \left(1 + \frac{m_a}{m}\right)ma = (1 + C_a)ma = C_m \cdot \rho \cdot \nabla \cdot a} \qquad \textbf{6-9}$$

Where

F_i	=	inertia force [N]
m_a	=	added mass [kg]
C_a	=	added mass coefficient
C_m	=	mass coefficient
a	=	fluid acceleration [m/s^2]

The mass coefficient, C_m, is determined by the size and shape of the object. The mass coefficient, C_m, is always greater than or equal to one. A conventional mass coefficient factor, C_m, is normally taken as 2 for an object with a circular cross section.

The total force estimated from Morison's equation for a moving object is a summation of drag and inertia force. It can be written by[34]:

$$\boldsymbol{F_n = -\frac{1}{2} \cdot C_d \cdot \rho \cdot A \cdot v_r \cdot |v_r| + \rho \cdot \nabla \cdot a - \rho \cdot C_a \cdot \nabla \cdot a_r} \qquad \textbf{6-1}$$

Where

F_n	=	total force [N]
v_r	=	$v_m - v$ is the relative velocity between the object and fluid [m/s]
a_r	=	$a_m - a$ is the relative acceleration between the object and fluid [m/s]

The relative acceleration is equal to the acceleration of the module subtracted by the acceleration of the fluid. Since the module travel with a constant velocity, the acceleration of the module becomes zero and the total force can be rewritten as:

$$\boldsymbol{F_n = -\frac{1}{2} \cdot C_d \cdot \rho \cdot A \cdot v_r \cdot |v_r| + \rho \cdot \nabla \cdot a - \rho \cdot C_a \cdot \nabla \cdot (-a)} \qquad \textbf{6-2}$$

$$\boldsymbol{F_n = -\frac{1}{2} \cdot C_d \cdot \rho \cdot A \cdot v_r \cdot |v_r| + \rho \cdot \nabla \cdot a \cdot (1 + C_a)} \qquad \textbf{6-3}$$

Force regimes, shown in figure 6-1, can be used to specify dominating wave forces in different conditions for the calculation of forces on the module when using Morison's equation.

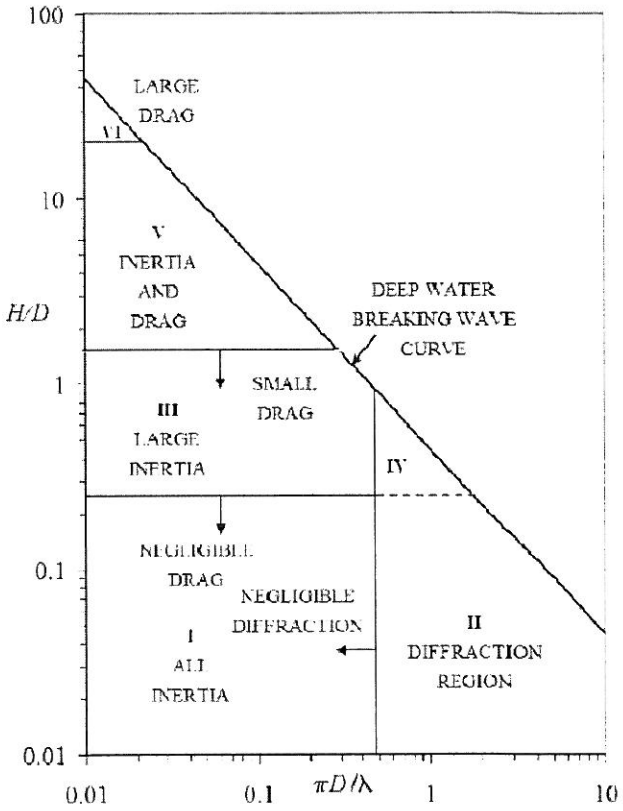

Figure 6-1 Different wave force regimes [34].

According to the values of the RT and WCP module in table A-3 appendix A, the RT and WCP are dominated by inertia and drag terms while the steel cable is governed by drag term.

Lift Forces

As the water particles flow across the submerged object, lift forces can be developed. For the RT and WCP module, the lift forces are assumed to be negligible because a velocity of water particle is low and the RT and WCP module are not streamlined to create the significant lift forces.

6.5 Moments

As descried previously, if fluid flow though any object, there will be forces that can cause the object move and rotate. Assumptions regarding uniform currents in deepwater and the projected areas of the RT and WCP module are established in appendix C.

6.6 Physical Pendulum

Assuming that the RT and WCP module hanging from a stationary point are subjected to waves, they could oscillate in a manner similar to the movement of a pendulum system. The pendulum system which a hanging object is attached to a wire with mass at a fixed point is specifically described as a physical pendulum, see figure 6-2.

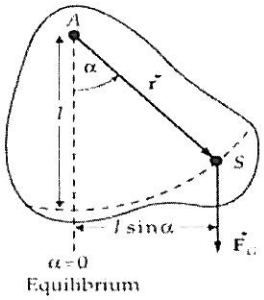

Figure 6-2 Physical pendulum[35].

Where

s = center of gravity [m]

F_G = weight force [N]

According to a basic law of rotational motion, torque of the weight, τ, is equal the product of the moment of inertia and the angular acceleration. The equations of the motion in the figure 6-2 can be given by[35]:

$$\tau = \dot{L} \qquad \textbf{6-10}$$

$$\tau = I_A \cdot \ddot{\alpha} \qquad \textbf{6-11}$$

$$\tau = -l \cdot m \cdot g \cdot sin\alpha = -l \cdot m \cdot g \cdot \alpha \qquad \textbf{6-12}$$

Where

L = angular momentum, $L = I_A \cdot \dot{\theta}$ [Nm s]

I_A = moment of inertia around A axis [kg m^2] $I_A = I_c + mr^2$

α = angular displacement [rad] **note:** for small angles α $(sin\alpha = \alpha)$

The period , T, and frequency , f, of pendulum is given by [35]:

$$T = 2\pi\sqrt{\frac{I_A}{mgl}} \qquad \textbf{6-13}$$

$$f = \frac{1}{2\pi}\sqrt{\frac{mgl}{I_A}} \qquad \textbf{6-14}$$

When designing mechanical parts in an oscillation system, the critical eigen frequency and period need to be identified to prevent excess loads to the system. If the system oscillates at the same frequency with the eigen frequency, the magnitude of the vibration can exponentially increase till it causes the degradation of the system.

7 Mathematical Models of the RT and WCP Module

Before the vehicles are built, the establishment of mathematical models is important for analyzing the effect of the forces and for designing control system of the vehicles. Mathematical models of marine vehicles are commonly involved dynamics, related with bodies having accelerated motion. The basic understanding of kinematic and kinetic theories is needed to explain vehicles motions. Kinematics describes translational and rotational movements in terms of position, velocity and acceleration regardless of the source causing movements (forces or moments). Kinetics represents forces or torques affecting on an object.

7.1 Notations and Reference Frames

Notations and reference frames need to be defined to refer the force and motions of the marine vehicles in six degrees of freedom (DOF).

DOF	Motions and rotations	forces and moments	linear and angular velocity	position and orientation (Euler angles)
1	motions in the x-direction (surge)	X	u	x
2	motions in the y-direction (sway)	Y	v	y
3	motions in the z-direction (heave)	Z	w	z
4	rotation about the x-axis (roll)	K	p	∅
5	rotation about the y-axis (pitch)	M	q	θ
6	rotation about the z-axis (yaw)	N	r	ψ

Table 7-1 Notation used for marine vehicles.

The first three degrees of freedom are used to determine position and translational motion along x-, y- and z-axis, while the last 3 DOFs are used to describe orientation and rotation. The dynamic equations of marine vehicles can be developed using a body-fixed frame and an earth-fixed reference frame, see figure 7-1.

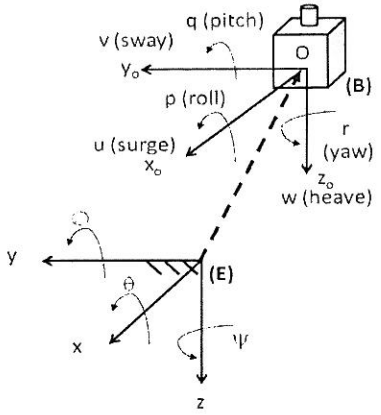

Figure 7-1 Body-fixed frame (B) and earth-fixed reference frame (E).

7.2 Hydrodynamic Forces and Moments

Hydrodynamic equations are introduced to characterize dynamic motions of marine vehicles in water. The complexity of hydrodynamic equations is due to six degrees of freedom, time

variant and nonlinear function so many assumptions are made to simplify the nonlinear equations. In Fossen [12], the nonlinear hydrodynamic equations of marine vehicles in six degrees of freedom can be expressed as:

$$\boldsymbol{M\dot{v} + C(v)v + D(v)v + g(n) = \tau_E + \tau} \qquad \textbf{7-1}$$

Where

M	=	inertia matrix (including added mass)
$C(v)$	=	matrix of Coriolis and centripetal terms (including added mass)
$D(v)$	=	hydrodynamic damping matrix
$g(n)$	=	vector of restoring force and moments
τ_E	=	vector of environmental force and moments
τ	=	vector of control inputs (propulsion forces and moments)

The vector n ^{n} = [x,y,z, ϕ,θ,ψ]^{T} is the position and Euler angles in the earth-fixed reference frame. The vector v = [u,v,w,p,q,r]^{T} is the linear and angular velocity in the body-fixed frame. The vector $\dot{v}$ is the linear and angular acceleration in the body-fixed frame.

Inertia and Added Mass

The inertia matrix can be expressed as[12]:

$$\boldsymbol{M \triangleq M_{RB} + M_A > 0} \qquad \textbf{7-2}$$

Where M_{RB} denotes the rigid-body inertia matrix, which is a 6 x 6 system matrix defined as[12]:

$$\boldsymbol{M_{RB} = \begin{bmatrix} m & 0 & 0 & 0 & mz_G & -my_G \\ 0 & m & 0 & -mz_G & 0 & mx_G \\ 0 & 0 & m & my_G & -mx_G & 0 \\ 0 & -mz_G & my_G & I_x & -I_{zx} & -I_{zx} \\ mz_G & 0 & -mx_G & -I_{zx} & I_y & -I_{yz} \\ -my_G & mx_G & 0 & -I_{zx} & -I_{yz} & I_z \end{bmatrix}} \qquad \textbf{7-3}$$

Where

r_g^b	=	vectors from the origin O to CG decomposed in the [B] frame.
m	=	mass of the rigid body

The inertia matrix $I_o \in \boldsymbol{R}^{3x3}$ is moment of inertia around the origin O, proofed in[12]:

$$\boldsymbol{I_o = I_c - m(rr^T - r^T r I_{3x3})} \qquad \textbf{7-4}$$

The inertia matrix $I_c = I_c^T \in \Re^{3x3}$ is the inertia matrix about the CG of the object. In[12], it can be expand as the following equations:

$$\boldsymbol{I_x = I_x^{cg} + m(y_g^2 + z_g^2)} \qquad \textbf{7-5}$$

$$\boldsymbol{I_y = I_y^{cg} + m(x_g^2 + z_g^2)} \qquad \textbf{7-6}$$

$$I_z = I_z^{cg} + m(x_g^2 + y_g^2) \qquad \textbf{7-7}$$

M_A is the hydrodynamic added mass term[12]:

$$M_A = -\begin{bmatrix} X_{\dot{u}} & X_{\dot{v}} & X_{\dot{w}} & X_{\dot{p}} & X_{\dot{q}} & X_{\dot{r}} \\ Y_{\dot{u}} & Y_{\dot{v}} & Y_{\dot{w}} & Y_{\dot{p}} & Y_{\dot{q}} & Y_{\dot{r}} \\ Z_{\dot{u}} & Z_{\dot{v}} & Z_{\dot{w}} & Z_{\dot{p}} & Z_{\dot{q}} & Z_{\dot{r}} \\ K_{\dot{u}} & K_{\dot{v}} & K_{\dot{w}} & K_{\dot{p}} & K_{\dot{q}} & K_{\dot{r}} \\ M_{\dot{u}} & M_{\dot{v}} & M_{\dot{w}} & M_{\dot{p}} & M_{\dot{q}} & M_{\dot{r}} \\ N_{\dot{u}} & N_{\dot{v}} & N_{\dot{w}} & N_{\dot{p}} & N_{\dot{q}} & N_{\dot{r}} \end{bmatrix} \qquad \textbf{7-8}$$

The expression of the notions can be expressed; for example, $X_{\dot{v}}$ denotes that the hydrodynamic added mass force X along x-axis due to acceleration $\dot{v}$ in the y-direction[12]:

$$X = X_{\dot{v}}\dot{v}, \qquad \textit{where} \qquad X_{\dot{v}} := \frac{\partial X}{\partial \dot{v}} \qquad \textbf{7-9}$$

Strip theory can be used to find three dimensional hydrodynamic derivatives[12]. By dividing the submerged part of the vehicle into a number of strips, two dimensional hydrodynamic coefficients for added mass can be computed for each strip and summarized over the length of the object to yield the three dimensional coefficient. The following formula can be used[12]:

$$-X_{\dot{u}} = \int_{-L/2}^{L/2} m_{11}^{(2D)}(y,z)\,dx \qquad \textbf{7-10}$$

$$-Y_{\dot{v}} = \int_{-L/2}^{L/2} m_{22}^{(2D)}(y,z)\,dx \qquad \textbf{7-11}$$

$$-Z_{\dot{w}} = \int_{-L/2}^{L/2} m_{33}^{(2D)}(y,z)\,dx \qquad \textbf{7-12}$$

$$-K_{\dot{p}} = \int_{-L/2}^{L/2} m_{44}^{(2D)}(y,z)\,dx \qquad \textbf{7-13}$$

$$-M_{\dot{q}} = \int_{-L/2}^{L/2} m_{55}^{(2D)}(y,z)\,dx \qquad \textbf{7-14}$$

$$-N_{\dot{r}} = \int_{-L/2}^{L/2} m_{66}^{(2D)}(y,z)\,dx \qquad \textbf{7-15}$$

The two-dimensional added inertia moment in roll, pitch and yaw can be written as[12]:

$$\int_{-L/2}^{L/2} m_{44}^{(2D)}(y,z)\,dx \triangleq \int_{-B/2}^{B/2} y^2 m_{33}^{(2D)}(x,z)\,dx + \int_{-H/2}^{H/2} m_{22}^{(2D)}(y,z)\,dz \qquad \textbf{7-16}$$

$$\int_{-L/2}^{L/2} m_{55}^{(2D)}(y,z)\,dx \triangleq \int_{-L/2}^{L/2} x^2 m_{33}^{(2D)}(y,z)\,dx + \int_{-L/2}^{L/2} m_{11}^{(2D)}(x,y)\,dz \qquad \textbf{7-17}$$

$$\int_{-L/2}^{L/2} m_{66}^{(2D)}(y,z)\,dx \triangleq \int_{-B/2}^{B/2} y^2 m_{11}^{(2D)}(x,z)\,dx + \int_{-H/2}^{H/2} m_{22}^{(2D)}(y,z)\,dz \qquad \textbf{7-18}$$

The two dimensional added mass coefficient can be found in appendix B.

From $M \triangleq M_{RB} + M_A > 0$, the inertia matrix, M, are[12]:

$$M = \begin{bmatrix} m - X_{\dot{u}} & -X_{\dot{v}} & -X_{\dot{w}} & -X_{\dot{p}} & mz_G - X_{\dot{q}} & -my_G - X_{\dot{r}} \\ -X_{\dot{v}} & m - Y_{\dot{v}} & -Y_{\dot{w}} & -mz_G - Y_{\dot{p}} & -Y_{\dot{q}} & mx_G - Y_{\dot{r}} \\ -X_{\dot{w}} & -Y_{\dot{w}} & m - Z_{\dot{w}} & my_G - Z_{\dot{p}} & -mx_G - Z_{\dot{q}} & -Z_{\dot{r}} \\ -X_{\dot{p}} & -mz_G - Y_{\dot{p}} & my_G - Z_{\dot{p}} & I_x - K_{\dot{p}} & -I_{zx} - K_{\dot{q}} & -I_{zx} - K_{\dot{r}} \\ mz_G - X_{\dot{q}} & -Y_{\dot{q}} & -mx_G - Z_{\dot{q}} & -I_{zx} - K_{\dot{q}} & I_y - M_{\dot{q}} & -I_{yz} - M_{\dot{r}} \\ -my_G - X_{\dot{r}} & mx_G - Y_{\dot{r}} & -Z_{\dot{r}} & -I_{zx} - K_{\dot{r}} & -I_{yz} - M_{\dot{r}} & I_z - N_{\dot{r}} \end{bmatrix} \quad \textbf{7-19}$$

Coriolis and Centripetal Forces

The Coriolis and centripetal matrix consists of rigid-body inertia, $C_{RB}(v)$, and added mass term, $C_A(v)$[12]:

$$\boldsymbol{C(v) \triangleq C_{RB}(v) + C_A(v)} \quad \textbf{7-20}$$

$C(v)$ becomes zero when a marine vehicle is at rest. $C_{RB}(v)$ represents forces and moments due to the mass of the vehicle while $C_A(v)$ accounts for forces and moments from the added mass.

Hydrodynamic Damping

Hydrodynamic damping is the forces that always resist the motions of the observed body. The forces depend on the magnitude of body velocity and the direction of its motion. The hydrodynamic damping matrix, $D(v)$, for ocean vehicles includes [12]:

$$\boldsymbol{D(v) \triangleq D_P(v) + D_v(v)} \quad \textbf{7-21}$$

$$\boldsymbol{D(v) \triangleq D_P(v) + D_s(v) + D_W(v) + D_M(v)} \quad \textbf{7-22}$$

$$\boldsymbol{D(v) > 0 \ \forall \ v \in \mathcal{R}^6} \quad \textbf{7-23}$$

$$\boldsymbol{D(v) = -\begin{bmatrix} X_u & X_v & X_w & X_p & X_q & X_r \\ Y_u & Y_v & Y_w & Y_p & Y_q & Y_r \\ Z_u & Z_v & Z_w & Z_p & Z_q & Z_r \\ K_u & K_v & K_w & K_p & K_q & K_r \\ M_u & M_v & M_w & M_p & M_q & M_r \\ N_u & N_v & N_w & N_p & N_q & N_r \end{bmatrix}} \quad \textbf{7-24}$$

Where

$D_P(v)$	=	radiation-induced potential damping due to forced body oscillations
$D_v(v)$	=	viscous damping matrix; $D_v(v) \triangleq D_s(v) + D_W(v) + D_M(v)$
$D_s(v)$	=	surface friction is a function of Reynolds number, $f(Re)$
$D_W(v)$	=	wave drift damping
$D_M(v)$	=	damping due to vortex shedding (Morison's equation)

Note: the drag and damping forces are related. The drag force is referred to forces caused when fluid flow through a fixed object whereas the damping force is force caused on an object moving through fluid.

Potential Damping

Potential damping or radiation-induced potential damping is caused due to the energy carried away by generated surface waves. The marine vehicle is forced to oscillate with wave excitation frequency and then there are no incident waves[12]. The potential damping should be considered when the marine vehicle operates in the wave zone. Compared with other terms (e.g. viscous damping) the potential damping terms can be negligible for underwater vehicles[12].

Skin Friction

For vehicles with the low-frequency motion, there will be a linear skin friction due to laminar boundary theory. In addition, there will be a nonlinear or quadratic skin friction due to turbulent boundary theory for a high-frequency motion of vehicles[12]. The skin friction acts tangentially to the surface of the vehicles.

Wave Drift Damping

Wave drift damping can be interpreted as resistance caused by waves when vehicles advance in waves [12]. As submerged vehicles operate at great depth, the effect of waves is significantly reduced. This resistance can be negligible for deeply marine vehicles.

Damping due to Vortex Shedding

When an object move passes though a viscous fluid, there will be viscous damping force due to vortex shedding. The force is associated with fluid density, velocity of the vehicle, the projected cross-sectional area and drag coefficient. This force is the drag term in Morison's equation[12]:

$$f(v) = -\frac{1}{2} \cdot C_D(Re) \cdot \rho \cdot A \cdot v \cdot |v| \qquad \textbf{7-25}$$

Restoring Forces and Moments

In marine control systems, restoring forces are referred to the gravitational and buoyant forces in the hydrodynamic terminology [12]. The gravitational force will act thought the center of gravity (CG) of the vehicle, $r_G = [x_G, y_G, z_G]^T$. The buoyant force will act thought the center of buoyancy (CB) of the vehicle, $r_B = [x_B, y_B, z_B]^T$. The restoring forces, g(n), can be written [12]:

$$g(n) = \begin{bmatrix} (W-B)s\theta \\ -(W-B)c\theta s\emptyset \\ -(W-B)c\theta c\emptyset \\ -(y_G W - y_B B)c\theta c\emptyset + (z_G W - z_B B)c\theta s\emptyset \\ (z_G W - z_B B)s\theta + (x_G W - x_B B)c\theta c\emptyset \\ -(x_G W - x_B B)c\theta s\emptyset - (y_G W - y_B B)s\theta\emptyset \end{bmatrix} \qquad \textbf{7-26}$$

Where

W = submerged weight of the vehicle $(m \cdot g)$ [N]

B = buoyancy force of the vehicle $(\rho \cdot \nabla \cdot g)$ [N]

Note $s \cdot = \sin(\cdot)\ and\ c \cdot = \cos(\cdot)$

Environmental Forces

Marine vehicles always experience several environmental disturbances from waves, winds and ocean currents[12].

$$\boldsymbol{\tau_E = \tau_{wave} + \tau_{wind} + \tau_{current}} \qquad \textbf{7-27}$$

Propulsive Forces and Moments

Propulsive forces and moments, τ, are applied to steer the vehicle towards desired positions and orientations. These forces and moments can be referred to the control inputs in the control system. The following expressions for the propeller thrust can be established [29]:

$$\boldsymbol{T = \rho D^2 K_T(J_o)|n|n} \qquad 7\text{-}28$$

Where

T	=	thrust [N]
ρ	=	water density [kg/m^3]
D	=	propeller diameter [m]
K_T	=	thrust coefficient
J_o	=	advance number, $\frac{V_a}{nD}$
V_a	=	advance speed (speed of the water going into the propeller)
n	=	propeller revolution

7.3 Simplification of Hydrodynamic Equations

The simplified mathematical model is important for estimating related forces and moments and for further development in control system on the RT system. The hydrodynamic model is quite complicated and requires many parameters to be considered. To reduce the complexity of the model, the following assumptions are applied, regardless of the effect of umbilical lines and steel cable.

- According to inherent metacentric stability and symmetrical planes of the RT and WCP module, the motion in roll and pitch can be negligible (i.e. p = q = 0 and $\theta = \emptyset = 0$). The metacentric stability is satisfied when the gravity (CG) of the RT and WCP module is located below the center of buoyancy (CB).
- Heave motions are negligible (i.e. w = 0 and $z = 0$). The winch system on the surface vessel is separately used to control the vertical movements (heave) of the module. The heave motions do not influence movements in other degrees of freedom.
- The RT and WCP module moves at low speed e.g. less than 2 m/s during the position adjustment.
- Environmental disturbances from waves can be negligible in deepwater zones.
- The origin of body fixed frame is located on the same z-axis as the center of gravity (CG) of the RT and WCP module, i.e. $\boldsymbol{x_G = y_G = 0}$.

- The motions of the RT and WCP module can be adjusted only one DOF at each time.
- The DOFs of the RT and WCP module are decoupled. Literatures suggest when vehicles operate at low speeds, the assumption of decoupling terms may be valid [36-38]. The decoupling terms mean that each degree of freedom can be treated individually.

Inertia and Added Mass

The expression for the inertia matrix, M, can be simplified by considering the symmetry of vehicle planes which the xz-plane of WCP is symmetry, $I_{xy} = I_{yz} = 0$. In addition, the RT and WCP module is assumed to have homogenous mass distribution. Accordingly, the simplified inertia matrix, M, is[12]:

$$M = \begin{bmatrix} m - X_{\dot{u}} & 0 & 0 \\ 0 & m - Y_{\dot{v}} & mx_G - Y_{\dot{r}} \\ 0 & mx_G - Y_{\dot{r}} & I_z - N_{\dot{r}} \end{bmatrix} \quad \textbf{7-29}$$

Other cases of the simplified inertia matrix, M, are described by Fossen [12].

Since $x_G = 0$ and decoupling assumption, the equation can be further simplified:

$$M = \begin{bmatrix} m - X_{\dot{u}} & 0 & 0 \\ 0 & m - Y_{\dot{v}} & 0 \\ 0 & 0 & I_z - N_{\dot{r}} \end{bmatrix} \quad \textbf{7-30}$$

Coriolis and Centripetal Forces

The Coriolis and centripetal forces are not decisive where the cruising speed of the vehicle is low [39]. The Coriolis and centripetal forces terms can be eliminated.

$$C(v)v = 0 \quad \textbf{7-31}$$

Hydrodynamic Damping

When potential damping and wave drift damping are negligible for deep marine vehicles, the expression of the hydrodynamic damping, $D(v)$, composes of surface friction, $D_s(v)$, and damping due to vortex shedding, $D_M(v)$:

$$D(v) \triangleq D_s(v) + D_M(v) \quad \textbf{7-32}$$

For low-speed underwater vehicles, a rough approximation of the hydrodynamic damping, $D(v)$, could be assumed that the vehicle is performing a decoupling motion. This suggests a diagonal structure of $D(v)$with linear and quadratic damping terms on the diagonal[12]:

$$D(v) = -diag\{X_u, Y_v, Z_w, K_p, M_q, N_r\} - diag\{X_{u|u|}|u|, Y_{v|v|}|v|, Z_{w|w|}|w|, K_{p|p|}|p|, M_{q|q|}|q|, N_{r|r|}|r|\} \quad \textbf{7-33}$$

The dampening terms, $D(v)$, can be divided into linear, D, and quadratic damping term, $D_n(v)$ [12]:

$$D(v) = D + D_n(v) \quad \textbf{7-34}$$

The linear damping, D, is caused by linear drift damping and laminar skin friction whereas quadratic damping ,$D_n(v)$, is caused by separation and vortex shedding [40].

Restoring Forces and Moments

As the winch system on the surface vessel supports all the submerged weight of the RT and WCP module, the effect of the restoring forces and moments can be neglected:

$$g(n) = 0 \quad \textbf{7-35}$$

Environmental Forces

For a shallow water zone, the effect of waves must be taken into account. The models for wave forces and moments can be found in Fossen [9]. As a vehicle is in deeper water depth, wave-induced forces significantly decrease and can be assumed to be negligible. There will be only current-induced forces defined as[12]:

$$\tau_E = \tau_{current} = \underbrace{M_{FK}\dot{v}_c}_{Froude-kriloff} + \underbrace{M_A\dot{v}_c + D_P(v)v_c}_{diffraction\ forces} + \underbrace{D_v(v)v_c}_{viscours\ forces} \quad \textbf{7-36}$$

Where M_{FK} = Froude-Kriloff inertia matrix (the inertia matrix of the displaced fluid)

According to Morrison formula, when the diameter of marine vehicle (or vehicle length), D, is large than one over five of wavelength i.e. D > 0.2 L (wavelength), the diffraction force must be taken into account because the acceleration of fluid will vary over the marine vehicle.

$$\underbrace{M_A\dot{v}_c + D_P(v)v_c}_{diffraction\ forces} = 0\ , when\ D < 0.2L \quad \textbf{7-37}$$

For a case of underwater vehicles working at great depths, the Frode-kriloff force is not considered due to the acceleration of the currents is negligible[41].

$$\underbrace{M_{FK}\dot{v}_c}_{Froude-kriloff} = 0 \quad \textbf{7-38}$$

Hence, the diffraction and the Frode-kriloff force for marine vehicles can be negligible and the environmental forces are from current:

$$\tau_{current} = \underbrace{D_v(v)v_c}_{viscours\ forces} \quad \textbf{7-39}$$

Propulsive Forces and Moments

In this thesis, the focus on detailed design of propellers is not a main task for the design of the new RT system. In addition many thrusters available in the market for underwater vehicles can be applied for the thruster system. Hence using specifications data from these

thruster applications appear practical for the design of the thruster system and estimation of the required energy.

7.4 Hydrodynamic Equations

The simplified hydrodynamic model for the RT and WCP module in deepwater zones can be:

$$\boldsymbol{M\dot{v} + Dv + D_n(v)v = \tau + \tau_{current}} \qquad \textbf{7-40}$$

For high speed maneuvers, the quadratic damping, $D_n(v)$, will dominate the linear damping. When the speed of the object is over 2 m/s, it can be defined as the high speed maneuvers [9]. Since the module travels at a low speed, not only is the quadratic damping term considered, but also the linear damping term, D, or skin friction should be included in the equations. The skin friction coefficient is dependent on the surface roughness of the material and it is based on experimental data from model tests. The maneuvering of the RT and WC module can be divided into three DOFs; two translational directions (surge and sway) and rotation motion (yaw).

Model for Controlling Translation

Surge motion:

$$\boldsymbol{(m - X_{\dot{u}})\dot{u} - X_u u, -X_{u|u|}|u|u = \tau + \tau_{current}} \qquad \textbf{7-41}$$

Sway motion:

$$\boldsymbol{(m - Y_{\dot{v}})\dot{v} - Y_v v - Y_{v|v|}|v|v = \tau + \tau_{current}} \qquad \textbf{7-42}$$

Model for Controlling Rotation

Yaw motion:

$$\boldsymbol{(I_z - N_{\dot{r}})\dot{r} - N_r r - N_{r|r|}|r|r = \tau + \tau_{current}} \qquad \textbf{7-43}$$

Once the equation of motion is found in terms of the mathematical model, the following time-stepping procedure can be used to solve the equation:

1. The position and orientation of the RT and WCP module is recognized in the earth-fixed reference frame. The linear velocity and angular velocity of the RT and WCP module is known in the body-fixed frame.
2. Calculate and substitute all forces and moments acting on the RT and WCP module in the equation of motion.
3. Solve the equation of motion and find, vector $\dot{v}$, the linear and angular acceleration in the body-fixed frame.
4. Integrate the linear and angular acceleration, $\dot{v}$, and find velocities, v= [u,v,w,p,q,r]^T, of the RT and WCP module in the body-fixed frame.
5. Integrate the linear and angular velocities , v, and find position and orientation of the RT and WCP module in the body-fixed frame.

The motion of the model is normally be simulated using a computer program if all important parameters are found. The parameters e.g. damping coefficient are determined based on experimental data from model tests.

The 1st-order Nomoto's model for Auto Heading Control

The 1st-order Nomoto's model for controlling rotation can be derived as follow:

$$\dot{r}T + r = K\delta \qquad \textit{7-44}$$

$$\dot{r} = -\frac{1}{T} \cdot r + \frac{K}{T}\delta \qquad \textit{7-45}$$

The model for controlling rotation can be manipulated in the similar equation as the Nomoto's model:

$$(I_z - N_{\dot{r}})\dot{r} - N_r r - N_{r|r|}|r|r = \tau + \tau_{current} \qquad \textit{7-46}$$

$$\dot{r} = \frac{N_r r + N_{r|r|}|r|r}{(I_z - N_{\dot{r}})} + \frac{\tau + \tau_{current}}{(I_z - N_{\dot{r}})} \qquad \textit{7-47}$$

Although, the equation (7-45) is similar to the Nomoto's model (7-47), the equation is partially highly complicated to solve due to the quadratic damping term. Both damping terms in the equation (7-47) should be linearised to comply with the Nomoto's model. Linearizing is to find a linear version of the model which will only be precise in a narrow space, i.e. around a certain point where the process is working.

Once the linear damping term has been found, the model can be:

$$\dot{r} = \frac{N_r r}{(I_z - N_{\dot{r}})} + \frac{\tau + \tau_{current}}{(I_z - N_{\dot{r}})} \qquad \textit{7-48}$$

With reference to the Nomoto's model, the expression shows that:

- time constant (*T*) = $(I_z - N_{\dot{r}})$
- process gain constant (*K*) = $\frac{1}{N_r}$

After the time constant and process gain constant have been determined, the system response and the control block diagram can be found to represent the relations of the input and output of the system. The transfer function of auto heading control can be written:

$$H(s) = \frac{r}{\delta}(s) = \frac{\frac{1}{N_r}}{[1 + (I_z - N_{\dot{r}})s]} = \frac{1}{N_r[1 + (I_z - N_{\dot{r}})s]} \qquad \textit{7-1}$$

Conclusion remark:

Linearizing of the model is normally accomplished by a model test. Nevertheless, for low speed maneuver, e.g. lower than 2m/s, only linear damping term can be a good approximation for the model and it is possible to neglect quadratic damping term[12].

8 Case Scenario: Angola Sea

Since there have been a great number of new explorations in offshore Angola, Angola Sea recently becomes one of the hottest spots for oil developments in the world and a key player in Africa's oil and gas exporters and producers. Angola Sea is selected as the potential location where the guidelineless RT can be operated.

8.1 Environmental Parameters

The Angola Current is a fast, narrow, and stable flow. The measurements of the water velocity at the surface from 9°S-16°S along the coast is 0.5 m/s and the average velocity decreases even more, down to 0.05-0.08 m/s, at 200-300 m southward flow along the edge of the shelf and over the continental slope[42]. Since the specific data of ultra-deepwater zones in the Angola Sea is not available, the sea state data in the West Africa area will be used instead.

The velocity of the surface current is assumed at 0.7 m/s. The current velocity decreases with increasing water depth and it is assumed to be 0.2 m/s from 400 m. water depths[43]. Figure 8-1 shows the assumption of the current profile used in this thesis.

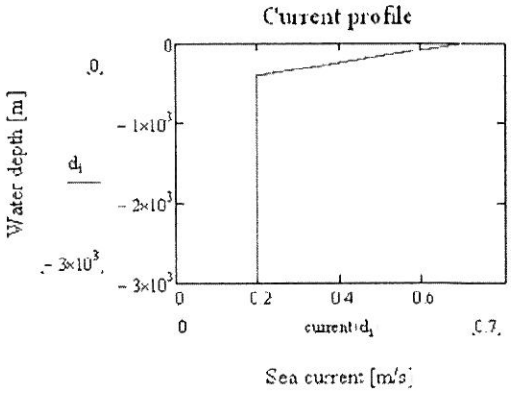

Figure 8-1 Current profile.

The main parameters used in this calculation are:

Water depth	=	3,000	[m]
Wave period (T)*	=	9.7	[s]
Significant wave height (Hs)*	=	3	[m]

* Maximum environmental condition for module deployment [44].

Figure 8-2 shows the maximum horizontal particle velocity and maximum horizontal particle acceleration, which can be neglected in deepwater zones. For shallow water zones, waves and sea current are the main factor influencing drag forces on the RT, WCP and steel cable. The maximum horizontal particle velocity and acceleration in a shallow water zone are shown in figure 8-3.

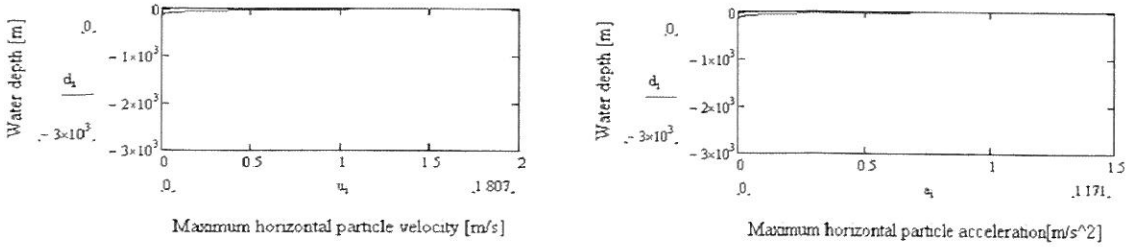

Figure 8-2 Maximum horizontal particle velocity (left) and acceleration (right).

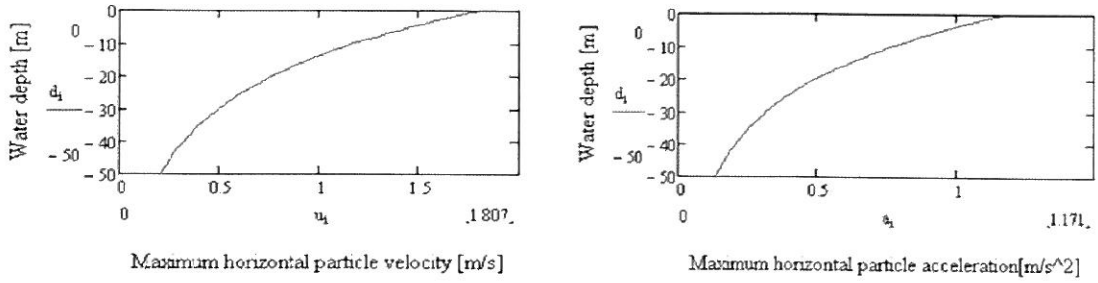

Figure 8-3 Maximum horizontal particle velocity (left) and acceleration (right) in a shallow water zone.

8.2 Force and Moment Estimations

With reference to the operations in chapter 3, the estimation of forces and moments can be followed the following operations:

1. The deployment of the RT and WCP to XT
2. The retrieval of the RT to the surface vessel
3. The deployment of the RT to WCP
4. The retrieval of the RT and WCP to the surface vessel

These four operations can also be categorized into two main water zones; ultra-deepwater zone and shallow water zone. The operation #1 and #3 are performed in the ultra-deep water zone while the operation #2 and #4 are in the shallow water zone.

The maximum horizontal estimations are calculated based on the superposition between the maximum horizontal forces due to waves and the forces due to current. Key parameters are listed in appendix A. The linear wave equation can be found in appendix B. Assumptions of the module rotations are explained in appendix C and the main calculations are shown in appendix D.

8.2.1 Forces in Ultra-deepwater Zone

In this zone, the influence from waves is negligible and the sea current becomes a main factor causing drag forces on the system. As can be seen from figure 8-4 the drag force of the steel cable is greater than the drag force on the RT and WCP module. From the result in appendix D, at 3,000 m water depths, the force of the steel cable is 3,691 N whereas the

force on the WCP is 357 N and the force on the RT is 34 N. The drag forces on the steel cable are equivalent to 90% of the total drag, 4,082 N. In essence, the total drag force will increase from 4,082 N to 10,652 N if the WCP is deployed with UTH, see figure 8-4. The additional drag forces are due to control and chemical umbilicals.

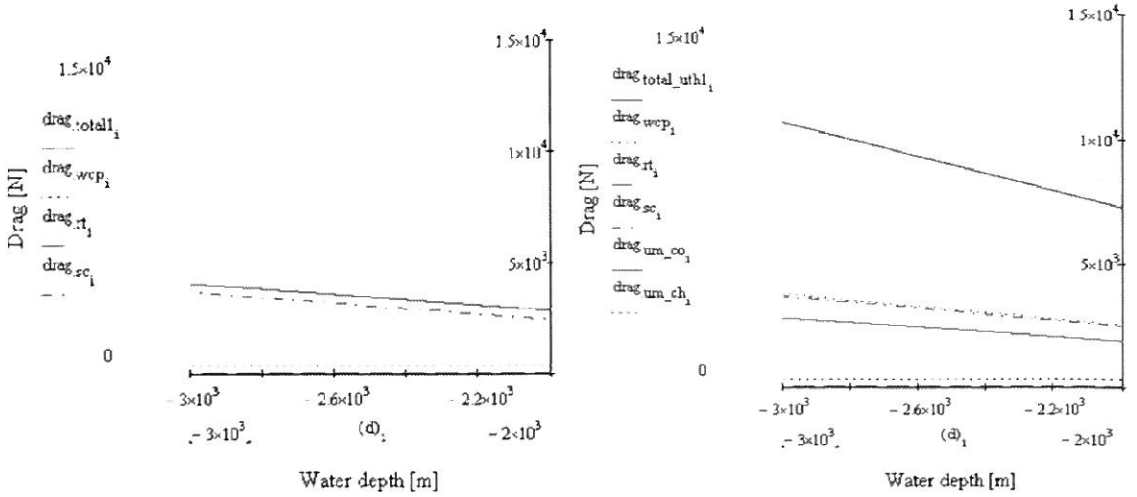

Figure 8-4 Total drag on the system when deploying the WCP without UTH (left) and with UTH (right) in the ultra-deepwater zone.

The geometry of a submerged line is much more significant than the geometry of the RT and WCP. In the ultra-deepwater zone, although the geometry of RT and WCP has been more streamlined, the improvement will not reduce the total force acting on the system.

8.2.2 Forces in Shallow Water Zone

In this zone the system will experience both drag and inertia forces from the waves and sea current. When the RT and WCP module is retrieved through the moon pool at 10 m below the sea level, the total force on the system will be around 103 kN. The force on the WCP is 97 kN, the force on the RT is 5 kN and the force of the steel cable is 1 kN. As seen from figure 8-5 in the shallow water zone, the total force on the WCP dominates the other forces. The force on the WCP is as much as 94% of the total force. The main reason is that the dimension of the WCP is relatively large compared with the RT and steel cable.

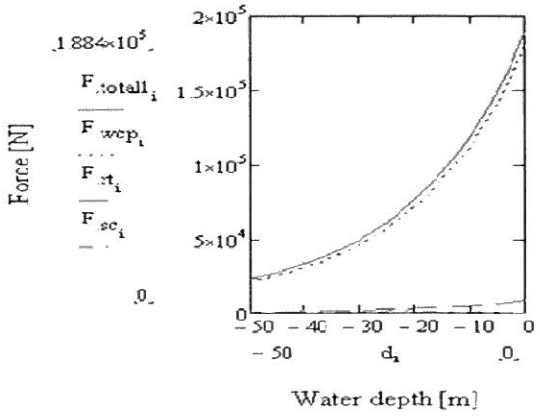

Figure 8-5 Total force of the system in the shallow water zone.

While deploying the WCP to the XT in the ultra-deepwater area, the most influence factor causing drag on the system is sea current. For a shallow water zone, both waves and current are the main factors that cause drag forces and inertia (or added mass) forces on the system. Table 8-1 shows the estimation of the forces experienced on the different operations of the RT and WCP in the ultra-deep zone and shallow water zone.

Operation	WD [m]	Max drag force (Fd) [N]				Max inertia force (Fi) [N]				Total drag and inertia forces [N]
		WCP	RT	Steel cable	Total	WCP	RT	Steel cable	Total	
1. Deployment of the RT and WCP to XT	3,000	357	34	3,691	**4,082**	0	0	0	**0**	**4,082**
2. Retrieval of the RT back to the surface vessel	10	0	3,003	1,072	**4,075**	0	1,979	31	**2,010**	**6,085**
3.Deployment of the RT to WCP	3,000	0	34	3,691	**3,725**	0	0	0	**0**	**3,725**
4.Retrieval of the RT and WCP back to the surface vessel	10	26,420	3,003	1,072	**30,495**	70,970	1,979	31	**72,980**	**103,475**

Table 8-1 A summary of the forces in the operations.

During the retrieval of the RT and WCP to the surface vessel, the system is expected to experience the maximum force around 103 kN which exceeds the performance of the thruster system to counteract this force.

From the result, the force on the system in the shallow water zone is much greater than the force in the ultra-deepwater zone. This is because the effect of a water particle velocity in the shallow zone, see table 8-2. Since the water particle flows fast in the shallow zone, water particle can cause more forces than in the ultra-deepwater zone.

Operation	WD [m]	Max. hor. particle velocity (waves) [m/s]	Max. hor. particle acceleration (waves) [m/s^2]	Current [m/s]	Max water particle waves& current [m/s]
1. Deployment of the RT and WCP to XT	3,000	0.00	0.00	0.20	0.20
2. Retrieval of the RT back to the surface vessel	10	1.18	0.76	0.69	1.87
3.Deployment of the RT to WCP	3,000	0.00	0.00	0.20	0.20
4.Retrieval of the RT and WCP back to the surface vessel	10	1.18	0.76	0.69	1.87

Table 8-2 A summary of sea conditions in the operations.

8.2.3 Moments on the RT and WCP module

When the WCP is prepared to connect to the XT re-entry hub, the orientation of the WCP is done by controlling thrusters on the RT. the minimum thrust required to counter the rotation can be estimated from the maximum moment on the RT and WCP module.

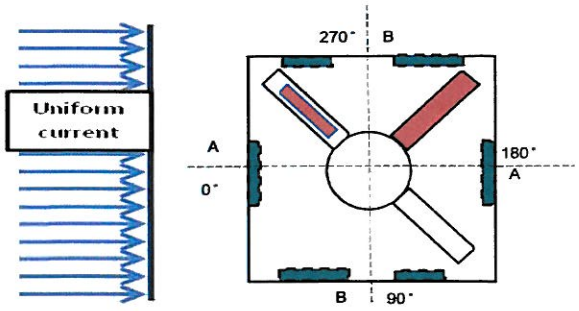

Figure 8-6 The sketch of uniform current towards the RT and WCP module.

According to the assumptions in appendix C, at 3,000 m water depths, when the direction of uniform current flow towards the 315 degrees side of the module, the maximum moment experienced on the RT and WCP module is 50 Nm, see figure 8-7. The numerical results can be found in appendix C.

In this thesis, the moments on the RT and WCP module in the shallow water zone are not determined the complexity of the inertia force acting on the RT and WCP geometry. However, the moments caused by drag force is calculated and the maximum moment experienced on the RT and WCP module is 4,319 Nm, see figure 8-8. The numerical results can be also found in appendix C.

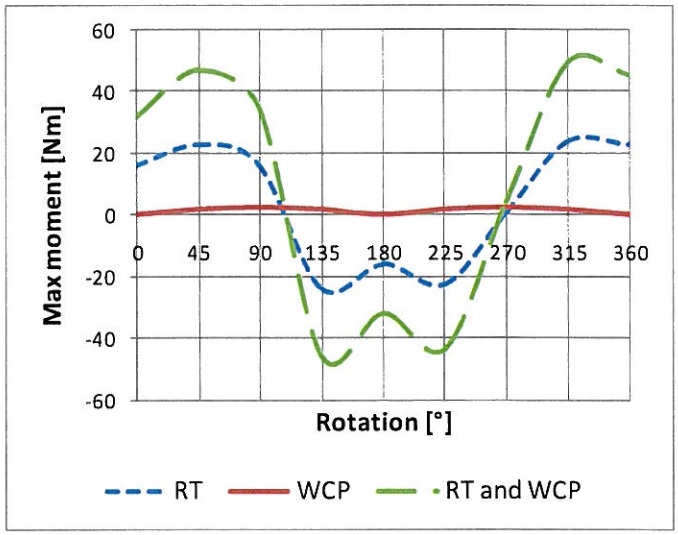

Figure 8-7 Maximum moment on the RT and WCP module at 3,000 m water depths.

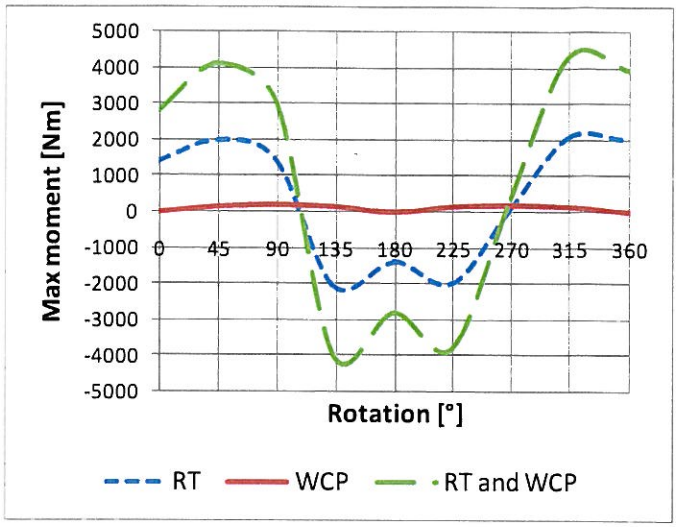

Figure 8-8 Maximum moment on the RT and WCP module at 10 m water depths.

If the thrusters are assumed to be placed at 950 mm radially from the center of the RT, i.e. the lever arm of the torque is designed at 950 mm, the minimum required thrust for the RT and WCP module is 53 N at 3,000 meters and 4,546 N at 10 meters when considering only drag force. Compared to the required thrust of the module for translation at the same depths, the required thrust for rotation is much lesser, thus the required thrust of the module for the translation is more critical.

8.3 Power and Energy Estimations

In order to estimate the power and energy required for the thruster system, the selection of the thrusts must be done to provide the specification of the thruster used in the operations. Table 8-3 shows DC thruster specifications taken from anonymous companies [45-49].

Company	Mass in air [kg]	Thrust[lbf]	Thrust [N]	Input power [W]	Thrust/power [N/kW]
A	35	635	2,845	15,500	184
B	25.5	505	2,262	12,900	175
C	**42**	**485**	**2,173**	**8,000**	**272**
D	45	100	448	1,950	230
E	4	38	170	1,125	151

Table 8-3 A summary of DC thruster specifications.

When comparing thrust and thrust/power ratio of available DC Thrusters, the thruster from C is chosen for the design of the new RT. The selected thruster provides the high ratio of the thrust to power input, at 272 N/kW. With the two steerable thrusters, the maximum thrust can be 4,346 N.

The maximum horizontal offset between the RT/WCP module and the surface vessel is calculated in accordance with an assumption that the direction of the uniform current does not change from the sea level to the sea bed. The equations used in the calculations can be found in appendix D. At 3,000 m water depths, the maximum horizontal offset while

deploying the RT and WCP module to XT (operation #1) is around 15 m and the maximum horizontal offset while deploying the RT to XT (operation #3) is around 29 m. At 10 m water depth, the maximum horizontal offset while deploying the RT back to the surface vessel (operation #2) is around 2 m and the maximum horizontal offset while retrieving the RT and WCP back to the surface vessel (operation #4) is 3 m.

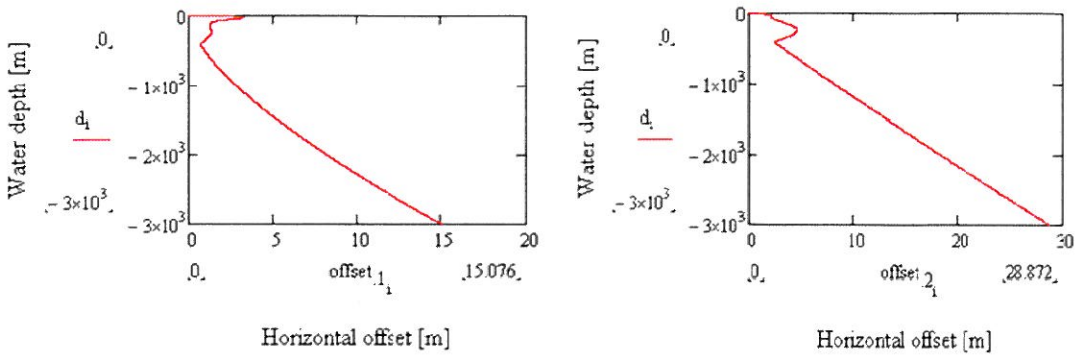

Figure 8-9 Maximum horizontal offset during the operation #1 and #4 (left) Maximum horizontal offset during the operation #2 and #3 (right).

From the result, the operator can either position the RT and WCP module during the operation #1 and #3 by moving the surface vessel or remotely operate thruster systems on the RT. The practical method is to move the surface vessel to minimize energy consumption of the thrusters and the operational time. Although the operator has maneuvered the surface vessel in the correct location, the final adjustment by using the thrusters is also expected. In this thesis, the final horizontal adjustment of the RT and WCP module was assumed at 2 m.

When the WCP moves in water, the WCP will always experience the drag force, which is a function of the relative speed of the module. Figure 8-10 shows the total force acts on the module during the operation #1, #2 and #3 with different advance speeds. To keep the thrust requirement to a minimum, the module should travel at low speed. The calculation of the WCP motion is based on an assumption that the advance speed of the module can immediately reach the set speed without any idle time.

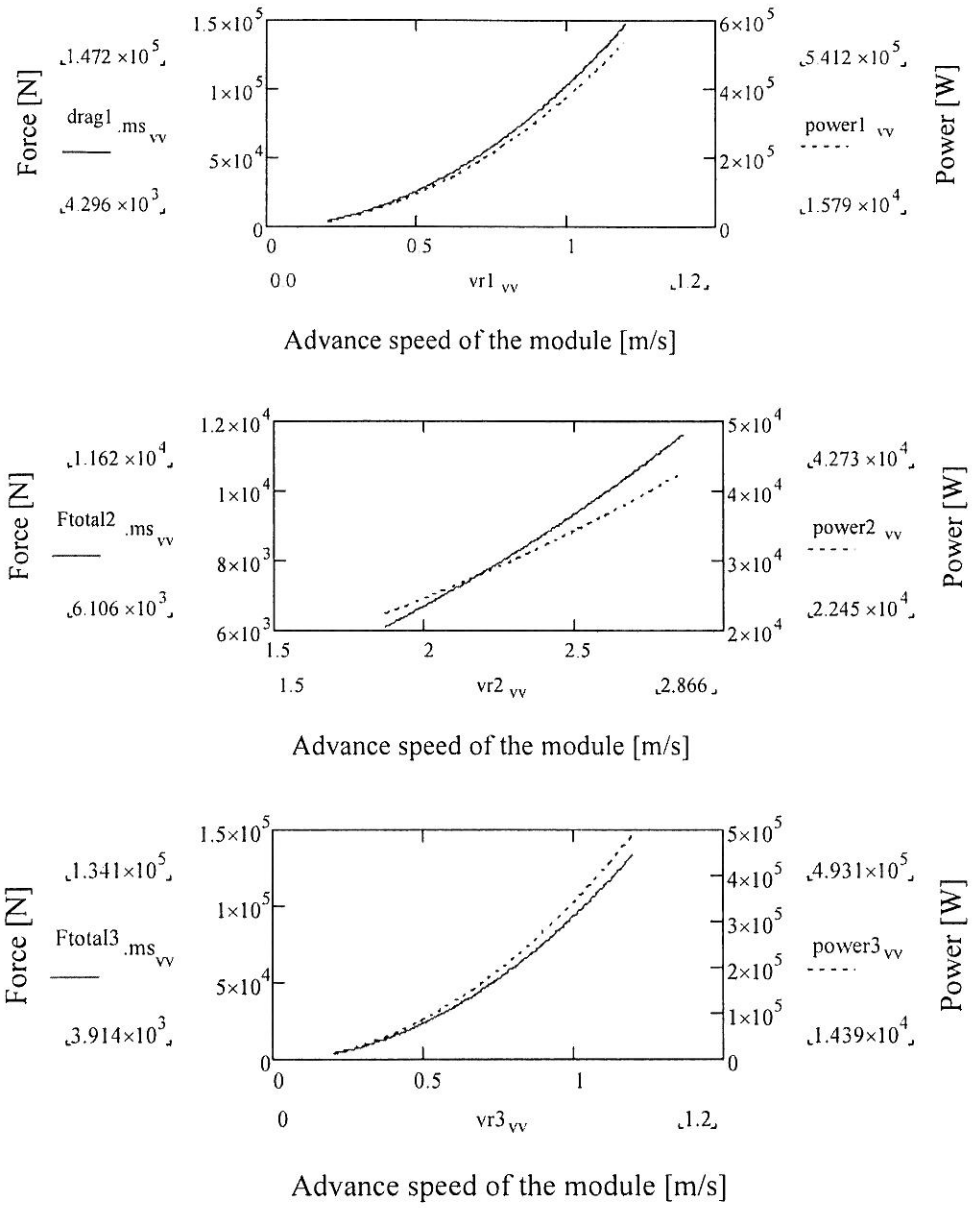

Figure 8-10 Forces experienced on the system during the operation #1 (top) #2 (middle) and #3 (bottom).

Once the speed of the module has been determined, the energy consumption can be calculated from the power and time values using the basic electrical theory. The amount of energy required for the thrusters is equal to the power multiplied with time that the thrusters operate. With increasing advance speed of the module, the input power of the thruster system increases while the operating time of the thruster system reduces.

Figure 8-11 illustrates the force and energy consumption of the RT and WCP module during the operation #1, #2 and #3 with different advance speeds.

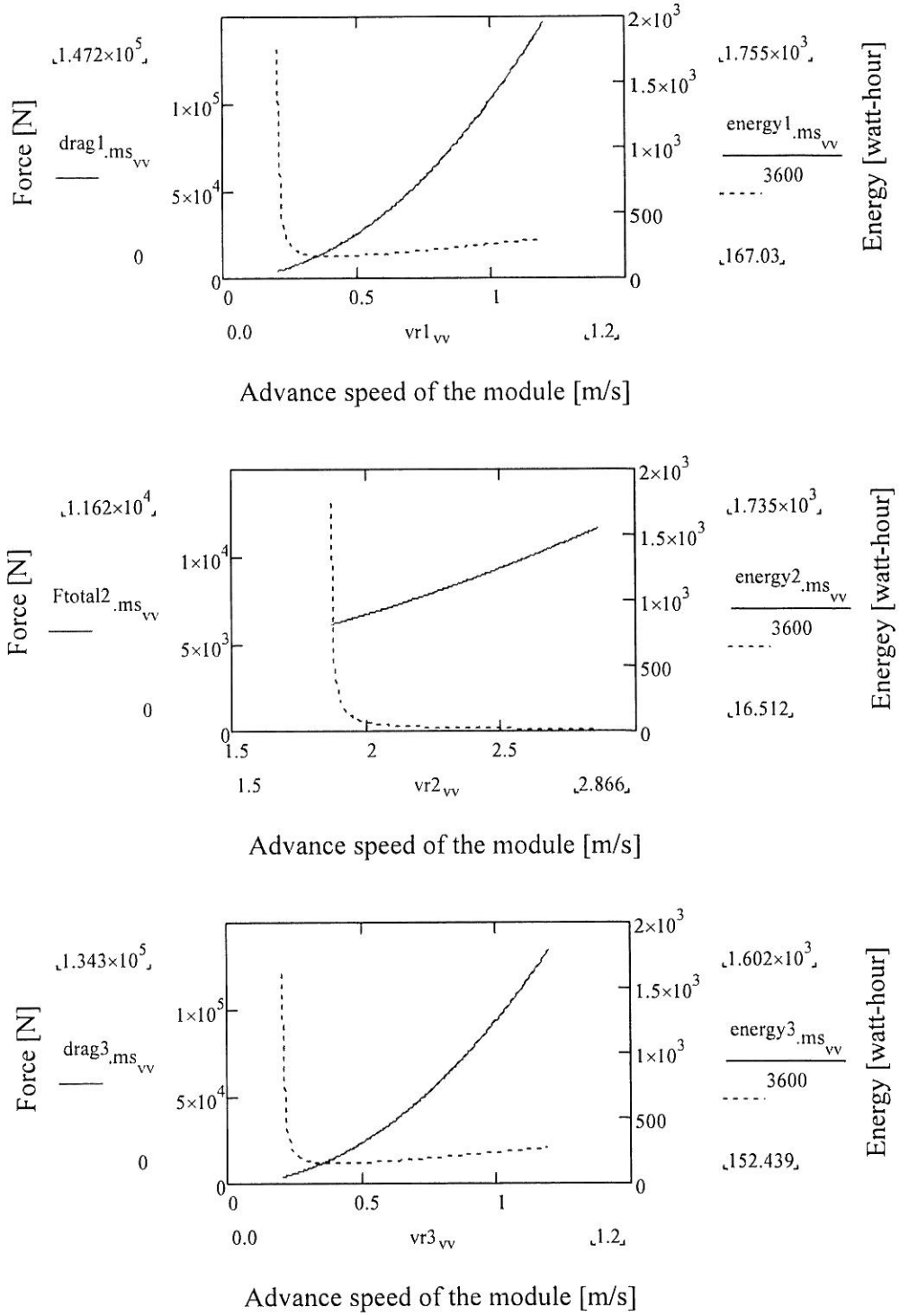

Figure 8-11 Energy and power requirement during the operation #1 (top) #2 (middle) and #3 (bottom).

Table 8-4 shows the minimum thrust that is required to counteract the environmental force in the operations.

Operation	Max water particle waves& current [m/s]	Total drag and inertia forces [N]	Translation requirement [m]	Minimum thrust requirement				
				Module speed [m/s]	Required thrust [N]	Power [W]	Energy [W-hr]	duration [s]
1.Deployment of the RT and WCP to XT	0.20	**4,082**	2	0.205	4,296	15,790	1,755	400
2.Retrieval of the RT back to the surface vessel	1.87	**6,085**	1.4	1.876	6,128	22,530	870	140
3.Deployment of the RT to WCP	0.20	**3,725**	2	0.205	3,914	14,390	1,599	400
4.Retrieval of the RT and WCP back to the surface vessel	1.87	**103,475**	2.5	N/A				

Table 8-4 A summary of required thrust in the operations.

For the deployment of WCP to XT (operation #1), when the module travel at speed 0.205 m/s, the drag experienced on the module is 4,296 N. For the deployment of RT to WCP (operation 3), when the module travel at speed 0.205 m/s, the drag experienced on the module is 3,914 N.

According to the design concept of the thruster system, the two steerable thrusters are previously selected to implement with the new RT. Although the two thrusters can provide enough thrust force 4,346 N, the RT should be equipped with three steerable thrusters to provide system redundancy. Therefore, the three steerable thrusters become the new design concept for the thruster system and they are expected to provide the maximum thrust around 6,500 N.

Table 8-5 shows the energy consumption when increasing advance speed of the module to the maximum speed of the thruster performance.

Operation	Max water particle waves& current [m/s]	Total drag and inertia forces [N]	Translation requirement [m]	Minimum energy consumption				
				Module speed [m/s]	Required thrust [N]	Power [W]	Energy [W-hr]	duration [s]
1.Deployment of the RT and WCP to XT	0.20	**4,082**	2	0.25	6,389	23,490	261	40
2.Retrieval of the RT back to the surface vessel	1.87	**6,085**	1.4	1.94	6,419	23,600	122	19
3.Deployment of the RT to WCP	0.20	**3,725**	2	0.26	6,296	23,150	214	33
4.Retrieval of the RT and WCP back to the surface vessel	1.87	**103,475**	2.5	N/A				

Table 8-5 A summary of required thrust in the operations.

When the module travels at slow speeds, thrusters need to operate long time thereby consuming large amount of energy. When deploying the RT and WCP to the XT (operation #1) with a advance speed at 0.205 m/s, the required thrust is 4,296 N and the energy consumption is 1,755 W-hr. In comparison, when the module travels at 0.25 m/s, the travelling time reduces, thereby saving energy consumption to 261 W-hr.

One high energy density battery of Li-ion battery technologies developed by Saft group, an advanced battery supplier, is selected to use in the estimation of the battery requirements , e.g. total quantity, weight and volume of batteries, for the operations. The VL 41M model is Li-ion battery suitable for underwater applications with excellent cycle life and high energy density – 136 Wh/kg [50]. The key characteristics of the VL 41M Li-ion battery can be found in table A-4 in appendix A. According to the table A-4, one cell can provide around 140 Wh with nominal voltage at 3.6 V and minimum current at 39 Ah. Table 8-6 shows the required battery packs for each operation with regard to minimum thrust requirement and minimum energy consumption.

Operation	Minimum thrust requirement			Minimum energy consumption		
	Required battery [kg]	Required battery [cell]	Required cells for 1 hr operation [cell]	Required battery [kg]	Required battery [cell]	Required cells for 1 hr operation [cell]
1.Deployment of the RT and WCP to XT	13	13	113	2	2	168
2.Retrieval of the RT back to the surface vessel	7	7	161	1	1	169
3.Deployment of the RT to WCP	12	12	103	2	2	166
4.Retrieval of the RT and WCP back to the surface vessel	N/A			N/A		

Table 8-6 A summary of battery requirement in the operations.

The total battery cells are estimated by combining the number of the batteries in operation #1 and #2, i.e. 20 cells for the minimum thrust case. The estimated energy capacity must be multiplied with some safety factor as several adjustments are required during the operations. However, it is difficult to determine the safety factor needed to be applied in the energy system according to several factors e.g. the RT and WCP positions, sea state, accuracy of the control system, etc.

From the previous results, it is possible to determine how much the reserved cells are needed to operate the RT for an hour. Based on the minimum energy consumption case, the reserved batteries for 1-hr operations for the operation #1 and #2 are equal to 168 cells and 169 cells respectively therefore the total reserved batteries are 337 cells or 350 kg. It is more conservative to estimate the cell requirement from the higher value. In addition, the estimations of energy system for the 1 hr-operations for the operation #1 and #2 are much higher than the previous estimated operational intervals, which are less than 1 minute, see table 8-5.

8.3.1 Conclusion

When considering system redundancy, it is prudent to install three steerable thrusters to enhance a system redundancy by 50 percent. With the three thrusters, the module will be able to travel at high speeds, minimizing overall energy consumption and translation interval. The maximum advance speed is limited by the thruster performance and sea state.

For a contingency plan, when one of the three thrusters fails, operating only two steerable thrusters can possibly accomplish the mission with a lower advance speed for the operation #1 and #3. However, the three thrusters must always be functional to accomplish the operation #2. The resultants from the #4 operation show that the thrusters are not applicable to control the RT and WCP module. During the #4 operation, the required thrust exceeds the thruster performance. In the shallow zone the RT and WCP module is subject to tremendous forces from waves and current. Additional systems are needed to be implemented to guide the RT and WCP module back to the moon pool during the operation #2 and #4.

Alternatively, the use of hydraulic motors can improve the performance of the thruster system. Hydraulic motors are generally more powerful than electrical ones and one hydraulic thruster system can provide thrust over 11,000 N[51], which is around 3 or 4 times more thrust than a electrical motor. Nevertheless, dealing with the available space for hydraulic subsystems and supplying hydraulic fluids will be challenges for the designer when implementing the hydraulic motors on the RT.

The energy consumption can vary from the estimations because there will be several adjustments due to uncertain variables in sea condition, control system and modules geometries. The sea condition is vastly dynamic, especially in the shallow zone where the direction and magnitude of forces due to waves are time variant. However, the energy supply is estimated by reserving the energy for 1-hour operations for each operation. Unlike AUVs or ROVs the total weight of the battery cells does not limits the capacity of the energy system; however the available space on the RT restricts the number of cells.

8.4 Physical Pendulum

According to the parameters in appendix A, the eigen period and frequency of the RT and WCP can be calculated using equation 6-13 and 6-14 in chapter 6. To simplify the calculation of moment of inertia, it is assumed that the geometry of the WCP is similar with a rectangular prism while the geometry of the RT and steel cable is assumed to be similar with a circular cylinder. The formula list of moment of inertia can be found in appendix B and the calculations are stored in the Excel file in the attachment.

Assuming that the position of the surface vessel is fixed and the effect of fluid viscosity is neglected. The eigen period and frequency of the system in shallow water can be determined as shown in figure 8-12.

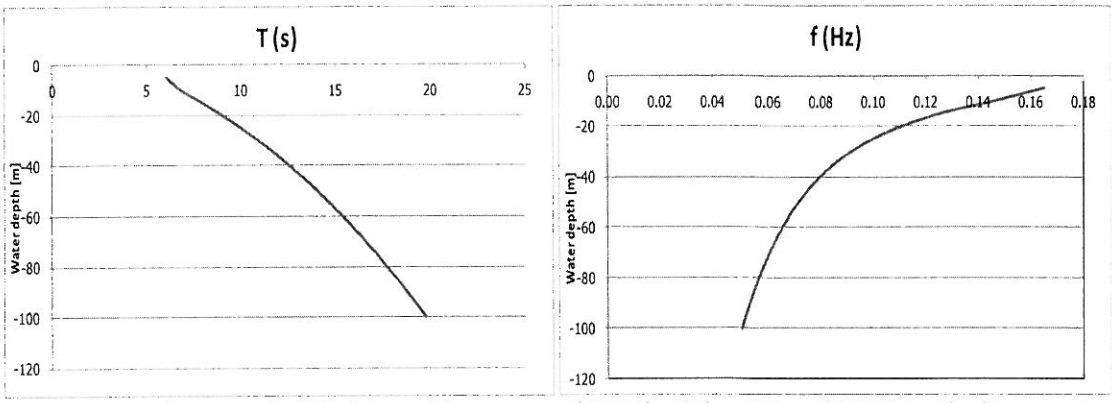

Figure 8-12 Eigen period (left) and frequency (right) of the RT and WCP in shallow water zones.

When the RT and WCP module is returned to the guide frame at 10 m water depths, the WCP may oscillate with 6.8 s period of pendulum. At the wave period equal to 9.7s, the critical water depth at which the WCP experience the maximum vibration is around 25 m water depths.

The frequency and period of pendulum are dependent on the length of the steel cable i.e. water depths. When water depth increases, the pendulum period increases whereas the pendulum frequency decreases.

Comments:

The above results are a rough estimation of eigen period and frequency of the RT and WCP in shallow water zones. In reality, the sea water is high viscous fluid resulting in a damping effect that will counteract against the oscillation of the system. So, the characteristic of the RT and WCP module may be not the same as physical pendulum and the eigen period may be longer than the above estimation.

In addition, since the surface vessel is always subjected to the environmental disturbances, the assumption of the fixed point cannot be valid. The real situation can be highly dynamic, thus analysis of eigan period would be complex.

9 Specification of the New Running Tool System

This chapter summarizes the essential applications for each system.

Thruster system

- Three DC brushless motors
- Three servo motors for steering units
- DC to DC converter
- Power monitor

Control system

- Autopilot control system and active surface controller
- Three controller systems for servo motors
- Three DC motor speed controllers

Navigation system

- MULBL for position tracking system
- HAIN system on the surface vessel
- INS system on the RT
    - Gyrocompass or fibre-optic gyrocompass (option)
    - Velocity sensor
    - Depth sensor (option)
    - Collision avoidance etc.

Communication system

- Underwater acoustic modems for hydroacoustic link.
- Direct connections for wire communication

Energy system

- VLM 41M Li-ion battery
- Energy monitor
- Umbilical connectors for the direct electricity from the surface

9.1 The Placement of the New Systems on the RT

This section illustrates the placement of the systems aforementioned on the RT. The placement of the thrusters is important in that the moment arm of their thrust forces, relative to the central mass of the vehicle, can improve maneuverability and controllability of the RT and WCP assembly. The larger the moment arm, the better the turning moment of the WCP module has. Therefore, the new three steerable thrusters can be placed on the RT frame as shown in figure 9-1.

According to the size of the thruster and the RT, a possible thruster placement proving the largest moment arm is around 950 mm radially from the center of the RT. However, the new systems attached on the RT must not restrict the operator's handing and ROV operations on the RT. The thrusters, for example, must not obstacle the access to the locking mechanism on the RT, see the red dash circular.

The other systems (e.g. battery packs, communication system and control system) can be placed around the RT under the thruster system as shown in figure 9-1. The room around the RT is roughly 0.3 m^3, at which battery cells and other electric systems are sufficiently stored here. This room could be used to store VL 41M battery as much as 600 cells.

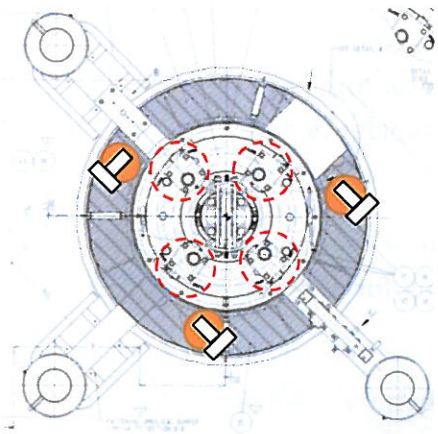

Figure 9-1 The placement of the thruster system on the RT.

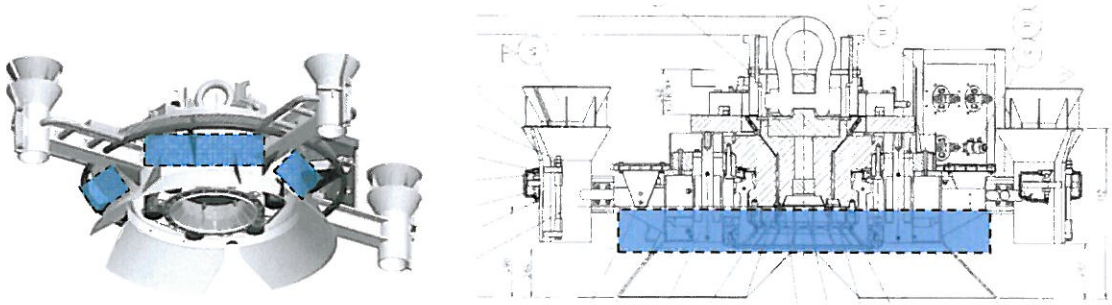

Figure 9-2 The placement of the battery system and the other systems on the RT.

Finally, the weight distribution of the new systems must be considered to prevent the change of the center of gravity of the RT.

10 Conclusions and Future Works

10.1 Conclusions

A discussion on the subsystems and the outcomes accomplished in this thesis is presented in this section.

During deploying the WCP without UTH to the XT at 3,000 m water depths, the maximum environmental force the RT and WCP will experience is around 4.1 kN while when deploying the WCP with UTH to the XT at the same depths, the maximum environmental force the RT and WCP will increase to 10.6 kN. When retrieving the RT and WCP without UTH at 10 m water depths, the maximum force on the RT and WCP is around 103 kN. In the shallow zone, there will be inertia force affecting on the RT and WCP module and the water particle velocity is much higher than in the deepwater zone.

The estimation of the drag and inertia forces may vary from the real situation due to uncontrolled variables such as the direction and magnitude of sea current and waves. However the large forces the RT and WCP module experience are when they are being deployed and retrieved in the shallow zone.

When the RT and WCP are in an ultra-deepwater area, small diameter steel cable is favorable to reduce the projected area, a main parameter generating large loads on the system. The composite materials can enhance the strength of the steel cable. The higher strength of the steel cable implies that the diameter of the string can be reduced and the total load on the system can be reduced. Hence, the operational limitation of the new RT can be extended based on the same thruster performance.

It is recommended that the deployment and retrieval of the WCP should be done without UTH to eliminate the drag from the two umbilicals and reduce the complexity of the operations (e.g. heading control of the WCP). The thrust from electric thrusters would not be sufficient to control the WCP as the maximum drag can exceed the thruster performance. Otherwise, the hydraulic thruster system may be introduced to yield more thrust to meet the requirement.

Thruster system

The bollard pull of thrusters and drag forces acting on the system determine the limitation of the new RT operation. The more powerful the thruster system of the RT, the stronger the sea current in which the RT can operate.

When the module travels at a low speed, it can minimize the thrust requirements but the thrusters will have long operational interval and consume large energy. To increase the advance speed of the module, the three steerable thrusters becomes the new design concept for the thruster system and they are expected to provide the maximum thrust around 6.5 kN. The three steerable thrusters are able to accomplish a wide range of RT

maneuvers while providing simplicity, modularization and redundancy being prime aspects in the design.

Control system

The characteristics of a control system for the RT should be of low output error and low overshooting with a quick response. The mathematical modeling of the hydrodynamic effects on marine vehicles can normally yield reasonable results. The algorism in control systems must be highly reliable and robust. In addition, as far as energy constraint of the RT system is concerned, an incorrect control model could cause loss of the energy, which finally could result in the loss of mobility.

Communication system

The implementation of hydroacoustic communication system may not show a sign of efficient system as the long transmission interval of signal can be the main problem during critical operations. For example, during stacking WCP onto the XT re-entry hub, the signal for controlling the thruster system will lack least 2 seconds after transmitted from the operator on the surface vessel.

An alternative practice is to connect an umbilical to the RT system by using ROV when the WCP is close to the XT to provide direct communication path and electricity for this critical operation. However, connecting the wire could be challenging operations while maneuvering the WCP and ROV.

Navigation system

The LBL system is suitable for the missions and works well in deep water operations as the SSBL system is inherently less accurate than the LBL system. The navigation system can be better by replacing the LBL system with the MULBL concept to reduce transponders employed in the field. The HAIN can also help to improve the accuracy of the navigation system.

Energy system

The properties of the Li-ion battery are superior among others, so the Li-ion battery is the chosen battery for the RT system. The energy density of the Li-ion can be higher than 130 Wh/kg. In addition, an umbilical connector should be available to supply energy and control signal from the surface vessel.

Compared to other systems, the thruster system is the main energy consumer on the RT. By considering the reserved energy needed to operate the RT for 1-hr operations for operation #1 and #2, the estimated reserved battery cells are 337 cells or 350 kg. These cells can provide abundant energy reserve for the thruster system and other systems. Furthermore, it is still possible to store more cells depending on the available room on the RT. Unlike AUVs or ROVs the total weight of the battery cells does not limits the capacity of the energy system; however the available space on the RT restricts the number of cells.

10.2 Future Works

This section presents suggestions for further work and investigation.

According to the tremendous environmental loads on the RT and WCP module in the shallow zone, the thruster system cannot provide enough thrust to control the movement of the RT and WCP module during the retrieval operation. The guide frame system need to be modified to assist the retrieval operation.

The ideal communication system is to transmit and receive data with real-time feedback. During adjusting the WCP onto the XT re-entry hub, the lack of real-time transmission demands that the communication and the control system should be more improved. The hydroacoustic link will take over 2 seconds to transmit the signal to the RT at 3,000 m water depths. A possibility of implementing the communications system through a dedicated line from the surface vessel or ROV umbilical should be further evaluated.

One should also study a possibility of implementing sliding bars at the XT adapter to assist the alignment operation between all pairs of guide frames (at XT adapter) and guideposts (at XT). The XT adapter with the sliding bars would limit the WCP motion in only 1 DOF (vertical movement) rather than 2 DOFs (horizontal and vertical movements) while stacking WCP on the XT en-entry hub.

The linear wave theory may not be applicable to non-linear conditions for the shallow water zone. Extensional simulations to the linear wave theory should be evaluated to improve the numerical models for the calculation of related forces.

The majority of future work in control system will involve in modeling of the RT and WCP and implementing the control system for the RT. Further investigations and model tests are required to determine correct parameters for the system. The identification of the model parameters need to be accomplished by analysis of scaled models. A combination empirical formulas, model tests and computational fluid dynamic (CFD) can be used to compare the result.

11 References

1. Jensen, Ø. *Riserless Light Well Intervention/RLWI - "A successful and efficient well intervention system for subsea completed fields".* 2008 [cited 2009 24 March]; Available from: http://aberdeen.spe.org/images/aberdeen/setup/18Nov%2015.30%20Riserless%20ight%20well%20intervention%20Oyvin%20Jensen,%20StatoilHydro.pdf.
2. *Description RLWI Mk II.* 2008, FMC Technologies.
3. Ligård, P., *INCREASED OIL RECOVERY WITH RLWI AND TTRD TECHNOLOGY*, in *PETROTECH.* 2009.
4. Mathiaseen, E., P.K. Munkerud, and H.B. Ske, *Well Intervention in Deep waters*, in *Offshore Technology Conference.* 2008: Houston, Texas, U.S.A.
5. Lindland, H.J., et al., *New Well Intervention Technology That Will Enable Increase In Recovery Rate*, in *Offshore Technology Conference.* 2003: Houston, Texas, U.S.A.
6. . 2009, FMC Production Services AS.
7. ISO, *Petroleum and natural gas industries -- Design and operation of subsea production systems -- Part 1: General requirements and recommendations.* Vol. ISO 13628-1: 2005. 2005.
8. *PID controller.* 2009 [cited 2009 17 February]; Available from: http://en.wikipedia.org/wiki/PID_controller.
9. Fossen, T.I., *Marine control systems: guidance, navigation and control of ships, rigs and underwater vehicles.* 2002, Trondheim: Marine Cybernetics. XIV, 570 s.
10. van de Ven, P.W.J., et al., *Neural network augmented identification of underwater vehicle models.* Control Engineering Practice, 2007. **15**(6): p. 715-725.
11. Ridao, P., et al., *On the identification of non-linear models of unmanned underwater vehicles.* Control Engineering Practice, 2004. **12**(12): p. 1483-1499.
12. Fossen, T.I., *Guidance and control of ocean vehicles.* 1994, Chichester: Wiley. XIV, 480 s.
13. Ridao, P., J. Batlle, and M. Carreras (2001) *MODEL IDENTIFICATION OF A LOW-SPEED UUV.*
14. *Instruction Manual - Introduction to underwater acoustics.* 2004, Kongsberg Maritime AS.
15. Crocker, M.J., *Handbook of acoustics.* 1998.
16. Elson, S., et al., *Underwater Communication, Navigation and Positioning in the Waters of Tomorrow* in *SPE Asia Pacific Oil and Gas Conference and Exhibition,.* 2004: Perth, Australia.
17. *Acoustic underwater positioning and navigation systems HiPAP and HPR* 2009 [cited 2009 19 February]; Available from: http://www.km.kongsberg.com/ks/web/NOKBG0240.nsf/AllWeb/FF57C18363FAD917C1256A7E002B9F2F?OpenDocument.
18. *Multi-User Long Base Line system.* [cited 2009 28 March]; Available from: http://www.km.kongsberg.com/ks/web/nokbg0397.nsf/AllWeb/C5FFDB36405C8EE3C1256C390046A6A6/$file/160057ad_MULBL_Product_specification.pdf?OpenElement.
19. Berntsen, M., *Hydroacoustic Aided Inertial Navigation System- HAIN A New Reference for DP*, in *DYNAMIC POSITIONING CONFERENCE.* 2007.
20. Griffiths, G., *Technology and applications of autonomous underwater vehicles.* 2003, London: Taylor & Francis. xviii, 342 s.
21. *HAIN Hydroacoustic Aided Inertial Navigation (Instruction Manual).* 2008 [cited 2009 19 February]; Available from:

http://www.km.kongsberg.com/ks/web/nokbg0397.nsf/AllWeb/9D7909B2241E7635C12574FE00374DF8/$file/164951ae-Hain-Instruction-manual.pdf?OpenElement.
22. Christ, R.D. and R.L. Wernli, *The ROV manual: a user guide for observation-class remotely operated vehicles*. 2007, Amsterdam: Elsevier. XVIII, 308 s.
23. *SoundLink Underwater Acoustic Modems*. [cited 2009 3 June]; LinkQuest Inc.]. Available from: http://www.link-quest.com/html/uwm_hr.pdf.
24. ZPower. *ZPower FAQs*. 2008 [cited 2009 19 February]; Available from: http://www.zpowerbattery.com/about/faq.htm.
25. Hawley, J.G., *Design aspects of underwater intervention systems*. 1996, Dubuque, Iowa: Kendall/Hunt. 1 b. (flere pag.).
26. Ramirez, J.A., et al. *Mechanical/naval design of an underwater remotely operated vehicle (ROV) for surveillance and inspection of port facilities*. 2008. New York, NY 10016-5990, United States: American Society of Mechanical Engineers.
27. *ROV chronicles*. 2008 [cited 2009 15 May]; Available from: http://dinkykitty.com/articles/rov/32-rov-chronicles-5-motors-and-controllers.
28. *Thrusters*. 2007 [cited 2009 8 April]; Available from: http://me-wserver.mecheng.strath.ac.uk/group2006/groupg/D12.pdf.
29. Workshop on Future Research Directions in Underwater, R. *Underwater robotic vehicles: design and control*. Albuquerque, N.M.: TSI Press.
30. Christ, R.D. and S. Robert L. Wernli. *Components of an ROV system - Part 1: Mechanical and electromechanical systems*. 2009 [cited 2009 13 April]; Available from: http://www.industrialcontroldesignline.com/howto/roboticsprototyping/215800262%3Bjsessionid=NTCQMAJ5BNEWAQSNDLQCKHSCJUNN2JVN?pgno=3.
31. Emadi, A., *Handbook of automotive power electronics and motor drives*. 2005: CRC Press.
32. Valentine, R., *Motor control electronics handbook*. 1998.
33. *Power Controller*. 2008 [cited 1 May 2009]; Available from: http://www.greenenergytechnologies.eu/productlist/22.
34. DNV, *ENVIRONMENTAL CONDITIONS AND ENVIRONMENTAL LOADS DNV-RP-C205*. 2007, Norway: Det Norske Veritas.
35. Harris, J.W., et al., *Handbook of physics*. 2002: Springer.
36. Indiveri, G., *Modelling and Identification of Underwater Robotics Systems*, in *Electronic Engineering and Computer Science*. 1998, University of Genova.
37. Gonzalez, L.A., *DESIGN, MODELLING AND CONTROL OF AN AUTONOMOUS UNDERWATER VEHICLE*, in *Centre for Intelligent Information Processing Systems, School of Electrical, Electronic and Computer Engineering,*. 2004, University of Western Australia.
38. Nickell, C.L., *Modular Modification of a Buoyant AUV for Low-Speed Operation*, in *the Faculty of the Virginia Polytechnic Institute and State University*. 2005: Virginia.
39. Berg, T.E., *Marine operations: submarines, AUVs, UUVs and ROVs*. 2007, [Trondheim]: Department of Marine Technology. 1 b. (flere pag.).
40. Breivik, M. *Mathematical Modelling Part 2*. 2009 [cited 2009 11 February]; Lecture note: TMR4240 Marine Control Systems]. Available from: http://www.ivt.ntnu.no/imt/courses/tmr4240/.
41. Bessa, W.M., M.S. Dutra, and E. Kreuzer, *Depth control of remotely operated underwater vehicles using an adaptive fuzzy sliding mode controller*. Robotics and Autonomous Systems, 2008. **56**(8): p. 670-677.
42. Gyory, J., et al. *The Angola Current*. [cited 2009 29 March]; Available from: http://oceancurrents.rsmas.miami.edu/atlantic/angola.html.

43. Patel, D. *SubseaUmbilicalsand Power Cables.* 2008 [cited 2009 20 March]; STEEGELecture 44]. Available from: http://www.steegekingston.co.uk/lecture44.pdf.
44. Friedberg, R., *Second Generation Well Intervention Units* 2006.
45. *SEA MAX TH-8000 Thruster.* [cited 2009 1 March]; Deep Sea Systems International, Inc.]. Available from: http://www.dssi.gexrov.com/8000.htm.
46. *Model 8020 DC BRUSHLESS THRUSTERS.* [cited 2009 1 March]; Tecnadyne]. Available from: http://www.tecnadyne.com/Brochure/Model%208020%20Brochure.pdf.
47. *SPE 380 Thruster.* 2009 [cited 2009 1 March]; Sub-Atlantic]. Available from: http://www.sub-atlantic.co.uk/userfiles/file/DC_Thruster_Drawings.pdf.
48. *THL 404-8 Sea Horse, a True Servo Thruster.* 1998 [cited 2009 1 March]; Available from: http://www.deepseasystems.com/thl404-8d.htm.
49. *Seaeye Brushless DC Thrusters.* [cited 2009 1 March]; Available from: http://www.seaeye.com/thrusters.html.
50. *Lithium-ion (Li-ion) - Large VLM cell range.* [cited 2009 1 May]; Saft group]. Available from: http://www.saftbatteries.com/MarketSegments/Marinedefence/tabid/154/Language/en-US/tabid/301/TypeControl/Produit/ProduitId/62/Default.aspx.
51. *HYDRAULIC THRUSTERS.* [cited 2009 1 April]; SMD]. Available from: http://www.smd.co.uk/products/thrusters.php.
52. Newman, J.N., *Marine hydrodynamics.* 1977, Cambridge, Mass.: MIT Press. xiii, 402 s.
53. *Mass Moment of Inertia Table.* [cited 2009 20 March]; Available from: http://web2.clarkson.edu/class/me324/MassMomInertiaTable.pdf.

Appendix A Key Parameters

Key Parameters

Parameters	Value	Unit
Current speed at the sea level	0.7	m/s
Wave Peak period (Tp)	9.7	s
Significant wave height wave height (Hs)	3	m

Table A-1 Maximum environmental condition[44].

Parameters	Value	Unit
The final adjustment between the WCP and XT	2	m.
WCP mass (in air)	50,000	[kg]
Width of WCP footprint	3.7	[m]
Length of WCP foot print	3.7	[m]
WCP height	4.7	[m]
$C_a$of WCP*	0.6	
C_d of WCP	1	
Existing RT mass (in air)	5,000	[kg]
Existing RT diameter	1.4	[m]
Existing RT height	1	[m]
$C_a$of RT*	0.64	
C_d of RT	1	
Steel cable	14	[kg/m]
Steel cable diameter	0.05	[m]
Chemical umbilical	10	[kg/m]
Chemical umbilical diameter	0.051	[m]
Control umbilical	2.5	[kg/m]
Control umbilical diameter	0.032	[m]
$C_a$of steel cable, chemical umbilical and control umbilical	1	
$C_d$of steel cable, chemical umbilical and control umbilical	1	
Wavelength (λ)	147	m
Wave number (k)	0.0428	m−1
Wave height (H)	5.6	m
$\lambda/5$	29.4	m
H/λ	0.038	

Table A-2 Key parameters for conceptual design.

*The values are mathematically interpolated from the appendix in DNV[34].

	WCP	RT	Steel cable
$\pi D/\lambda$	0.08	0.03	0.001
H/D	1.51	4	112

Table A-3 Calculated parameters and properties.

According to the table A-1 and A-2, the following parameters can be calculated.

Electrical characteristics	value	unit
Nominal voltage	3.6	[V]
Average capacity C/3 after charge to 4.0 V/cell	41	[Ah]
Minimum capacity C/3 after charge to 4.0 V/cell	39	
Specific energy after charge to 4.0 V/cell	136	Wh/kg
Energy density after charge to 4.0 V/cell	285	Wh/dm^3
Mechanical characteristics		
Diameter	54.3	[mm]
Height	222	[mm]
Typical weight	1.07	[kg]
Volume	0.51	$[dm^3]$

Table A-4 Key characteristics of VL 41M lithium-ion battery[50].

Appendix B Formula

Linear wave equation

Parameter	*Airy wave theory*		*Stokes second-order wave theory*
	General water depth	*Deep water*	
Velocity potential, φ	$\frac{\pi H}{kT}\frac{\cosh[k(z+d)]}{\sinh(kd)}\sin\theta$ = $\frac{gH}{2\omega}\frac{\cosh[k(z+d)]}{\cosh(kd)}\sin\theta$	$\frac{\pi H}{kT}e^{kz}\sin\theta$ = $\frac{gH}{2\omega}e^{kz}\sin\theta$	$\varphi_t+\frac{3}{8}\frac{\pi H}{kT}\left(\frac{\pi H}{\lambda}\right)\frac{\cosh[2k(z+d)]\sin 2\theta}{\sinh^4(kd)}$ Note that in deep water the Stokes second-order wave potential is equal to the first order Airy wave potential
Phase velocity, celerity, c	$\sqrt{\frac{g}{k}\tanh(kd)}$	$gT/(2\pi)$	$\sqrt{\frac{g}{k}\tanh(kd)}$
Wavelength, λ	cT	$gT^2/(2\pi)$	cT
Surface elevation, η	$\frac{H}{2}\cos\theta$	$\frac{H}{2}\cos\theta$	$\eta_t+\frac{\pi H^2}{8\lambda}\frac{\cosh kd}{\sinh^3 kd}[2+\cosh 2kd]\cos 2\Theta$
Horizontal particle displacement, ξ	$-\frac{H}{2}\frac{\cosh[k(z+d)]}{\sinh(kd)}\sin\theta$	$-\frac{H}{2}e^{kz}\sin\theta$	$\xi_t+\frac{H}{8}\left(\frac{\pi H}{\lambda}\right)\frac{1}{\sinh^2(kd)}\left\{1-\frac{3\cosh[2k(z+d)]}{2\sinh^2(kd)}\right\}\sin 2\theta$ $+\frac{H}{4}\left(\frac{\pi H}{\lambda}\right)\frac{\cosh[2k(z+d)]}{\sinh^2(kd)}(\omega t)$
Vertical particle dis-placement, ζ	$-\frac{H}{2}\frac{\sinh[k(z+d)]}{\sinh(kd)}\cos\theta$	$\frac{H}{2}e^{kz}\cos\theta$	$\zeta_t+\frac{3H}{16}\left(\frac{\pi H}{\lambda}\right)\frac{\sinh[2k(z+d)]}{\sinh^4(kd)}\cos 2\theta$
Horizontal particle velocity, u	$\frac{\pi H}{T}\frac{\cosh[k(z+d)]}{\sinh(kd)}\cos\theta$	$\frac{\pi H}{T}e^{kz}\cos\theta$	$u_t+\frac{3}{4}\frac{\pi H}{T}\left(\frac{\pi H}{\lambda}\right)\frac{\cosh[2k(z+d)]}{\sinh^4(kd)}\cos 2\theta$
Vertical particle velocity, w	$\frac{\pi H}{T}\frac{\sinh[k(z+d)]}{\sinh(kd)}\sin\theta$	$\frac{\pi H}{T}e^{kz}\sin\theta$	$w_t+\frac{3}{4}\frac{\pi H}{T}\left(\frac{\pi H}{\lambda}\right)\frac{\sinh[2k(z+d)]}{\sinh^4(kd)}\sin 2\theta$
Horizontal particle acceleration, $\dot{u}$	$\frac{2\pi^2 H}{T^2}\frac{\cosh[k(z+d)]}{\sinh(kd)}\sin\theta$	$\frac{2\pi^2 H}{T^2}e^{kz}\sin\theta$	$\dot{u}_t+\frac{3\pi^2 H}{T^2}\left(\frac{\pi H}{\lambda}\right)\frac{\cosh[2k(z+d)]}{\sinh^4(kd)}\sin 2\theta$
Vertical particle acceleration, $\dot{w}$	$-\frac{2\pi^2 H}{T^2}\frac{\sinh[k(z+d)]}{\sinh(kd)}\cos\theta$	$-\frac{2\pi^2 H}{T^2}e^{kz}\cos\theta$	$\dot{w}_t-\frac{3\pi^2 H}{T^2}\left(\frac{\pi H}{\lambda}\right)\frac{\sinh[2k(z+d)]}{\sinh^4(kd)}\cos 2\theta$
Subsurface pressure, p	$-\rho gz+\frac{1}{2}\rho gH\frac{\cosh[k(z+d)]}{\cosh(kd)}\cos\theta$	$-\rho gz+\frac{1}{2}\rho gHe^{kz}\cos\theta$	$p_t+\frac{3}{4}\rho gH\frac{\pi H}{\lambda\sinh(2kd)}\left\{\frac{\cosh[2k(z+d)]}{\sinh^2(kd)}-\frac{1}{3}\right\}\cos 2\theta$ $-\frac{1}{4}\rho gH\frac{\pi H}{\lambda\sinh(2kd)}\{\cosh[2k(z+d)]-1\}$
Group velocity, c_g	$\frac{c}{2}\left\{1+\frac{2kd}{\sinh(2kd)}\right\}$	$\frac{c}{2}$	$(c_g)_t$
Average energy density, E	$\frac{1}{8}\rho gH^2$	$\frac{1}{8}\rho gH^2$	$\frac{1}{8}\rho gH^2$
Energy flux, F	Ec_g	$\frac{1}{2}Ec$	Ec_g
Notation: d = mean water depth; g = acceleration of gravity; H = trough-to-crest wave height; $k=2\pi/\lambda$ = wave number; λ = wave length; T = wave period; t = time; x = distance of propagation; z = distance from mean free surface positive upward; $\theta=kx-\omega t=k(x-ct)$; $\omega=2\pi/T$ = angular wave frequency. Subscript t denotes linear small-amplitude theory. (Continued) (Continued) (Continued)			

Table B-1 Gravity wave theory[34].

Added Mass Forces and Moments

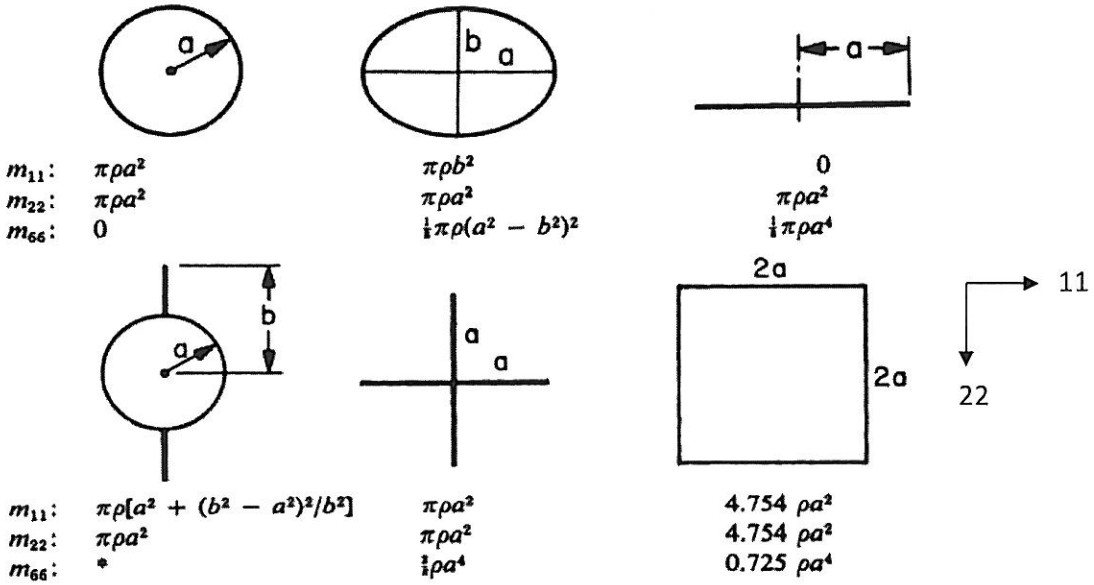

m_{11}:	$\pi\rho a^2$	$\pi\rho b^2$	0
m_{22}:	$\pi\rho a^2$	$\pi\rho a^2$	$\pi\rho a^2$
m_{66}:	0	$\frac{1}{8}\pi\rho(a^2 - b^2)^2$	$\frac{1}{8}\pi\rho a^4$
m_{11}:	$\pi\rho[a^2 + (b^2 - a^2)^2/b^2]$	$\pi\rho a^2$	4.754 ρa^2
m_{22}:	$\pi\rho a^2$	$\pi\rho a^2$	4.754 ρa^2
m_{66}:	*	$\frac{3}{8}\rho a^4$	0.725 ρa^4

Figure B-1 A list of added-mass coefficient for various two-dimensional bodies[52].

*For the finned circle the added moment of inertia is given by the formula

$$m_{66} = \rho a^4(\pi^{-1}csc^4\alpha\left[2\alpha^2 - \alpha sin4\alpha + \frac{1}{2}sin^2 2\alpha\right] - \frac{\pi}{2}) \qquad \textbf{B-1}$$

Where

$$\alpha = \frac{2ab}{a^2+b^2} and \frac{\pi}{2} < \alpha < \pi \qquad \textbf{B-2}$$

Formula list of moment of inertia[53]

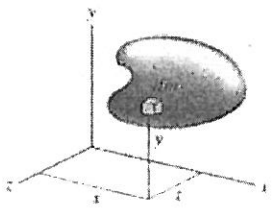

The mass moments of inertia of the object in terms of the xyz coordinate system are

$$I_{(x\text{ axis})} = I_{xx} = \int_m (y^2 + z^2)\, dm,$$

$$I_{(y\text{ axis})} = I_{yy} = \int_m (x^2 + z^2)\, dm,$$

$$I_{(z\text{ axis})} = I_{zz} = \int_m (x^2 + y^2)\, dm$$

$$I_{xy} = \int_m xy\, dm, \qquad I_{yz} = \int_m yz\, dm.$$

$$I_{zx} = \int_m zx\, dm$$

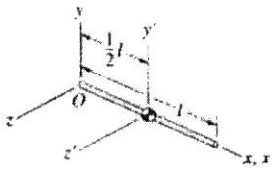

Slender Bar

$$I_{(x\text{ axis})} = 0, \qquad I_{(y\text{ axis})} = I_{(z\text{ axis})} = \frac{1}{3}ml^2.$$

$$I_{xy} = I_{yz} = I_{zx} = 0.$$

$$I_{(x'\text{ axis})} = 0, \qquad I_{(y'\text{ axis})} = I_{(z'\text{ axis})} = \frac{1}{12}ml^2.$$

$$I_{x'y'} = I_{y'z'} = I_{z'x'} = 0$$

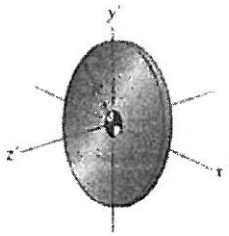

Thin Circular Plate

$$I_{(x'\text{ axis})} = I_{(y'\text{ axis})} = \frac{1}{4}mR^2, \qquad I_{(z'\text{ axis})} = \frac{1}{2}mR^2.$$

$$I_{xy} = I_{yz} = I_{zx} = 0$$

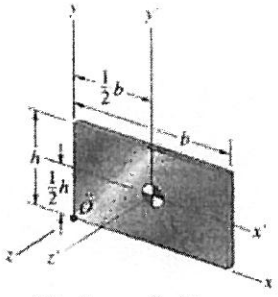

Thin Rectangular Plate

$$I_{(x\text{ axis})} = \frac{1}{3}mh^2, \qquad I_{(y\text{ axis})} = \frac{1}{3}mb^2, \qquad I_{(z\text{ axis})} = \frac{1}{3}m(b^2 + h^2).$$

$$I_{xy} = \frac{1}{4}mbh, \qquad I_{yz} = I_{zx} = 0.$$

$$I_{(x'\text{ axis})} = \frac{1}{12}mh^2, \qquad I_{(y'\text{ axis})} = \frac{1}{12}mb^2 \qquad I_{(z'\text{ axis})} = \frac{1}{12}m(b^2 + h^2)$$

$$I_{x'y'} = I_{y'z'} = I_{z'x'} = 0.$$

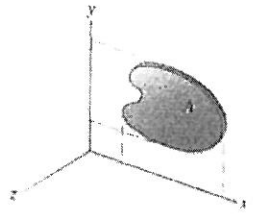

Thin Plate

$$I_{(x\text{ axis})} = \frac{m}{A} I_x^A, \qquad I_{(y\text{ axis})} = \frac{m}{A} I_y^A \qquad I_{(z\text{ axis})} = I_{(x\text{ axis})} + I_{(y\text{ axis})},$$

$$I_{xy} = \frac{m}{A} I_{xy}^A, \qquad I_{yz} = I_{zx} = 0$$

(The superscripts A denote moments of inertia of the plate's cross-sectional area A.)

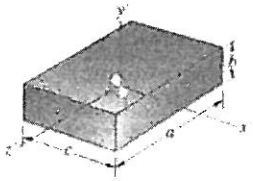

Rectangular Prism

$$\text{Volume} = abc$$

$$I_{(x'\text{ axis})} = \frac{1}{12} m(a^2 + b^2), \qquad I_{(y'\text{ axis})} = \frac{1}{12} m(a^2 + c^2),$$

$$I_{(z'\text{ axis})} = \frac{1}{12} m(b^2 + c^2), \qquad I_{x'y'} = I_{y'z'} = I_{z'x'} = 0$$

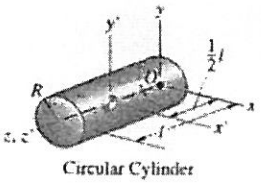

Circular Cylinder

$$\text{Volume} = \pi R^2 l$$

$$I_{(x\text{ axis})} = I_{(y\text{ axis})} = m\left(\frac{1}{3} l^2 + \frac{1}{4} R^2\right), \qquad J_{(z\text{ axis})} = \frac{1}{2} m R^2$$

$$I_{xy} = I_{yz} = I_{zx} = 0,$$

$$I_{(x'\text{ axis})} = I_{(y'\text{ axis})} = m\left(\frac{1}{12} l^2 + \frac{1}{4} R^2\right), \qquad I_{(z'\text{ axis})} = \frac{1}{2} m R^2,$$

$$I_{x'y'} = I_{y'z'} = I_{z'x'} = 0$$

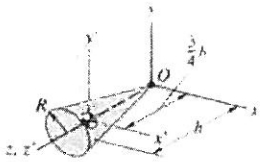

Circular Cone

$$\text{Volume} = \frac{1}{3} \pi R^2 h$$

$$I_{(x\text{ axis})} = I_{(y\text{ axis})} = m\left(\frac{3}{5} h^2 + \frac{3}{20} R^2\right), \qquad I_{(z\text{ axis})} = \frac{3}{10} m R^2,$$

$$I_{xy} = I_{yz} = I_{zx} = 0,$$

$$I_{(x'\text{ axis})} = I_{(y'\text{ axis})} = m\left(\frac{3}{80} h^2 + \frac{3}{20} R^2\right), \qquad I_{(z'\text{ axis})} = \frac{3}{10} m R^2,$$

$$I_{x'y'} = I_{y'z'} = I_{z'x'} = 0$$

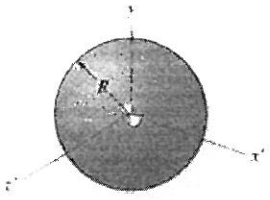

Sphere

$$\text{Volume} = \frac{4}{3} \pi R^3$$

$$I_{(x'\text{ axis})} = I_{(y'\text{ axis})} = I_{(z'\text{ axis})} = \frac{2}{5} m R^2,$$

$$I_{x'y'} = I_{y'z'} = I_{z'x'} = 0$$

Appendix C Assumptions of the Moments on RT and WCP Module

Assumptions of the Moment on the WCP

The following figures are assumed to be side areas of WCP to demonstrate an approach to obtain a moment caused by current-induced force.

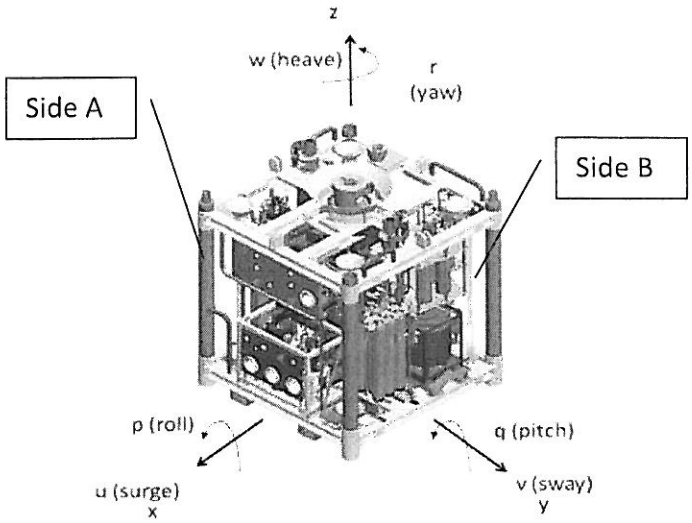

Figure C-1 Sketch of side A and B on WCP.

Uniform currents are assumed to act on only one horizontal side of the WCP at each time. The projected area along x axis is referred to side A, whereas the projected area along y axis is referred to side B. The WCP module is assumed to have xz-symmetry plan, see figure C-2. When a uniform current acts on the projected area A, area along x-axis, the net moment around vertical axis should be zero. The drag forces acting in x-direction cannot cause rotation because the WCP module has xz-symmetry plan.

In contrast, the WCP is asymmetry on y-z plan, see figure C-2, thus when uniform currents flow though the projected area B, the module can rotate if currents flow in the y- direction.

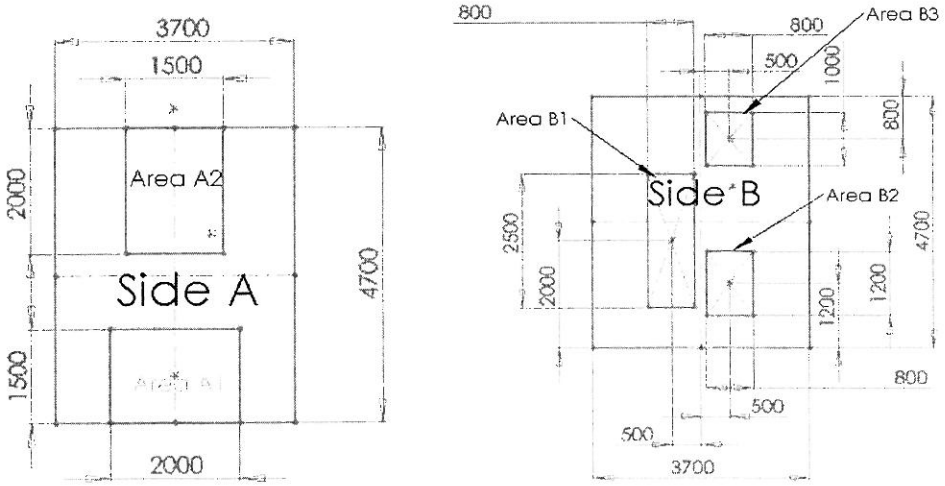

Figure C-2 The projected area side A (left) and side B (right).

From the figure C-2, the net moment can be calculated by finding clockwise and counterclockwise moments around z-axis. The moments are equal a sum of products of drag forces and projected areas on the side:

$$\boldsymbol{M = \sum F_d \cdot r_m} \quad \textbf{C-1}$$

Where

F_d = net drag forces [N]

r_m = moment arm (the distance between the center line of the side B and the center of each projected area) [m]

In case the uniform current flows are perpendicular to the side B.

The clockwise moment is give by:

$$\boldsymbol{M_c = \frac{1}{2} \cdot C_d \cdot \rho \cdot A_{B1} \cdot v_r \cdot |v_r| \cdot r_{m,B1}} \quad \textbf{C-2}$$

Where

M_c = clockwise moment around z-axis [Nm]

A_{B1} = projected area on B1 [m^2]

= $2{,}500 \cdot 800 = 2{,}000{,}000\ mm^2 = 2[m^2]$

$r_{m,B1}$ = the distance between the center line of the side B and the center of area B1 = 0.5 [m]

The clockwise moment around z-axis is:

$$\boldsymbol{M_c = 0.50 \cdot C_d \cdot \rho \cdot v_r \cdot |v_r|} \quad \textbf{C-3}$$

The counterclockwise moment is give by:

$$\boldsymbol{M_{cc} = \left[\frac{1}{2} \cdot C_d \cdot \rho \cdot A_{B2} \cdot v_r \cdot |v_r| \cdot r_{m,B2}\right] + \left[\frac{1}{2} \cdot C_d \cdot \rho \cdot A_{B3} \cdot v_r \cdot |v_r| \cdot r_{m,B3}\right]} \quad \textbf{C-4}$$

Where

M_{cc} = counter clockwise moment around z-axis [Nm]

A_{B2} = projected area on B2 [m^2]

= $1{,}200 \cdot 800 = 960{,}000\ mm^2 = 0.96$ [m^2]

$r_{m,B2}$ = the distance between the center line of the side B and the center area of area B2 = 0.5 [m]

A_{B3} = projected area on B3 [m^2]

= $1{,}000 \cdot 800 = 800{,}000\ mm^2 = 0.8$ [m^2]

$r_{m,B3}$ = the distance between the center line of the side B and the center area of area B3 = 0.5 [m]

The clockwise moment around z-axis is:

$$\boldsymbol{M_{cc} = 0.44 \cdot C_d \cdot \rho \cdot v_r \cdot |v_r|} \quad \textbf{C-5}$$

The net moment around z-axis is equal:

$$\boldsymbol{M = M_c - M_{cc}} \quad \textbf{C-6}$$

$$\boldsymbol{M = [0.50 \cdot C_d \cdot \rho \cdot v_r \cdot |v_r|] - [0.44 \cdot C_d \cdot \rho \cdot v_r \cdot |v_r|]} \quad \textbf{C-7}$$

$$\boldsymbol{M = 0.06 \cdot C_d \cdot \rho \cdot v_r \cdot |v_r|} \quad \textbf{C-8}$$

Hence, the module starts to rotate in clockwise direction around z-axis with the magnitude of moment equal to $M = 0.06 \cdot C_d \cdot \rho \cdot v_r \cdot |v_r|$ [Nm].

Assumptions of the Moment on the RT

When considering projected area on the RT, there are two main parts that can cause rotation; ROV receptacle on WCP RT and a guide frame **as shown below.**

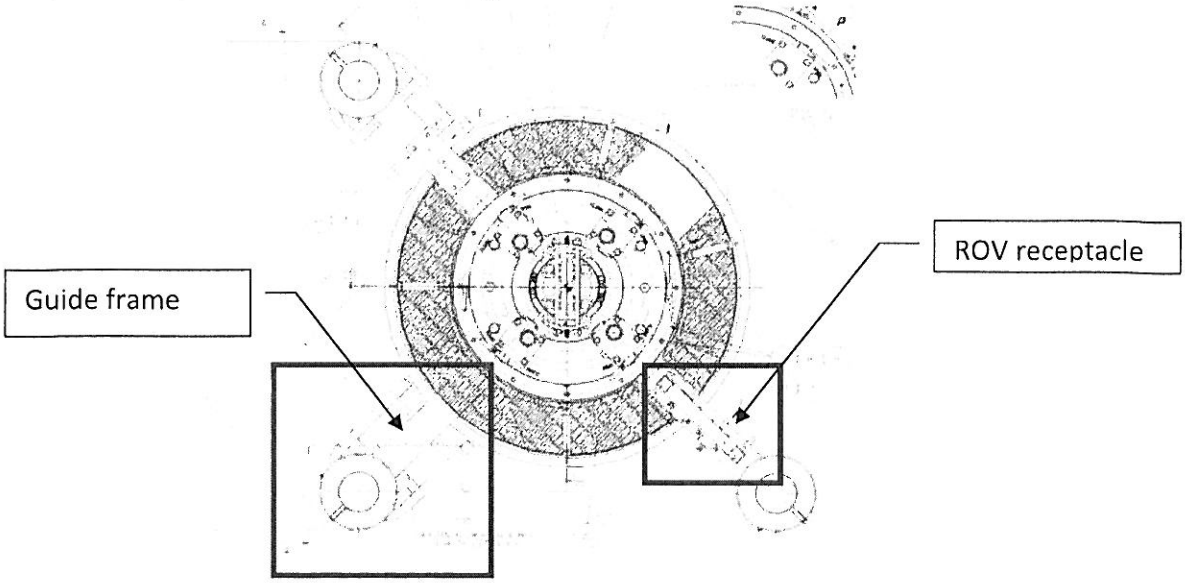

Figure C-3 RT from the top view [6].

1 The moment caused by the force acting on the ROV receptacle is:

$$M_r = -\frac{1}{2} \cdot C_d \cdot \rho \cdot A_r \cdot v_r \cdot |v_r| \cdot r_m \qquad \textbf{C-9}$$

Where

M_r = moment around z-axis [Nm]

C_d = 2

A_r = projected area on ROV receptacle [m^2] = $0.69 \cdot 0.69 = 0.476\ m^2$

$r_{m,r}$ = the distance between the center line of the RT and the center of the ROV receptacle = 1.15 [m]

The moment caused by ROV receptacle is:

$$M_r = 0.55 \cdot \rho \cdot v_r \cdot |v_r| \qquad \textbf{C-10}$$

2 The guide frame is made by the force acting on the two main parts; the funnel and I-beam frame. The moment can be written by:

$$M_a = M_{a1} + M_{a2} \qquad \textbf{C-11}$$

$$M_a = \frac{1}{2} \cdot C_{d,a1} \cdot \rho \cdot A_{a1} \cdot v_r \cdot |v_r| \cdot r_{m,a1} + \frac{1}{2} \cdot C_{d,a2} \cdot \rho \cdot A_{a2} \cdot v_r \cdot |v_r| \cdot r_{m,a2} \qquad \textbf{C-12}$$

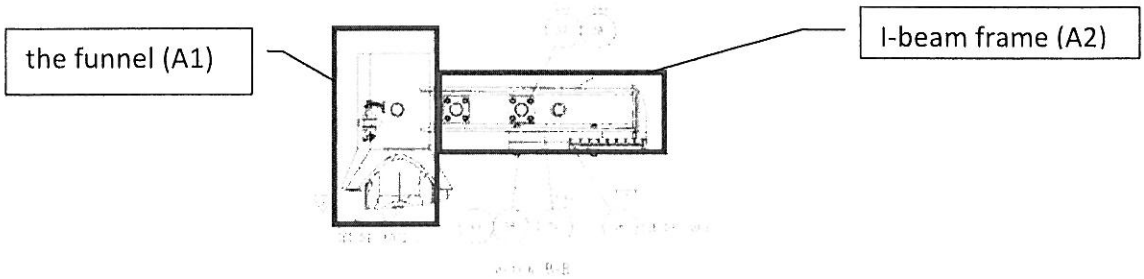

Figure C-4 The guide frame on the RT [6].

Where

M_a = moment around z-axis [Nm]

M_{a1} = moment caused by the force acting on the funnel [Nm]

M_{a2} = moment caused by the force acting on the I-beam frame [Nm]

$C_{d,a1}$ = 1.2

$C_{d,a2}$ = 2

A_{a1} = projected area on the funnel [m^2] = $0.296\ m^2$

A_{a2} = projected area on the I-beam frame [m^2] = $0.211\ m^2$

$r_{m,a1}$ = the distance between the center line of the RT and the center of the funnel = 1.84 [m]

$r_{m,a2}$ = the distance between the center line of the RT and the center of the funnel = 1.173 [m]

The moment caused by ROV receptacle is:

$$\boldsymbol{M_a = \frac{1}{2} \cdot 0.653 \cdot \rho \cdot v_r \cdot |v_r| + \frac{1}{2} \cdot 0.495 \cdot \rho \cdot v_r \cdot |v_r|} \qquad \textbf{C-13}$$

$$\boldsymbol{M_a = 0.58 \cdot \rho \cdot v_r \cdot |v_r|} \qquad \textbf{C-14}$$

With the same current velocity, the moment caused by projected area of the ROV receptacle is less than that of the guide frame therefore it can be assumed that the maximum drag force experienced on the RT is on the guide frame.

The moment in the ultra-deepwater zone and shallow zone

It is assumed that the velocity of sea current at 3,000 meters is equal to 0.2 m/s, while the water particle velocity caused by waves and sea current at 10 meters is equal to 1.87 m/s. According to the previous assumptions of the RT and WCP module and the assumed water velocities, the maximum moment of the RT and WCP module for the ultra-deepwater and shallow water zone can be calculated as shown in the following tables.

Degree	Max moment[Nm]				
	RT			WCP	RT and WCP
	Guide frame	ROV receptacle	Total		
0	0	16	16	0	32
45	0	23	23	2	47
90	0	16	16	2	34
135	-24	0	-24	2	-46
180	0	-16	-16	0	-32
225	0	-23	-23	2	-43
270	17	-16	1	2	4
315	24	0	24	2	49
360	0	23	23	0	45

Table C-1 Maximum moment on the RT and WCP module at 3,000 m water depths.

Degree	Max moment[Nm]				
	RT			WCP	RT and WCP
	Guide frame	ROV receptacle	Total		
0	0	1,397	1,397	0	2,793
45	0	1,975	1,975	152	4,103
90	0	1,397	1,397	215	3,009
135	-2,083	0	-2,083	152	-4,014
180	0	-1,397	-1,397	0	-2,793
225	0	-1,975	-1,975	152	-3,798
270	1,473	-1,397	76	215	368
315	2,083	0	2,083	152	4,318
360	0	1,975	1,975	0	3,950

Table C-2 Maximum moment on the RT and WCP module at 10 m water depths.

Appendix D Calculations

Density of sea water

$\rho := 1027\frac{kg}{m^3}$

Water depth [m]

wd := 300

i := 0.. wd

$d_i := -i$

$depth_i := (-d)_i m$

Sea state

$T_w := 9.7s$

$H_w := 5.58m$

wavelength for deep water

$\lambda := g\cdot\frac{T_w^2}{2\pi} = 146.853m$

wave number

$k := 2\frac{\pi}{\lambda} = 0.043\frac{1}{m}$

Current speed for deep water

$v_{current} := -0.2\frac{m}{s}$

$v_{module} := 0$

Relative velocity

$vr := v_{module} - v_{current}$

$\rho_{steel} := 7800\frac{kg}{m^3}$

WCP dimension

$w_{wcp} := 3.7m$

$l_{wcp} := 3.7m$

$h_{wcp} := 4.7m$

Projected area

$area_{wcp} := w_{wcp}\cdot h_{wcp} = 17.39m^2$

Cross section area

$crossarea_{wcp} := w_{wcp}\cdot l_{wcp} = 13.69m^2$

Volum

$vol_{wcp} := w_{wcp}\cdot l_{wcp}\cdot h_{wcp} = 64.343m^3$

$cd_{wcp} := 1$

$ca_{wcp} := 0.6$

Mass of the WCP in the air

$m_{wcp\_inair} := 50000kg$

Submerged mass of the WCP in the sea water

$$m_{wcp} := m_{wcp\_inair}\cdot\left(1 - \frac{\rho}{\rho_{steel}}\right) = 4.342\times 10^{4}\,kg$$

RT dimension

$h_{rt} := 1m$

$d_{rt} := 1.4m$

Projected area

$area_{rt} := h_{rt}\cdot d_{rt} = 1.4m^{2}$

Volum

$$vol_{rt} := \frac{\pi}{4}\left(d_{rt}\right)^{2}\cdot h_{rt} = 1.539\,m^{3}$$

$cd_{rt} := 1.2$

$ca_{rt} := 0.64$

Mass of the RT in the air

$m_{rt\_inair} := 5000kg$

Submerged mass of the RT in the sea water

$$m_{rt} := m_{rt\_inair}\cdot\left(1 - \frac{\rho}{\rho_{steel}}\right) = 4.342\times 10^{3}\,kg$$

Steel cable dimension

$cd_{cable} := 1.2$

$ca_{cable} := 1$

Diameter

$d_{sc} := 0.05m$

Length

$l_{sc_i} := i\cdot 1m$

$area_{sc_i} := d_{sc}\cdot l_{sc_i}$

$$\rho_{um\_sc} := 7000\frac{kg}{m^{3}}$$

Mass of the steel cable in the air

$$m_{sc\_air} := \rho_{um\_sc}\cdot\left[\pi\cdot\frac{\left(d_{sc}\right)^{2}}{4}\right] = 13.744\frac{kg}{m}$$

Submerged mass of the steel cable in the sea water

$$m_{sc} := m_{sc\_air} \cdot \left(1 - \frac{\rho}{\rho_{um\_sc}}\right) = 11.728 \frac{kg}{m}$$

Chemical Umbilical dimension

Diameter

$$d_{um\_ch} := 0.051m$$

Length

$$l_{um\_ch_i} := i \cdot 1m$$

$$area_{um\_ch_i} := d_{um\_ch} \cdot l_{um\_ch_i}$$

$$\rho_{um\_ch} := 2500 \frac{kg}{m^3}$$

Mass of the chemical umbilical in the air

$$m_{um\_ch\_inair} := \rho_{um\_ch} \cdot \left[\pi \cdot \frac{(d_{um\_ch})^2}{4}\right] = 5.107 \frac{kg}{m}$$

Submerged mass of the chemical umbilical in the sea water

$$m_{um\_ch} := m_{um\_ch\_inair} \cdot \left(1 - \frac{\rho}{\rho_{um\_ch}}\right) = 3.009 \frac{kg}{m}$$

Control Umbilical dimension

Diameter

$$d_{um\_co} := 0.038m$$

Length

$$l_{um\_co_i} := i \cdot 1m$$

$$area_{um\_co_i} := d_{um\_co} \cdot l_{um\_co_i}$$

$$\rho_{um\_co} := 1800 \frac{kg}{m^3}$$

Mass of the control umbilical in the air

$$m_{um\_co\_air} := \rho_{um\_co} \cdot \left[\pi \cdot \frac{(d_{um\_co})^2}{4}\right] = 2.041 \frac{kg}{m}$$

Submerged mass of the control umbilical in the sea water

$$m_{um\_co} := m_{um\_co\_air} \cdot \left(1 - \frac{\rho}{\rho_{um\_co}}\right) = 0.877 \frac{kg}{m}$$

Waves profile

Maximum horizontal velocity for deep water

$z_i := d_i\,m$

$u_i := \left(\pi \cdot \frac{H_W}{T_W}\right) \cdot e^{(k \cdot z_i)}$

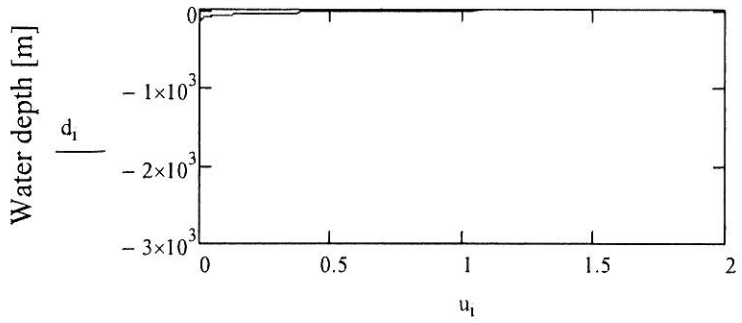

Maximum horizontal particle velocity [m/s]

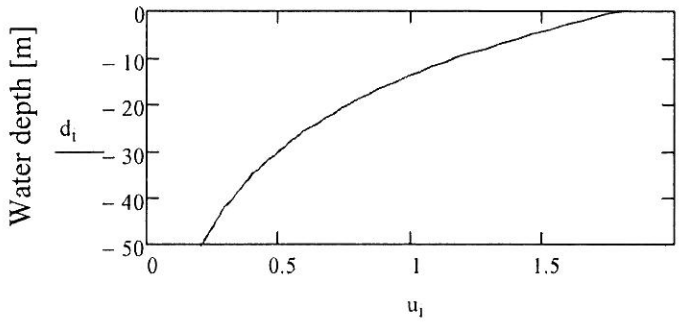

Maximum horizontal particle velocity [m/s]

$u_{3000} = 0\frac{m}{s}$

$u_{10} = 1.178\frac{m}{s}$

$a_i := \left[2\pi^2 \cdot \frac{H_W}{(T_W)^2}\right] \cdot e^{(k \cdot z_i)}$

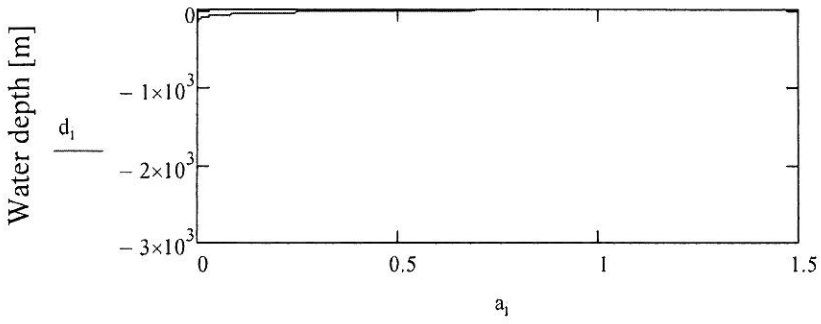

Maximum horizontal particle acceleration[m/s^2]

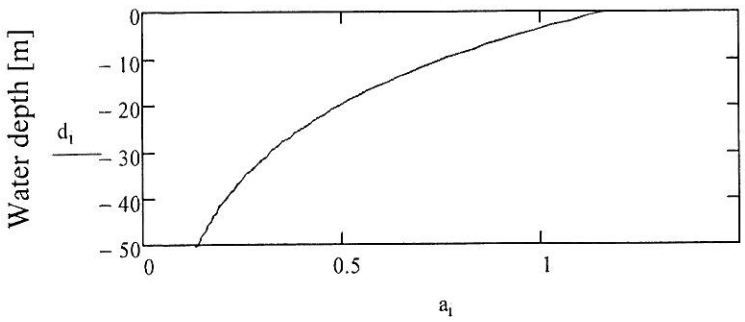

Maximum horizontal particle acceleration[m/s^2]

$a_{3000} = 0\frac{m}{s^2}$

$a_{10} = 0.763\frac{m}{s^2}$

Current profile

$$current(d) := if\left[-400 \le d \le 0, \left[\frac{-0.5\cdot(-d)}{400}\right] + 0.7, 0.2\right]\cdot\frac{m}{s}$$

Current profile

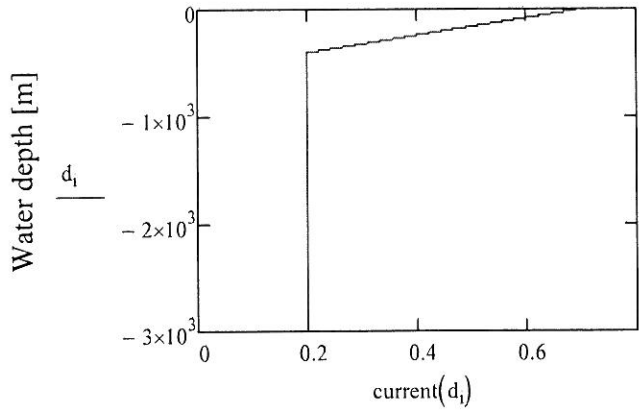

Sea current [m/s]

$velocity_i := current(d_i) + u_i$

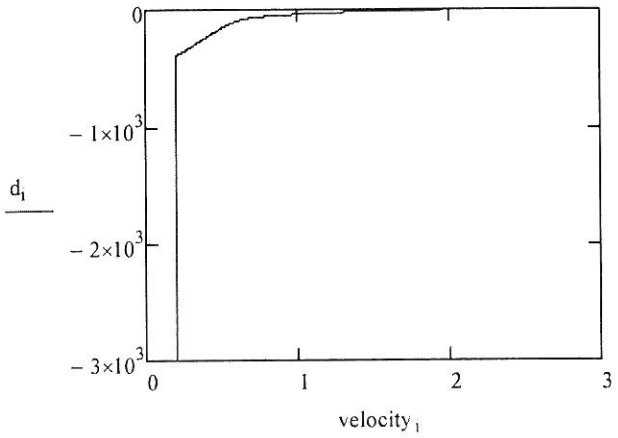

Drag forces experienced on the RT, WCP and steel cable

$$drag_{wcp_i} := \frac{1}{2} \cdot cd_{wcp} \cdot area_{wcp} \cdot \rho \cdot \left[\left(velocity_i \right)^2 \right]$$

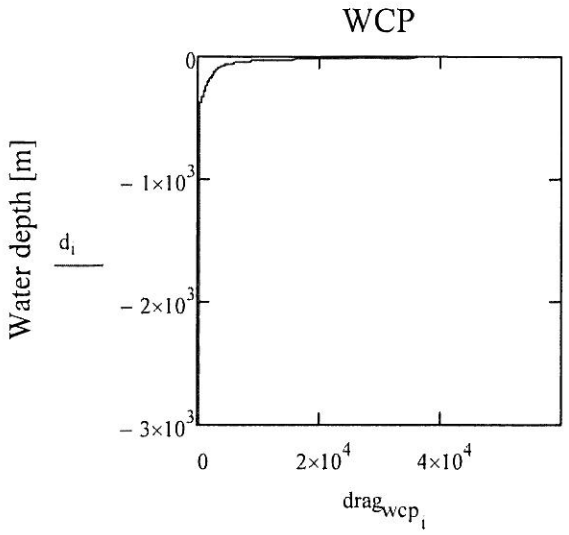

$$drag_{rt_i} := \frac{1}{2} \cdot cd_{rt} \cdot area_{rt} \cdot \rho \cdot \left[\left(velocity_i \right)^2 \right]$$

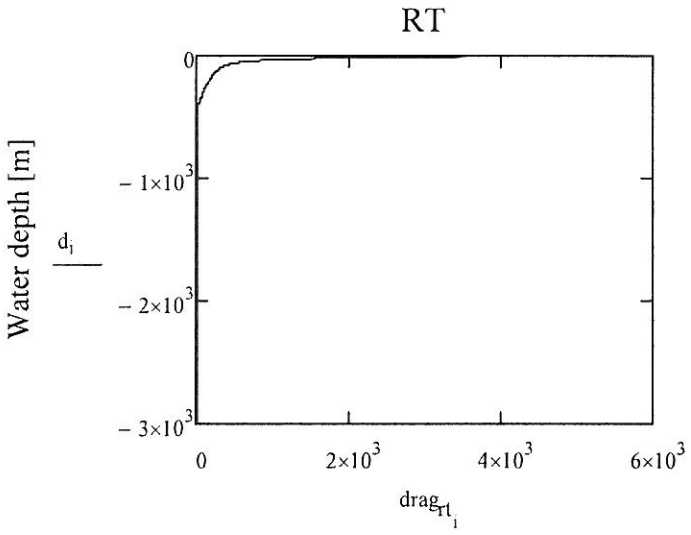

$$drag_{module_i} := \left(drag_{wcp_i} + drag_{rt_i} \right)$$

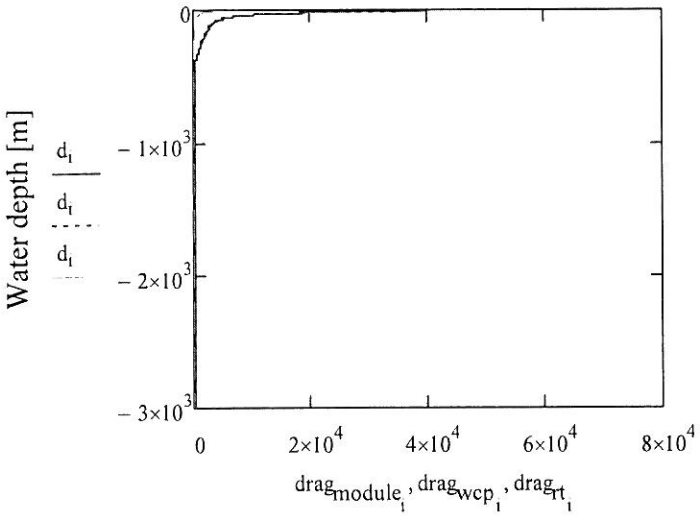

$$drag_{sc_i} := \frac{1}{2}\cdot cd_{cable}\cdot area_{sc_i}\cdot\rho\cdot\left[\left(velocity_i\right)^2\right]$$

Steel cable

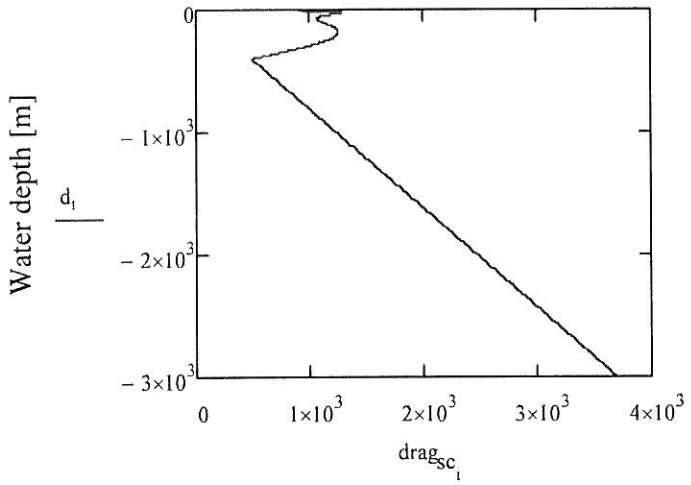

$$drag_{um\_ch_i} := \frac{1}{2}\cdot cd_{cable}\cdot area_{um\_ch_i}\cdot\rho\cdot\left[\left(velocity_i\right)^2\right]$$

Chemical umbilical

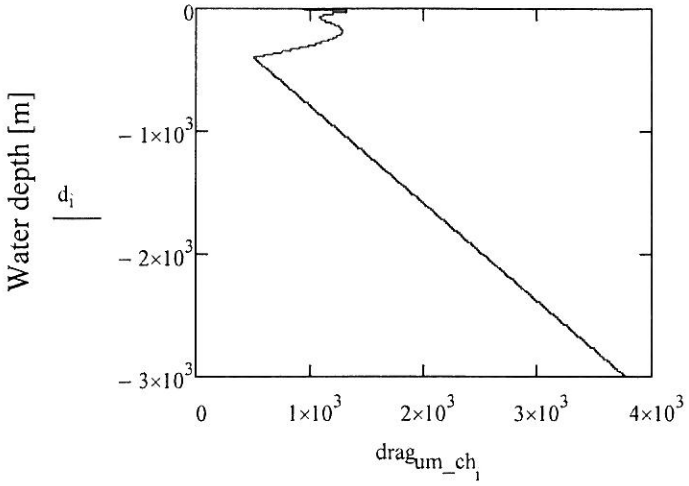

Drag force [N]

$$drag_{um\_co_i} := \frac{1}{2}\cdot cd_{cable}\cdot area_{um\_co_i}\cdot\rho\cdot\left[\left(velocity_i\right)^2\right]$$

Control umbilical

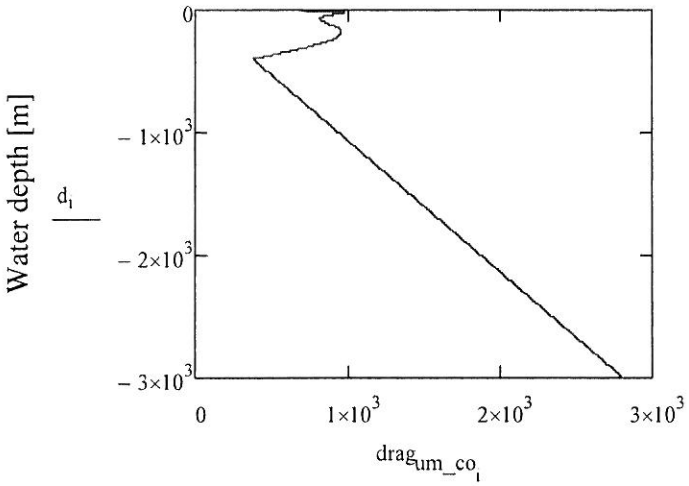

Drag force [N]

$$drag_{total1_i} := drag_{wcp_i} + drag_{rt_i} + drag_{sc_i}$$

WD from 0-3,000 m-without UTH

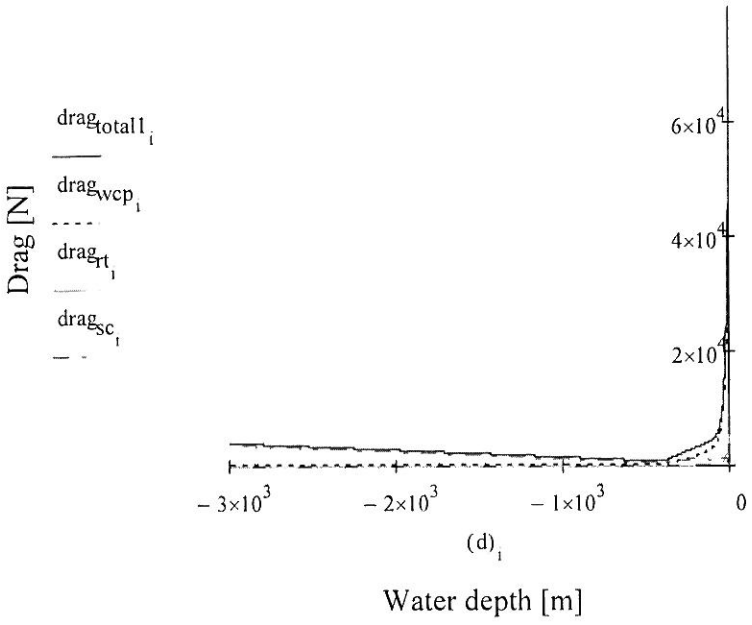

WD from 2,000-3,000 m-without UTH

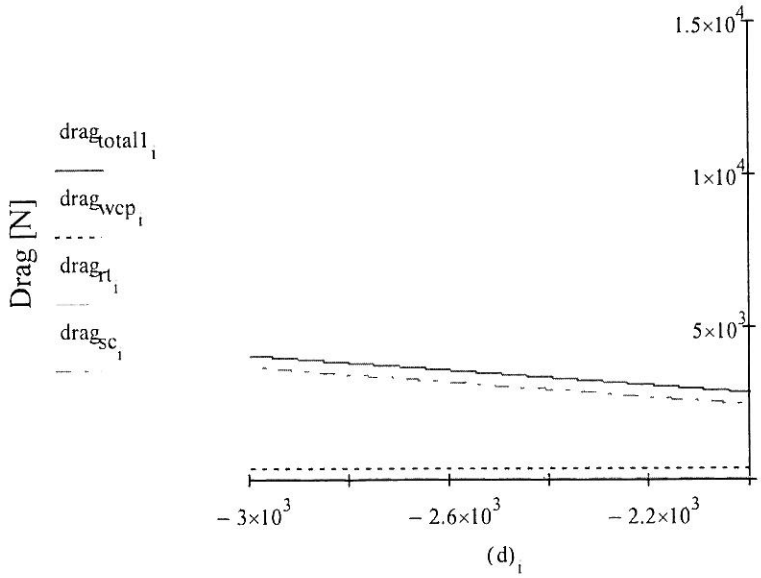

WD from 0-3,000 m-with UTH

$drag_{total\_uth1_i} := drag_{wcp_i} + drag_{rt_i} + drag_{sc_i} + drag_{um\_co_i} + drag_{um\_ch_i}$

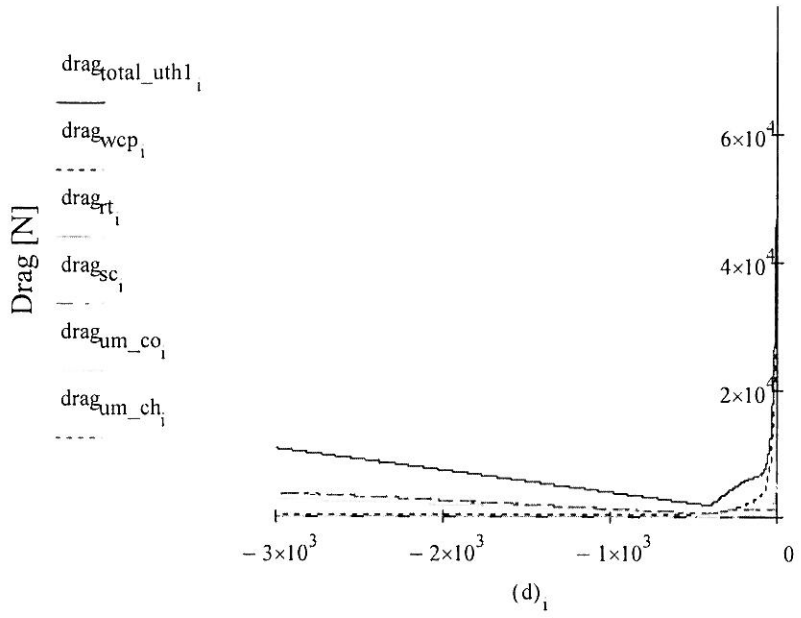

Water depth [m]

WD from 2,000-3,000 m-without UTH

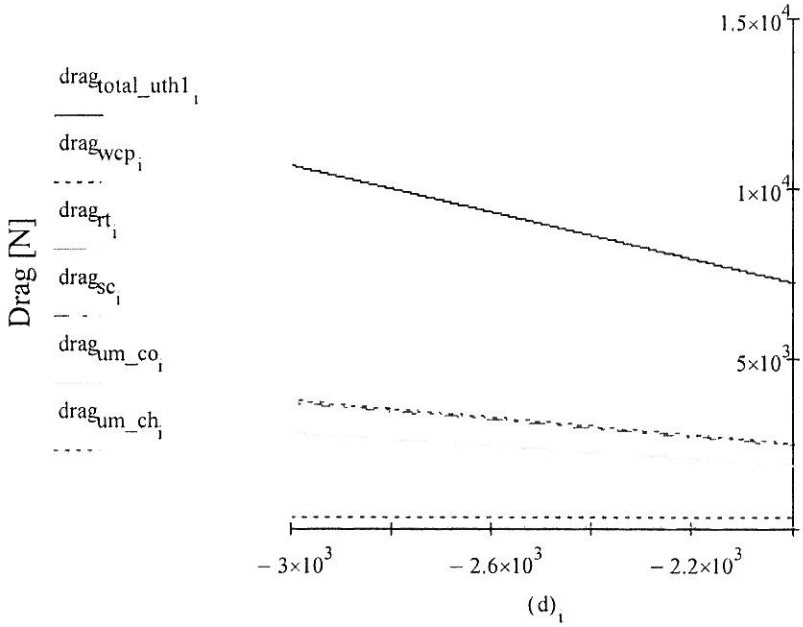

Water depth [m]

$drag_{wcp_{2997}} = 357.191N$

$drag_{rt_{2995}} = 34.507N$

$drag_{sc_{2995}} = 3.691 \times 10^3 N$

$drag_{um\_co_{2995}} = 2.805\times 10^{3}\ N$

$drag_{um\_ch_{2995}} = 3.765\times 10^{3}\ N$

Inertia forces on the RT, WCP and steel cable

the inertia force affects the object in shallow water zones (operation #2 and #4).

$Fi_{wcp_i} := \rho \cdot crossarea_{wcp} \cdot h_{wcp} \cdot a_i \cdot (1 + ca_{wcp})$

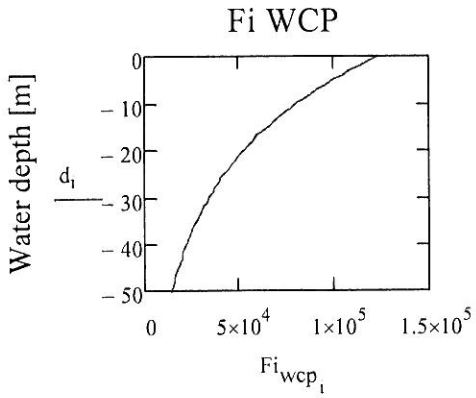

The Fi is estimated by taking the fa at 13 m WD

$Fi_{wcp_{13}} = 7.097\times 10^{4}\ N$

$Fi_{rt_i} := \rho \cdot \frac{\pi (d_{rt})^2}{4} \cdot h_{rt} \cdot a_i \cdot (1 + ca_{rt})$

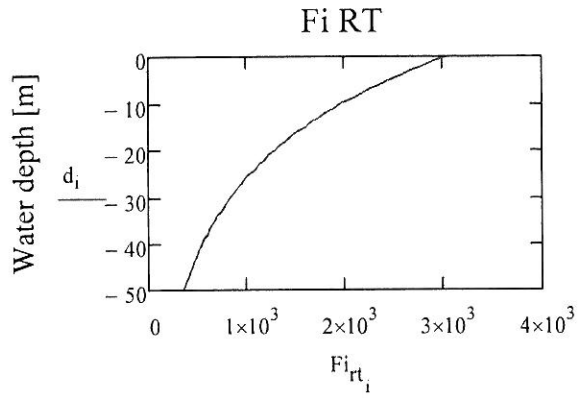

For RT and steel cable, the inertia forces are estimated at 10 m

$Fi_{rt_{10}} = 1.979\times 10^{3}\ N$

$Fi_{sc_i} := \rho \cdot \frac{\pi (d_{sc})^2}{4} \cdot a_i \cdot (1 + ca_{cable}) \cdot (-d)_i m$

Fi SC

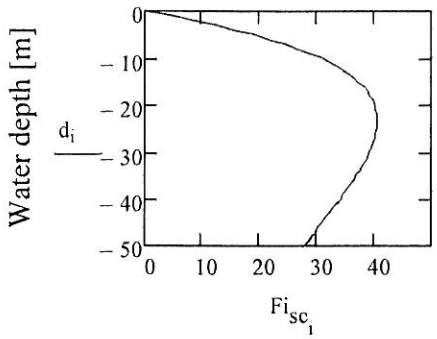

Inertia force[N]

$Fi_{sc_{10}} = 30.778N$

For operation #2

$Fi_{total2_i} := Fi_{rt_i} + Fi_{sc_i}$

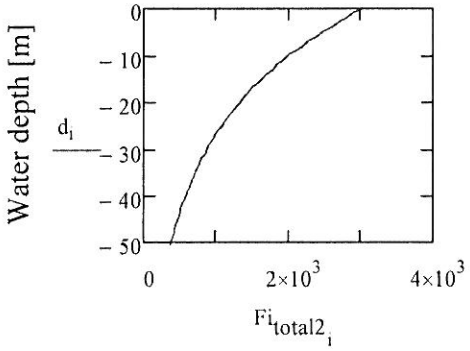

Total inertia force [N]

For operation #4

$Fi_{total4_i} := Fi_{rt_i} + Fi_{wcp_i} + Fi_{sc_i}$

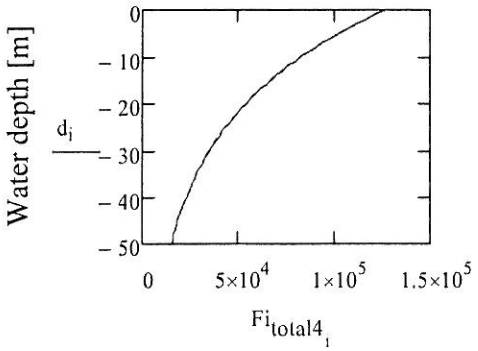

Inertia force [N]

$F_{total1_i} := drag_{total1_i} + Fi_{total4_i}$

$F_{wcp_i} := drag_{wcp_i} + Fi_{wcp_i}$

$F_{rt_i} := drag_{rt_i} + Fi_{rt_i}$

$F_{sc_i} := drag_{sc_i} + Fi_{sc_i}$

$F_{total2_i} := F_{rt_i} + F_{sc_i}$

the total force on the system

WD from 0-50 m

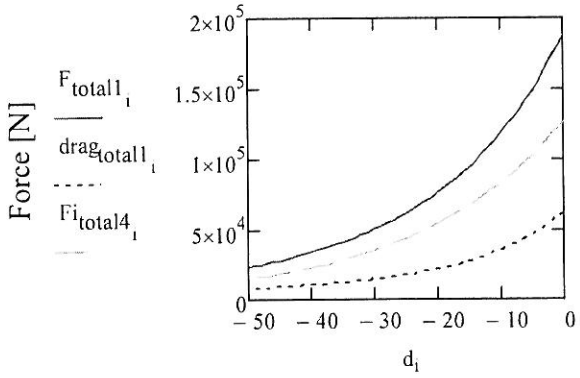

WD from 2,000-3,000 m

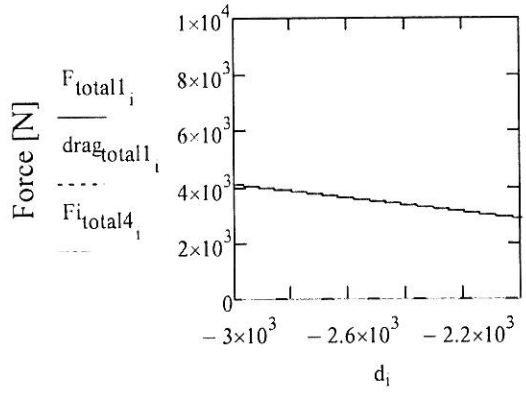

The total force acting on each object

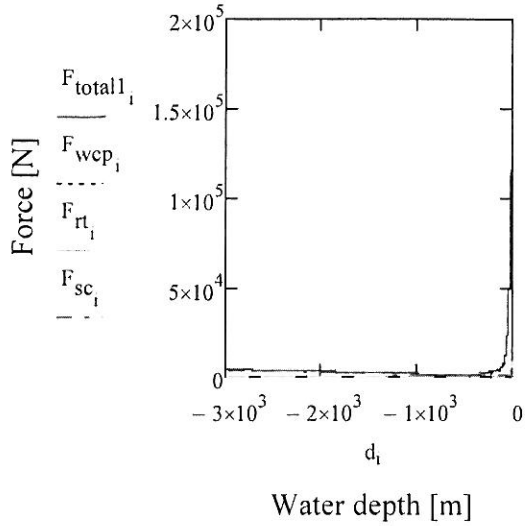

WD from 0-50 m

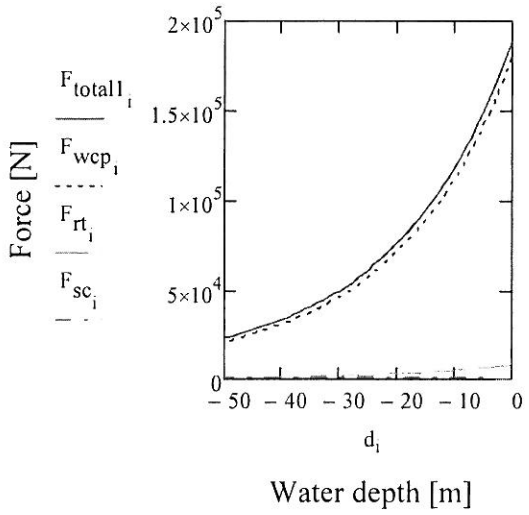

WD from 2,000-3,000 m

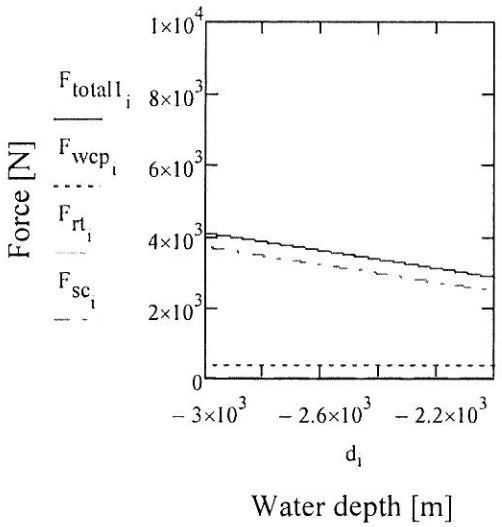

the total force on each module

$F_{wcp_{13}} = 9.738 \times 10^4 \text{ N}$

$F_{rt_{10}} = 4.981 \times 10^3 \text{ N}$

$F_{sc_{10}} = 1.103 \times 10^3 \text{ N}$

$F_{wcp_{2997}} = 357.191 \text{N}$

$F_{rt_{2995}} = 34.507 \text{N}$

$F_{sc_{2995}} = 3.691 \times 10^3 \text{ N}$

Drag forces experienced on the system during operation #1

WD from 2,000-3,000 m

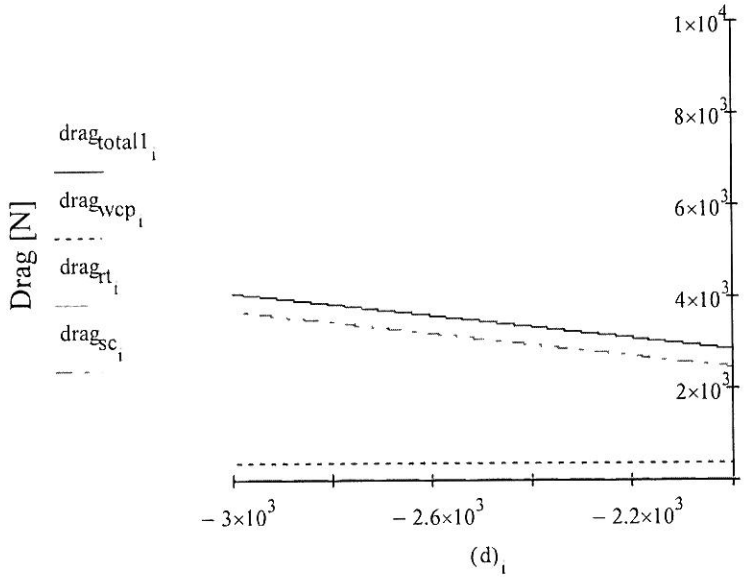

Drag force in operation #1

For WCP, the drag is estimated at 3,000 m

For RT and steel cable, the drag forces are estimated at 2,995 m

$drag_{wcp_{wd}} = 357.191 \text{N}$

$drag_{rt_{2995}} = 34.507 \text{N}$

$drag_{sc_{2995}} = 3.691 \times 10^3 \text{ N}$

The drag forces experienced on the RT and steel cable during operation #2 and #3

$drag_{total2_i} := drag_{rt_i} + drag_{sc_i}$

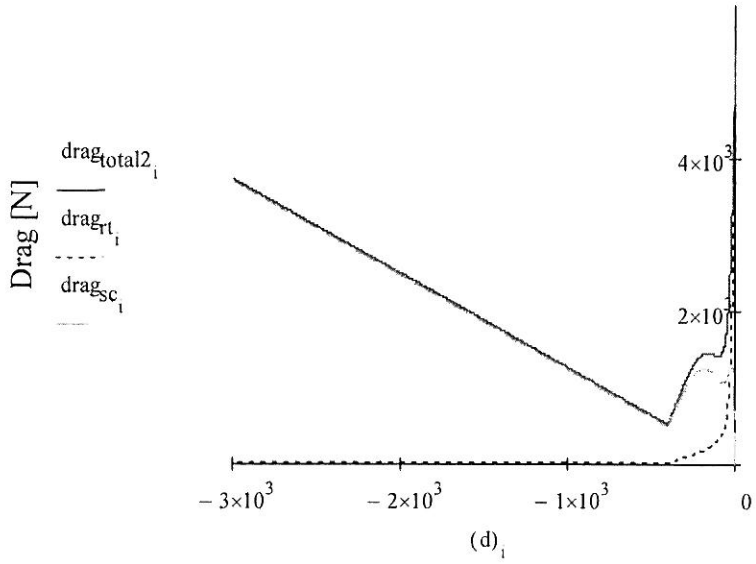

Water depth [m]

The drag forces experienced on the RT and steel cable during operation #2

WD from 0-50 m

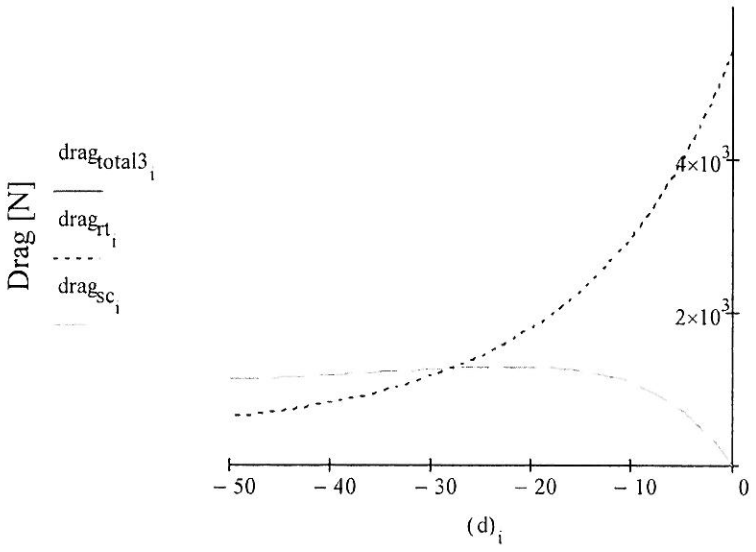

Water depth [m]

2

Drag force in operation #2

$drag_{rt_{10}} = 3.003 \times 10^3\ N$

$drag_{sc_{10}} = 1.072 \times 10^3\ N$

$drag_{total2_{10}} = 4.075 \times 10^3\ N$

Inertia force in operation #2

$Fi_{rt_{10}} = 1.979 \times 10^3\ N$

$Fi_{sc_{10}} = 30.778N$

$Fi_{total2_{10}} = 2.009 \times 10^3\ N$

The drag forces experienced on the RT and steel cable during operation #3

WD from 2,000-3,000 m

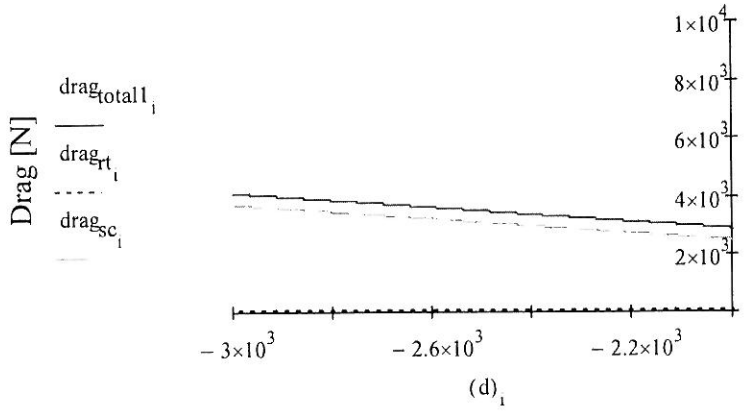

Drag force in operation #3

$drag_{rt_{2995}} = 34.507N$

$drag_{sc_{2995}} = 3.691 \times 10^3\ N$

$drag_{total2_{2995}} = 3.726 \times 10^3\ N$

Drag forces experienced on the system during operation #4

WD from 0-50 m

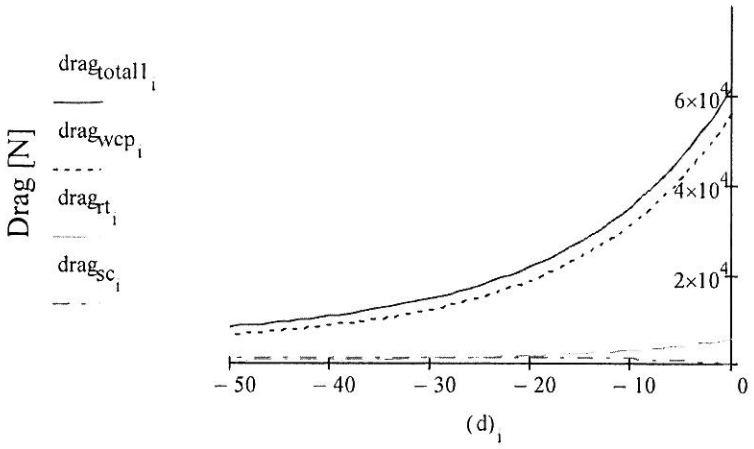

Drag force in operation #4

For WCP, the drag is estimated at 13 m

For RT and steel cable, the drag forces are estimated at 10 m

$drag_{wcp_{13}} = 2.642\times 10^{4}\ N$

$drag_{rt_{10}} = 3.003\times 10^{3}\ N$

$drag_{sc_{10}} = 1.072\times 10^{3}\ N$

Inertia forces in operation #4

$Fi_{rt_{10}} = 1.979\times 10^{3}\ N$

$Fi_{sc_{10}} = 30.778N$

$Fi_{wcp_{13}} = 7.097\times 10^{4}\ N$

Mass

$m_{sc\_d_i} := (depth_i)\cdot m_{sc}$

$m_{total1_i} := m_{wcp} + m_{rt} + m_{sc\_d_i}$

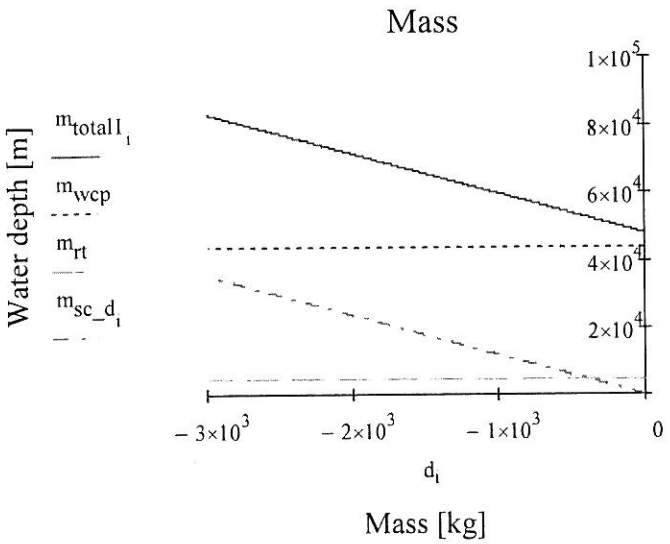

$$W_{total.1_i} := m_{total1_i} \cdot 9.81 \frac{m}{s^2}$$

Mass in operation #2 and #3

$$m_{total2_i} := m_{rt} + m_{sc\_d_i}$$

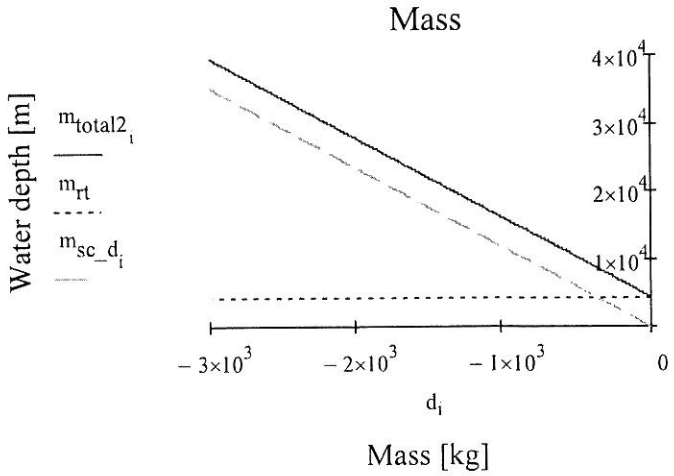

$$W_{total.2_i} := m_{total2_i} \cdot 9.81 \frac{m}{s^2}$$

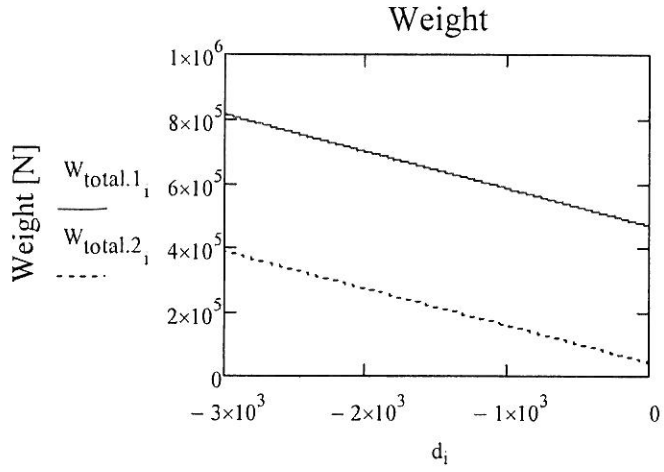

Operation #1 and #4

$$\text{theta}_{1_i} := \text{atan}\left(\frac{W_{total.1_i}}{F_{total1_i}}\right)\cdot\frac{180}{\pi}$$

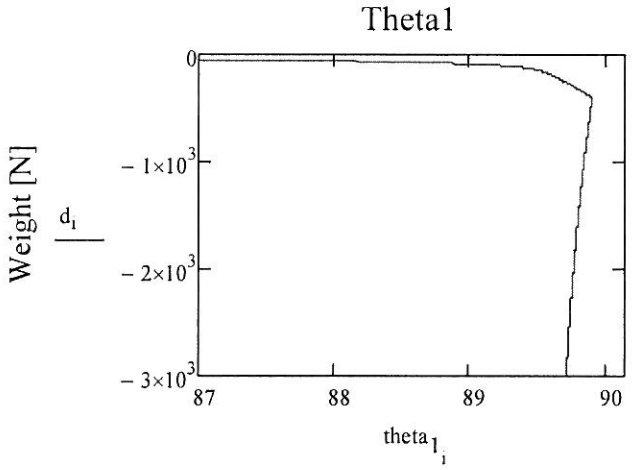

$\text{theta}_{1_{wd}} = 89.712$

Operation #1 and #3

$$\text{theta}_{2_i} := \text{atan}\left(\frac{W_{total.2_i}}{F_{total2_i}}\right)\cdot\frac{180}{\pi}$$

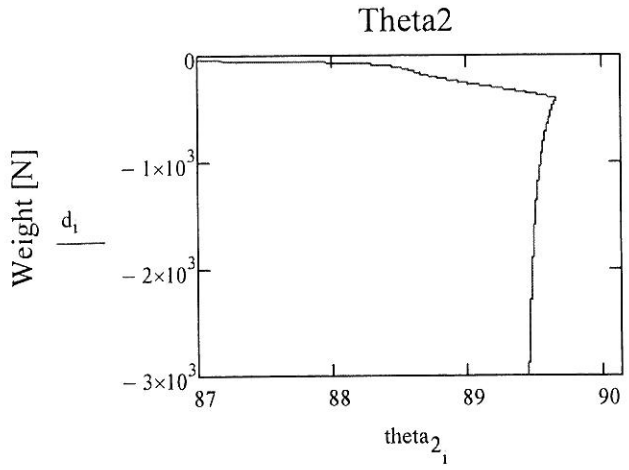

$theta2_{wd} = 89.449$

$$offset1_i := \frac{depth_i}{\tan\left(theta1_i \cdot \frac{\pi}{180}\right)}$$

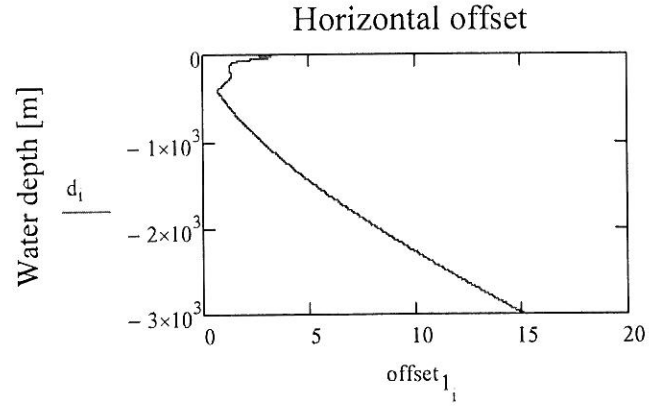

Operation #1

$offset1_{wd} = 15.076m$

Operation #4

$offset1_{10} = 2.509m$

$$offset2_i := \frac{depth_i}{\tan\left(theta2_i \cdot \frac{\pi}{180}\right)}$$

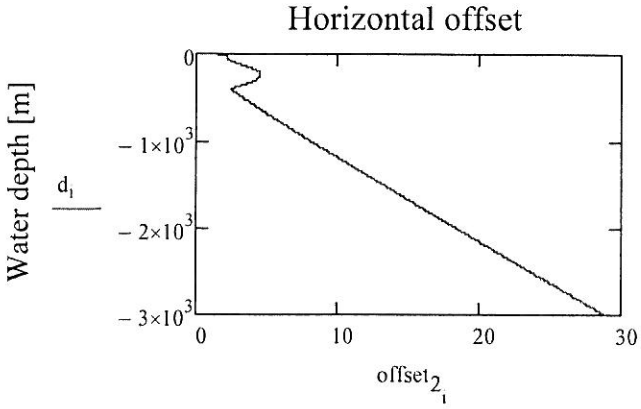

Operation #2

$offset2_{10} = 1.391m$

Operation #3

$offset2_{wd} = 28.872m$

Power and Energy calculations

$v_{current} := -0.2\frac{m}{s}$

th_ratio $\frac{thrust}{kw}$

$th\_ratio := 272\frac{N}{kW}$

Increasing speeds

$vv := 1..200$

Operation #1

$v1ms_{vv} := \frac{vv}{200}\frac{m}{s}$

Relative velocity of the module

$vr1_{vv} := v1ms_{vv} - v_{current}$

$f_{drag\_dv1} := \frac{drag_{total1_{wd}}}{vr^2} = 1.022\times 10^5\frac{kg}{m}$

Required power

$drag1ms_{vv} := f_{drag\_dv1}\cdot\left(vr1_{vv}\right)^2$

$power1_{vv} := \frac{drag1ms_{vv}}{th\_ratio}$

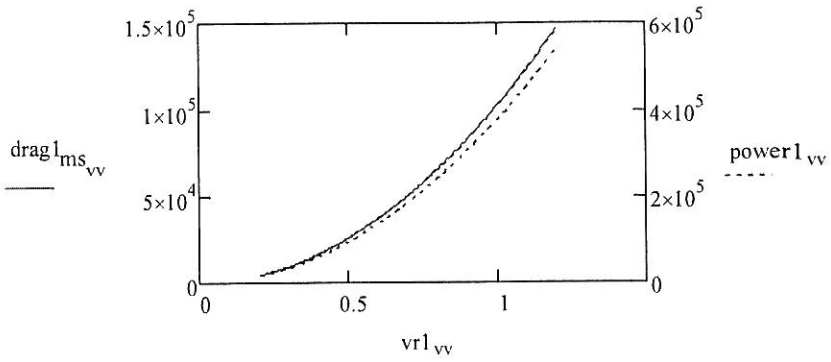

Advance speed of the module [m/s]

Minimum required thrust

$vr1_1 = 0.205\frac{m}{s}$

$drag1ms_1 = 4.296\times 10^3\ N$

$power1_1 = 1.579\times 10^4\ W$

Operation #2, WD 10 m

$drag_{total2_{10}} = 4.075\times 10^3\ N$

$Fi_{total2_{10}} = 2.009\times 10^3\ N$

$drag_{total2_{10}} = 4.075\times 10^3\ N$

$current(d_{10}) = 0.688\frac{m}{s}$

$u_{10} = 1.178\frac{m}{s}$

Increasing speeds

$v2ms_{vv} := \frac{vv}{200}\frac{m}{s}$

$$f_{drag\_dv2} := \frac{drag_{total2_{10}}}{\left(current(d_{10}) + u_{10}\right)^2} = 1.171\times 10^3\ \frac{kg}{m}$$

Relative velocity of the module

$vr2_{vv} := v2ms_{vv} + current(d_{10}) + u_{10}$

Required power

$Ftotal2ms_{vv} := f_{drag\_dv2}\cdot\left(vr2_{vv}\right)^2 + Fi_{total2_{10}}$

$$power2_{vv} := \frac{Ftotal2ms_{vv}}{th\_ratio}$$

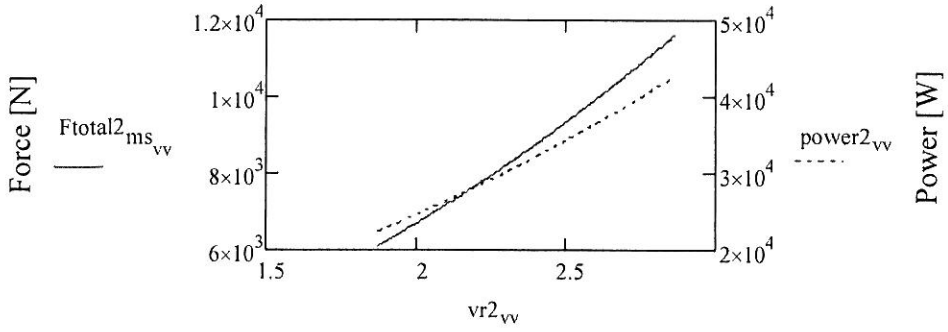

Advance speed of the module [m/s]

Minimum required thrust

$vr2_1 = 1.871 \frac{m}{s}$

$Ftotal2ms_1 = 6.106 \times 10^3 \, N$

$power2_1 = 2.245 \times 10^4 \, W$

Operation #3

$$f_{drag\_dv3} := \frac{drag_{total2_{2995}}}{\left(current\left(d_{2995}\right)\right)^2} = 9.314 \times 10^4 \frac{kg}{m}$$

Relative velocity of the module

$$vr3_{vv} := v2ms_{vv} + current\left(d_{2995}\right)$$

Required power

$$Ftotal3ms_{vv} := f_{drag\_dv3} \cdot \left(vr3_{vv}\right)^2$$

$$power3_{vv} := \frac{Ftotal3ms_{vv}}{th\_ratio}$$

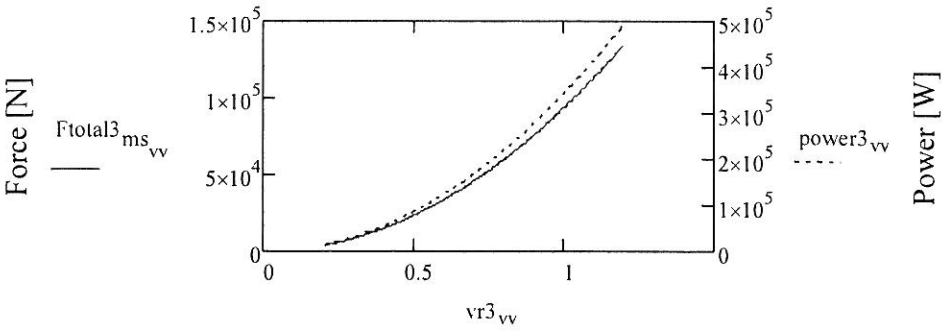

Advance speed of the module [m/s]

Minimum required thrust

$vr3_1 = 0.205 \frac{m}{s}$

$Ftotal3_{ms_1} = 3.914 \times 10^3\ N$

$power3_1 = 1.439 \times 10^4\ W$

Operation #1

The offset distance

$offset1_{wd} := 2m$

$time1_{ms_{vv}} := \left(\frac{offset1_{wd}}{v1_{ms_{vv}}} \right)$

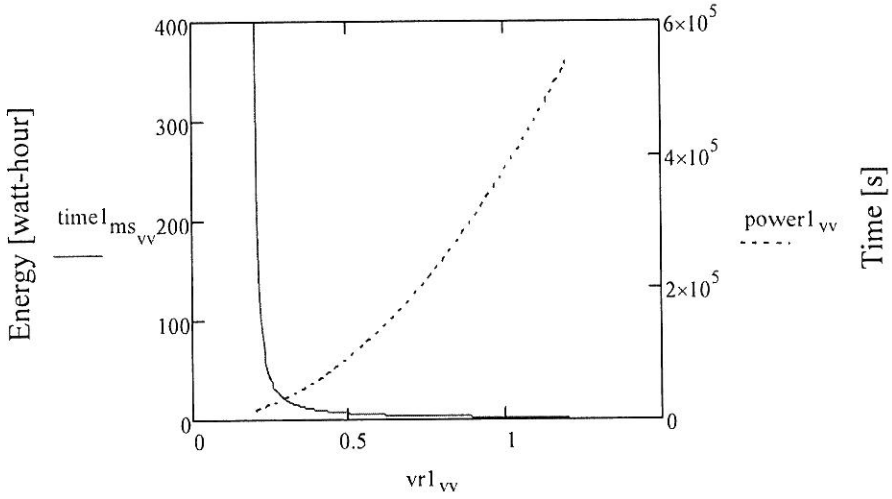

Energy converted into watt hour

$energy1_{ms_{vv}} := \left(time1_{ms_{vv}} \cdot power1_{vv} \right)$

1 watt hour = 3600 J

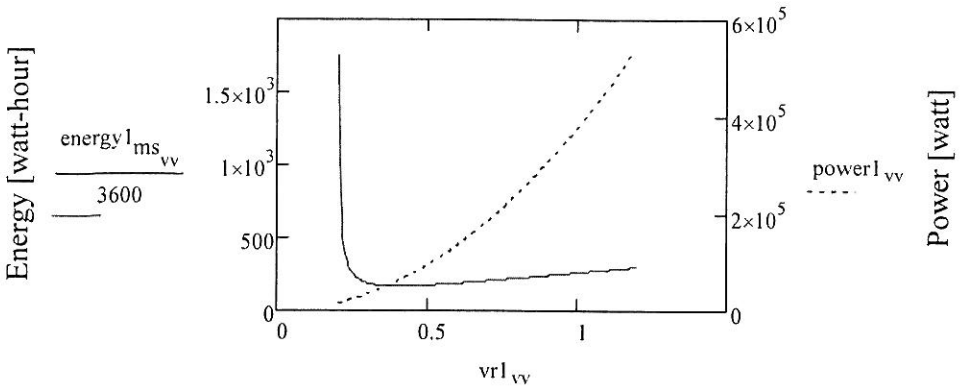

Advance speed of the module [m/s]

Minimum required thrust

$$vr1_1 = 0.205\frac{m}{s}$$

$$drag1_{ms_1} = 4.296\times 10^3\ N$$

$$power1_1 = 1.579\times 10^4\ W$$

$$time1_{ms_1} = 400s$$

$$energy1_{ms_1} = 1.755\times 10^3\cdot W\cdot hr$$

Minimum energy consumption

The minimum value can be found from a differential equation

$$energy1_{ms_{vv}} = time1_{ms_{vv}}\cdot power1_{vv} = \left(\frac{offset1_{wd}}{v1_{ms_{vv}}}\right)\cdot\left(\frac{Ftotal2_{ms_{vv}}}{th\_ratio}\right)$$

$$energy1_{ms_{vv}} = \left(\frac{offset1_{wd}}{v1_{ms_{vv}}}\right)\cdot\frac{\left[f_{drag\_dv1}\cdot\left(vr1_{vv}\right)^2\right]}{th\_ratio}$$

$$energy1_{ms_{vv}} = 2\cdot\frac{\left(1.022\times 10^5\right)}{272}\cdot\frac{\left(v1_{ms_{vv}}+0.2\right)^2}{v1_{ms_{vv}}}$$

$$energy1_{ms_{vv}} = 751\cdot\frac{\left(v1_{ms_{vv}}+0.2\right)^2}{v1_{ms_{vv}}}$$

$$\frac{d}{dvm}\frac{751(vm+0.2)^2}{vm} \rightarrow \frac{751\cdot(2\cdot vm+0.4)}{vm} - \frac{751\cdot(vm+0.2)^2}{vm^2}$$

Solving the equation

$$\frac{751\cdot(2\cdot vm+0.4)}{vm} - \frac{751\cdot(vm+0.2)^2}{vm^2} = 0 \text{ solve} \rightarrow \begin{pmatrix}-0.2\\0.2\end{pmatrix}$$

So vm=0.2 m/s

Where vm = the net velocity of the module

The advance speed giving the minimum energy is vm+v.current, 0.4 m/s

$$vr1_{40} = 0.4\frac{m}{s}$$

$$drag1_{ms_{40}} = 1.636\times 10^{4}\,N$$

$$power1_{40} = 6.013\times 10^{4}\,W$$

$$time1_{ms_{40}} = 10\,s$$

$$energy1_{ms_{40}} = 167.03\,W\cdot hr$$

The max advance velocity is around 0.25 m/s according to the thrust performance

$$vr1_{10} = 0.25\frac{m}{s}$$

$$drag1_{ms_{10}} = 6.389\times 10^{3}\,N$$

$$power1_{10} = 2.349\times 10^{4}\,W$$

$$time1_{ms_{10}} = 40\,s$$

$$energy1_{ms_{10}} = 260.985\,W\cdot hr$$

running 2 thrusters

Energy requirement

$$vr1_{1} = 0.205\frac{m}{s}$$

$$drag1_{ms_{1}} = 4.296\times 10^{3}\,N$$

$$power1_{2} = 1.657\times 10^{4}\,W$$

$$time1_{ms_{2}} = 200\,s$$

$$energy1_{ms_{2}} = 920.754\,W\cdot hr$$

Operation #2

The offset distance

$$offset2_{10} = 1.391\,m$$

$$time2_{ms_{vv}} := \left(\frac{offset2_{10}}{v2_{ms_{vv}}}\right)$$

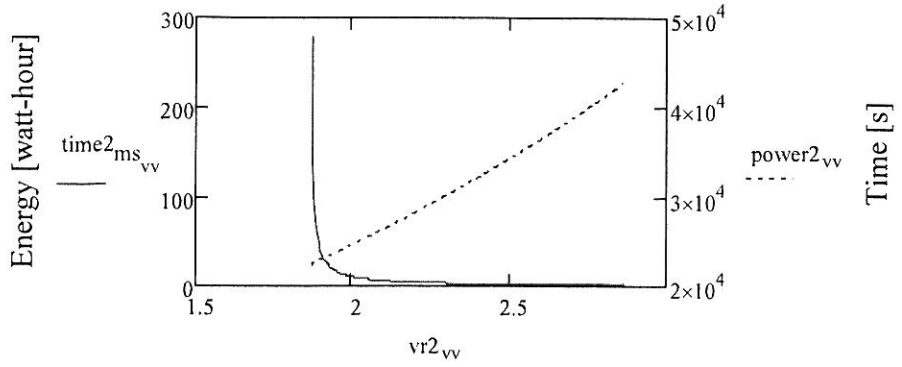

Velociy of the module [m/s]

$$energy2ms_{vv} := \left(time2ms_{vv} \cdot power2_{vv}\right)$$

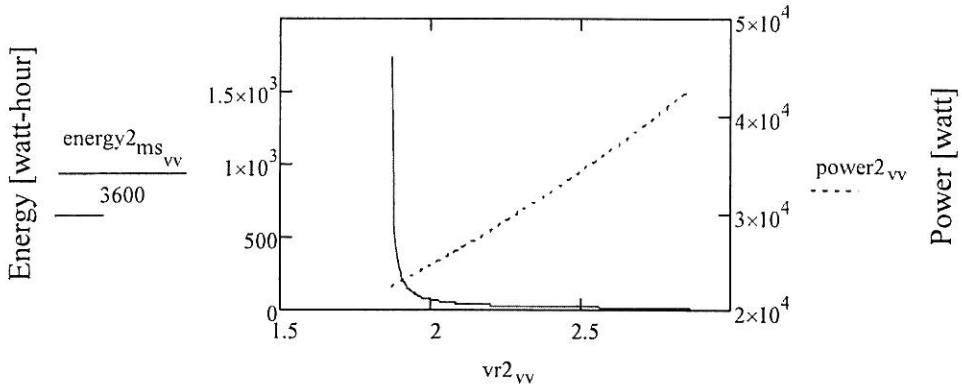

Advance speed of the module [m/s]

Minimum required thrust

$vr2_2 = 1.876\frac{m}{s}$

$Ftotal2ms_2 = 6.128\times 10^3\ N$

$power2_2 = 2.253\times 10^4\ W$

$time2ms_2 = 139.098s$

$energy2ms_2 = 870.535\,W\cdot hr$

Minimum energy consumption

$vr2_{15} = 1.941\frac{m}{s}$

$Ftotal2ms_{15} = 6.419\times 10^3\ N$

$power2_{15} = 2.36\times 10^4\ W$

$time2ms_{15} = 18.546s$

$energy2ms_{15} = 121.572\,W\cdot hr$

Operation #3

The offset distance

$offset_3 := 2m$

$time3_{ms_{vv}} := \left(\frac{offset_3}{v2_{ms_{vv}}} \right)$

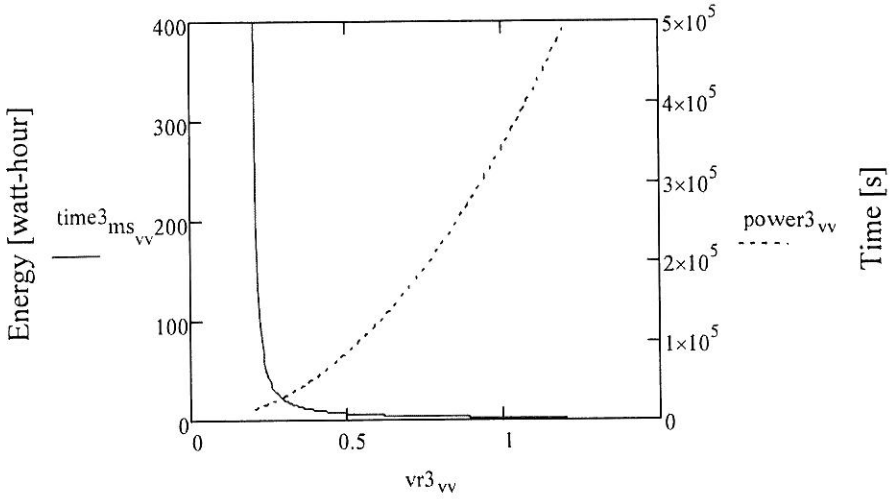

Velociy of the module [m/s]

Energy converted into watt hour

$energy3_{ms_{vv}} := \left(time3_{ms_{vv}} \cdot power3_{vv} \right)$

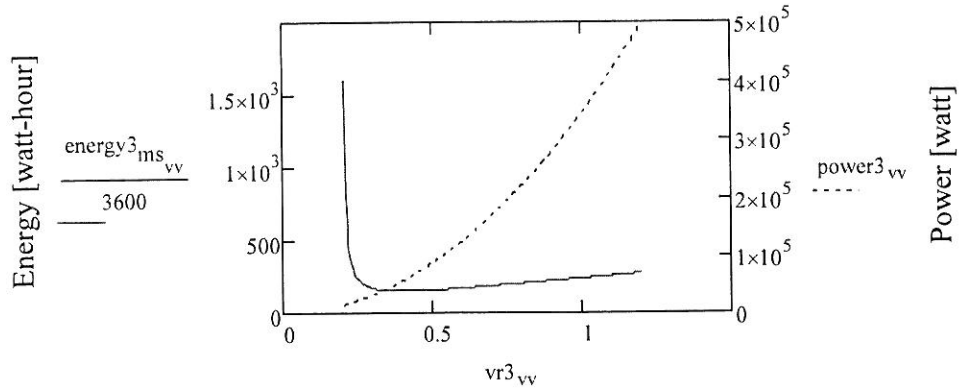

Advance speed of the module [m/s]

Minimum required thrust

$vr3_1 = 0.205 \frac{m}{s}$

$Ftotal3_{ms_1} = 3.914 \times 10^3 N$

$power3_1 = 1.439 \times 10^4 W$

$time3_{ms_1} = 400s$

$energy3_{ms_1} = 1.599 \times 10^3 \cdot W \cdot hr$

running 3 thrusters

Minimum energy consumption

$$vr3_{12} = 0.26\frac{m}{s}$$

$$Ftotal3_{ms_{12}} = 6.296\times 10^{3}\,N$$

$$power3_{12} = 2.315\times 10^{4}\,W$$

$$time3_{ms_{12}} = 33.333s$$

$$energy3_{ms_{12}} = 214.33\,W\cdot hr$$

running 2 thrusters

Energy requirement

$$vr3_{3} = 0.215\frac{m}{s}$$

$$Ftotal3_{ms_{3}} = 4.305\times 10^{3}\,N$$

$$power3_{3} = 1.583\times 10^{4}\,W$$

$$time3_{ms_{3}} = 133.333s$$

$$energy3_{ms_{3}} = 586.238\,W\cdot hr$$